

University of
Strathclyde
Glasgow

**Investigation into The Mechanism of
Wet Electrostatic Scrubber (WES) for
Fine Particles Capture**

by

Lin Yang

A thesis submitted in fulltime of the requirements for the degree of

Doctor of Philosophy

Department of Naval Architecture, Ocean and Marine Engineering

University of Strathclyde, Glasgow

November 2024

Declaration

This thesis is the result of the author's original research. It has been composed by the author and has not been previously submitted for examination which has led to the award of a degree.

The copyright of this thesis belongs to the author under the terms of the United Kingdom Copyright Acts as qualified by University of Strathclyde Regulation 3.50. Due acknowledgement must always be made of the use of any material contained in, or derived from, this thesis.

Signed:

Date:

Abstract

In the context of increasing global maritime trade, emissions from marine diesel engines, primarily using Heavy Fuel Oil (HFO) and Marine Gas Oil (MGO), pose significant environmental and health risks. These emissions, especially particulate matter (PM), contribute to climate change, acid rain, and ecosystem damage. Among the methods for reducing PM from marine diesel engines, electrohydrodynamic techniques show promise.

This thesis proposes a theoretical model to describe particle movement in a wet electrostatic scrubber (WES) for capturing emissions from marine diesel engines. In the WES, exhaust gases pass through a high-voltage electric field, ionizing particles which then interact with oppositely charged water droplets. These droplets capture the particles through electrostatic attraction, resulting in cleaner exhaust gas. A detailed scientific explanation of this particle-droplet interaction is uncommon.

The model presented considers various factors such as electric field strength, gas flow conditions, particle characteristics, and droplet size. By optimally selecting conditions for electric and flow fields, particle removal efficiency can be enhanced. The framework aligns gas flow, temperature, and electrostatic fields

to optimize particle capture.

The thesis investigated the mechanism of particle capturing process in a WES. The thesis proposes that through developing a theoretical description and analysing the motion characteristics. The core of this thesis is threefold:

(1) A mathematical model incorporating electrostatic force and flow field distribution around the droplet is developed. By solving equations for particle movement and stream function distribution, the model describes particle-droplet interactions under an electrostatic field. Analysis shows that electric fields increase particle velocity and capture efficiency, with larger particles being more affected. Smaller droplet sizes enhance particle collection.

(2) A co-simulation method using ANSYS Fluent and MATLAB simulates the particle motion process. Simulation results are consistent with mathematical calculation data, showing an average error of 1.5%.

(3) An experimental platform was established to observe and record particle motion using a high-speed camera. Analysis confirms that charged droplets effectively capture charged particles, with increased electric field strength boosting capture efficiency.

In conclusion, this thesis develops a theoretical electrohydrodynamic method to explain particle movement in WES, providing a scientific framework for reducing PM emissions from marine diesel engines. A co-simulation method is obtained to simulate this motion process and verify the theoretical results. Also, an experiment is conducted to verify the results of the theoretical model.

Contents

Abstract	ii
List of Figures	vii
List of Tables	xi
Acknowledgements	xiii
1 Introduction	16
1.1 Background and motivation	16
1.2 Aims and objectives	21
1.3 Organisation of the thesis	23
2 Literature review	25
2.1 Combatting air pollution: policy approaches and emission challenges	25

2.2	Gas emission from marine diesel engine	28
2.2.1	Air pollutants from marine exhaust emissions	28
2.2.2	PM emission status from marine vessels	33
2.2.3	Policies to limit the gas emission from marine diesel engine	38
2.3	Method to reduce PM emission from marine diesel engines	41
2.3.1	Technologies for reducing PM emission from marine diesel engines	41
2.3.2	Comparison of methods on reducing PM emission from marine applications	44
2.4	Research progress on WES technology	47
3	Adopted approach and innovations	50
3.1	Approach adopted in this work	50
3.2	Innovations of this work	51
3.3	The advantages of WES technology	52
4	Mathematical model development	55
4.1	Introduction	55
4.2	Theoretical model assumptions	56
4.3	Particle motion mechanism	58

4.4	Air flow field distribution	61
4.5	Derived Mathematical Model for particle motion in WES	62
4.6	Summary	64
5	Characteristics of particle motion process	66
5.1	Introduction	66
5.2	Effect of electrostatic field strength	67
5.3	Effect of particle size	74
5.4	Effect of droplet size	76
5.5	Effect of particle density	80
5.6	Summary	82
6	Co-simulation of Ansys fluent and MATLAB	84
6.1	Introduction	84
6.2	Co-simulation mechanism	85
6.3	3-D model development	88
6.4	Co-simulation results	90
6.5	Comparison of simulation and theoretical results	95
6.6	Summary	99

7	Experiment on particle capture process	101
7.1	Introduction	101
7.2	Experimental set up	102
7.3	Data processing of particle moving towards the droplet	106
7.4	Particle motion behaviour of different conditions	107
7.5	Experimental results	111
7.6	Summary	116
8	Conclusions and future work	118
8.1	Conclusions	118
8.2	Recommendations for future research	120
	Bibliography	121

List of Figures

1.1	Annual average contribution of shipping to PM2.5 concentrations (in $\mu\text{g}/\text{m}^3$) [27]	19
1.2	Cardiopulmonary mortality attributable to ship PM2.5 emissions worldwide [27]	19
1.3	An overview of WES on particle capturing process.	22
2.1	Annual PM10 emissions from water transportation in EU (2008-2022)(data from OECD).	34
2.2	Proportion of PM10 emissions from water transportation to total emissions in EU transportation sector (2008-2021)(data from OECD).	35
2.3	Annual PM2.5 emissions from water transportation in EU (2008-2022) (data from OECD).	36

2.4	Proportion of PM _{2.5} emissions from water transportation to total emissions in EU transportation sector (2008-2021)(data from OECD).	37
3.1	Mind map of the approach adopted.	51
3.2	An example of WES with counter-current gas flow.	53
4.1	Forces acting on the particle and flow field near the droplet. . . .	57
5.1	Trend of distance change with and without electric force when droplet radius is 1 mm and particle radius is 10 μm	69
5.2	Trend of velocity change with and without electric force when droplet radius is 1 mm and particle radius is 10 μm	70
5.3	Trends of velocity under different electric field strength when droplet radius is 1 mm and particle radius is 10 μm	72
5.4	Magnitude comparison of drag force and electric force when droplet radius is 1 mm and particle radius is 10 μm	73
5.5	Trends of distance change under different particle diameters when droplet radius is 1 mm and electric field strength is 20 kV.	75
5.6	particle velocity changes with time under different particle diameters when droplet radius is 1 mm and the electric field strength is 20 kV.	76

5.7	Distance between particle to the droplet surface changes with time under different droplet diameters when particle radius is 10 μm and electric field strength is 20 kV.	77
5.8	Particle velocity changes with time under different droplet diameters when particle radius is 10 μm and electric field strength is 20 kV.	78
5.9	Drag Force to Electrostatic Force Ratio (F_D/F_E) as a Function of Droplet to Particle Size Ratio (r_c/r_p)	80
5.10	Particle velocity distribution of different particle densities.	81
6.1	Flow chart of the computational procedures for the co-simulation approach.	87
6.2	Coupled motion model of particle and droplet for simulation.	88
6.3	Illustration of the particle overset mesh.	89
6.4	Contour plot of the velocity magnitude when the particle is approaching the droplet when droplet radius is 1mm and particle radius is 10 μm and electric field strength is 20kV.	91
6.5	Comparison of the velocities of particles with different particle radii when droplet radius is 1 mm.	92
6.6	Comparison of the velocities of particles with different droplet radii when particle radius is 10 μm	92

6.7	Instantaneous velocity distribution plots of particle and flow field when droplet radius is 1 mm and electric field strength is 20 kV.	94
6.8	Comparison of simulation and theoretical results under the electric field strength of 20 kV.	96
6.9	Side view of instantaneous velocity magnitude profiles when droplet radius is 1mm and particle radius is 10 μm and electric field strength is 20 kV.	97
7.1	Particles production process	102
7.2	Schematic diagram of the experimental system	103
7.3	An example of particle trajectory processed by the software.	107
7.4	Droplet deformation with the electric field strength increases.	108
7.5	Droplet deform and fall off when the electric field strength is 10 kV.	109
7.6	Velocity distribution before arriving at the droplet surface under different electrostatic field strengths in lab condition.	110
7.7	Comparison of particle velocity distribution before arriving at the droplet between the theoretical result and experimental test data.	112
7.8	Standard deviation for six sets of experimental data	114
7.9	Four photographs taken during an experiment involving particle adhesion on a droplet under varying electric field strengths.	115

List of Tables

2.1	Comparison of methods applied for marine vessel diesel PM emission. [69, 75]	45
5.1	Model properties.	67
6.1	Results of mathematical calculation and simulation of different particle sizes when droplet radius is 1 mm.	98
6.2	Results of mathematical calculation and simulation of different droplet sizes when particle radius is 10 μm	98
7.1	Results of mathematical calculation and simulation of different droplet sizes when particle radius is 10 μm	104
7.2	Results of mathematical calculation and simulation of different droplet sizes when particle radius is 10 μm	105

Acknowledgements

Firstly, I would like to express my deepest gratitude to my supervisor, Prof. Peilin Zhou, for his expert guidance and invaluable mentorship throughout this research. I am also grateful to Prof. Peilin Zhou for giving me the opportunity to pursue a PhD degree in the NAOME department. This thesis was completed with his constant encouragement and supervision.

My sincere thanks go to Prof. Ning Mei from Ocean University of China, who supervised me during my time at the university and supported me with experiments. Many thanks to my second supervisor Dr. Byongug Jeong for his kind encouragement. Thanks to Dr. Haibin Wang, Dr. Zhiming Yuan, and Dr. Han Yuan for their steadfast support over the years.

I would like to express my thankfulness to the researchers and staff of NAOME department for their kind assistance.

I must acknowledge my colleagues for their support and camaraderie in the laboratory, which made my life in Glasgow very meaningful.

My heartfelt thanks to my parents, whose love and unwavering support have sustained me. I also wish to thank my partner, Dr Shuangrui Yu, for providing

relief from the pressures of academic life with his companionship and understanding.

This accomplishment would not have been possible without the collective support of all who were involved.

Chapter 1

Introduction

1.1 Background and motivation

Against the backdrop of contemporary economic globalisation, approximately 90% of global trading shipments utilise maritime routes, of which nearly 70% are concentrated within a distance of 400 kilometres from the coastline [1–5]. As the OECD (Organisation for Economic Co-operation and Development) reports: As demand for global freight increases, maritime trade volumes are set to triple by 2050 [6]. This brings opportunities for economic growth and technological advancements, but also poses challenges in infrastructure capacity, environmental impact, and regulatory oversight. The dominant energy sources currently used in shipping are traditional fossil fuels like Heavy Fuel Oil (HFO) and Marine Gas Oil (MGO), with HFO being the most common due to its cost-effectiveness. Diesel engines are favoured for their efficiency and reliability. However, due to environmental concerns, there is a growing interest in cleaner alternatives like

liquefied natural gas (LNG) and various forms of renewable energy. Despite this shift towards greener options, diesel remains the dominant fuel source in the maritime industry due to its widespread availability and established infrastructure [7,8]. The current state of marine conditions reveals that the emission of marine diesel engines causes serious pollution to both the air and ocean environments. Shipping emissions have a significant impact on air quality far from the source, and some pollutants disperse globally, leading to effects on the climate as well [9–11].

The exhaust gas discharged by marine diesel engines contains various pollutants, including sulphur dioxide (SO_2), nitrogen oxide (NO_x), and particulate matter (PM) [12–18]. In terms of potential to harm human health, PM poses the greatest risk, as it penetrates into sensitive regions of the respiratory system and can lead to health problems and premature mortality [19]. Although ships contribute a relatively small fraction of global particulate emissions compared to other sources, but has significantly affect environmental pollution levels in key regions [20–22]. Most of the ship emissions occur within 400 kilometers of coastlines [5], significantly affecting air quality in coastal regions [23–25]. However, these emissions can disperse and travel hundreds of kilometers inland, influencing air pollution across a much wider region [3, 26]. In his comprehensive study, James J. Corbett [27] assesses the emissions of particulate matter (PM) from shipping and their negative health impacts. Detailed distributions of these shipping-related PM emissions and their global health impacts are illustrated in Fig. 1.1 and 1.2. Fig. 1.1 shows the annual average contribution of shipping to PM_{2.5} concentrations in various regions worldwide. From this map, high concentrations of PM_{2.5} are observed in density trafficked shipping lanes and coastal regions. For example, Europe, the Mediterranean, the eastern United States, and

parts of Asia show significant increases in PM_{2.5} levels due to shipping activities on this map. The areas with the darkest shades coincide with major shipping routes and port cities. Fig. 1.2 shows the cardiopulmonary mortality rates attributable to PM_{2.5} emissions from ships, represented by circles of varying sizes and colours. From this map, higher mortality rates are observed in areas with increased PM_{2.5} concentrations due to shipping, aligning with the observations from Fig. 1.1. Europe, the eastern United States, and parts of Asia, particularly around major ports and densely populated coastal areas, show significant cardiopulmonary mortality. The size and colour of the circles indicate the number of deaths, with darker and larger circles representing higher mortality rates. It can be concluded from these two figures that there is a clear correlation between regions with high PM_{2.5} concentrations due to shipping and areas with elevated cardiopulmonary mortality rates. Besides, The data suggest a significant health impact of shipping-related air pollution, particularly in regions with heavy maritime traffic and dense populations. Studies have estimated that these emissions are responsible for 60,000 cardiopulmonary and lung-cancer deaths every year worldwide, with a majority of fatalities occurring in coastal areas near major ports. More recent estimates indicate that this figure has increased to 87,000 deaths per year globally [27–29].

The particulate emissions from ships can contribute to environmental issues such as acid rain and eutrophication of water bodies. These emissions can also deposit on soil and water, affecting agriculture and aquatic ecosystems. Diesel particles are mainly solid carbon (41%), unburned lubricant (25%), sulphate/water (14%), and other ash and unburned contents, which accounts for less than 20% of the DPM [30–32]. Some components of ship particulate emissions, particularly black carbon (a component of soot), are known to contribute to global warming.

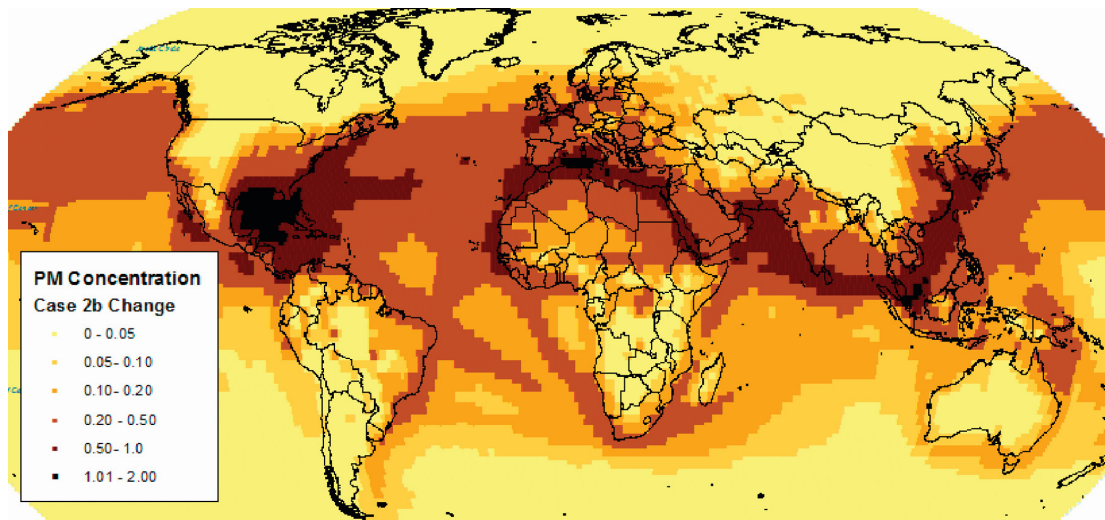


Figure 1.1: Annual average contribution of shipping to PM2.5 concentrations (in µg/m³) [27]

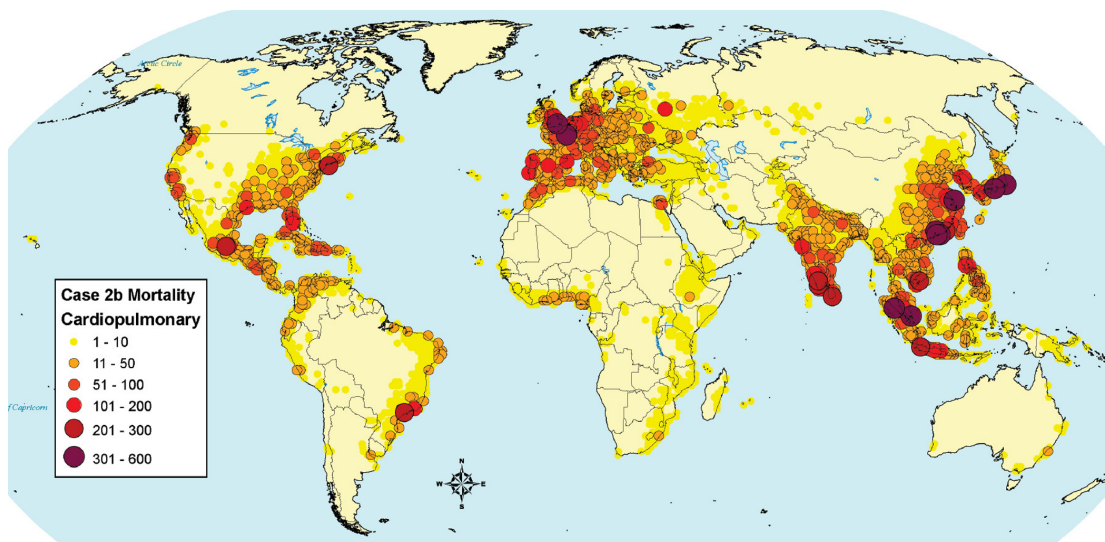


Figure 1.2: Cardiopulmonary mortality attributable to ship PM2.5 emissions worldwide [27]

Black carbon particles absorb sunlight and heat the atmosphere. When deposited on ice and snow, they can accelerate melting by increasing solar absorption. Moreover, particulate matter from ships can contribute to the formation of secondary pollutants like ozone and fine particulate matter, further exacerbating air quality issues. The impact of ship emissions is a growing concern, leading to increased regulation and efforts to develop cleaner maritime outcomes. Reducing particulate emissions from ships is essential for improving air quality, protecting public health, and mitigating environmental damage.

Unlike SO_2 and NO_x , PM emissions are more complex to measure and control due to their varying composition and the technical limitations of current measurement technologies. The difficulty in developing accurate and reliable PM emission measurement methods for marine engines has hindered the establishment of appropriate regulations [10] [33]. Therefore, efficient removal of PM emissions from marine diesel engines remains a major technological challenge. Novel technologies need to be investigated to reduce PM pollution effectively. According to Regulation (EU) 2016/1628 [34], a limit on PN (the number of particles with a diameter over 23 nm) was added into it. The gradual introduction of PN emission control is also one of the trends in ship emission precision control development in the future. The International Maritime Organization (IMO) has set limits on the sulphur content of marine fuels, which indirectly reduce PM emissions. In designated Emission Control Areas (ECAs), stricter limits are enforced. Additionally, IMO 2020 regulations [35] mandate a significant reduction in sulphur oxide emissions, aiming to improve air quality and reduce health risks. Ships can comply with these regulations by using low sulphur fuel oils or installing exhaust gas cleaning systems, such as scrubbers.

As PM emissions from ships are harmful and emission regulations are becoming increasingly strict, conducting relevant research on controlling PM emissions from marine diesel engines has become imperative with significant theoretical and practical importance. Controlling PM emissions from ships is vital for environmental sustainability, public health, regulatory compliance, and the industry's social license to operate.

1.2 Aims and objectives

The primary aim of the present work is to reveal the fundamental mechanisms and characterise the phenomena of electrostatic field interactions within WES, seeking to essentially enhance the efficiency of PM abatement from marine diesel engine emissions. An overview of the particle capturing process is shown in Fig. 1.3.

The specific research objectives are listed as follows:

1. To develop a novel theoretical model that integrates electrostatic and hydrodynamic forces, predicting particle trajectories with high-level accuracy in a WES environment.
2. To design and implement a series of experimental and simulation studies about particle motion, aiming to uncover new relationships between particle characteristics and the combined effects of flow and electric fields.
3. To discover and characterise the mechanisms through which modifications in field strength and droplet dynamics affect PM capture rates, assessing

WES's effectiveness in addressing the particle matter abatement in marine diesel engines.

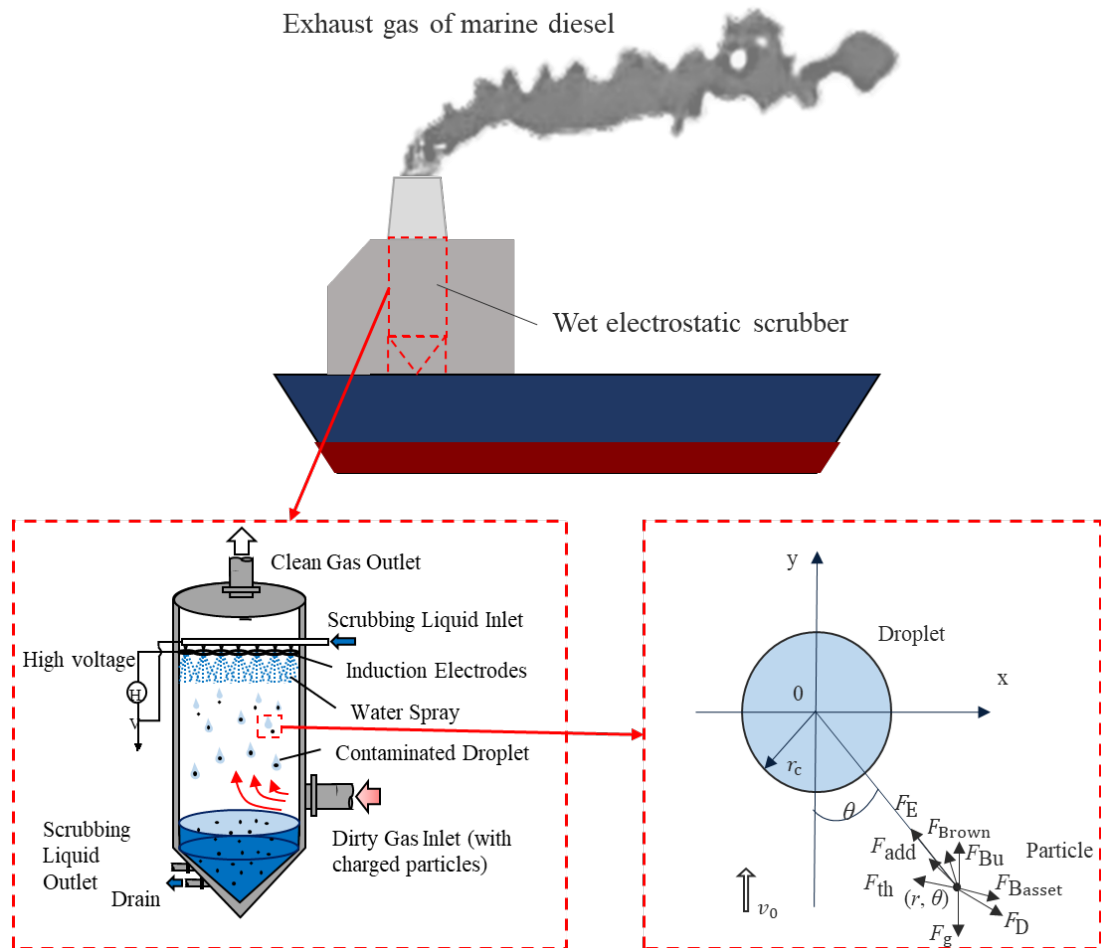


Figure 1.3: An overview of WES on particle capturing process.

1.3 Organisation of the thesis

This thesis is organised to the following chapters and a brief outline of the content of each chapter is given below:

- Chapter 1 Introduction

Give a brief introduction to the background of removal of PM emission from marine diesel engines. Emphasis on the effective method of using WES for PM abatement. Also, a summary of the research objectives of this work is given in this chapter.

- Chapter 2 Literature review

Present a detailed and comprehensive literature review on particle emission situation, relative regulations, and abatement methods on marine diesel engines. A review of the research progress on WES is proposed in this chapter. For the application of WES technology, some frontier researches are introduced in this chapter.

- Chapter 3 Adopted approach and innovations

Present the methodology used in this research work and the innovation of this work. Besides, the working process and advantages of WES are introduced in the part.

- Chapter 4 Mathematical model development

Establish and develop the theoretical model to describe the particle movement characteristic when moving to approach the droplet in a gas flow field under an electrostatic field. Present the solving process of the mathematical model.

- Chapter 5 Characteristics of particle motion process
Give the results of the theoretical model and analyse the effect of several features on the particle motion process, such as electric field strength, particle size, droplet size, and particle density.
- Chapter 6 Co-simulation of Ansys fluent and MATLAB
Illustrate a co-simulating method of Ansys Fluent and MATLAB to simulate the particle motion process when associating the electrostatic field with a gas flow field. Give the computational procedures, model development, and simulation results of distinctive features.
- Chapter 7 Experiment on particle capture process
Introduce the designation and combination of an experimental platform. Describe the experiment process and recorded data. Give the experimental results processing and analysis.
- Chapter 8 Conclusions and future work
Conclude the work of this thesis and outline future work plans.

Chapter 2

Literature review

2.1 Combatting air pollution: policy approaches and emission challenges

The air pollution is the foremost global threat to the public health and is a significant contributor to the environmental decline. Those atmospheric pollutants are generated from energy transformation, energy consumption, and industrial processes. The most common air pollutants include particulate matter (PM_{2.5} and PM₁₀), nitrogen dioxide (NO₂), sulphur dioxide (SO₂), carbon monoxide (CO), ground-level ozone (O₃), and volatile organic compounds (VOCs) [36, 37]. Particulate matter (PM_{2.5} and PM₁₀) is generated from combustion processes, industrial activities, and transportation emissions. PM_{2.5}, in particular, poses severe health risks as it can penetrate deep into the lungs and enter the bloodstream. Nitrogen dioxide (NO₂) is primarily produced from traffic and energy production. It contributes to respiratory problems and the formation of ground-

level ozone. Sulphur dioxide (SO_2) is emitted from burning fossil fuels at power plants and industrial facilities. SO_2 can lead to acid rain, which harms ecosystems and buildings. Unlike other pollutants, ground-level ozone is not emitted directly but forms when NO_2 and VOCs react in sunlight. It is a key component of smog and can cause various respiratory issues. Moreover, greenhouse gases like carbon dioxide contribute to global warming and climate change, altering weather patterns and disrupting ecosystems worldwide. Air pollution is a leading cause of premature death globally, with millions of deaths attributed to conditions such as heart disease, stroke, lung cancer, and chronic respiratory diseases. The World Health Organisation (WHO) estimates that air pollution is responsible for over 7 million deaths annually. Moreover, air pollution has significant environmental impacts, including reduced agricultural yields, acidification of water bodies, and damage of forests [36]. Overall, atmospheric pollutants have far-reaching and detrimental effects on the environment, affecting both natural systems and human societies.

To reduce these emissions, action is taken on three aspects, transport, energy and agricultural sectors. Such as using cleaner fuels instead of dirty ones, developing cleaner industries, reducing consumption of polluting products and adopting cleaner technologies. Besides, some countries and organizations tailor policies to specific local circumstances.

The 1979 Convention on Long-Range Transboundary Air Pollution (LRTAP) is the first multilateral agreement addressing transboundary air pollution and sets emission reduction targets for various air pollutants, including sulphur dioxide (SO_2), nitrogen oxides (NO_x), ammonia (NH_3), volatile organic compounds (VOCs), fine particulate matter (PM_{2.5}), and black carbon [38]. With the in-

creasing attention to air pollution and the advancement of scientific and technological levels, more rigorous and specific policies and regulations have been proposed.

India National Clean Air Programme (NCAP), which launched in 2019, aims to reduce particulate matter (PM₁₀ and PM_{2.5}) concentrations by 20-30% by 2024 compared to 2017 levels in 122 Indian cities. It focuses on city-specific action plans, technology interventions, and source-based initiatives to combat air pollution.

China publishes action plan to reduce air pollution in 2023. The plan contains a series of measures to achieve bluer skies by 2025. Its goals are to reduce PM_{2.5} density at the level and above by 10 percent by 2025 and to cut emissions of nitrogen oxides (NO_x) and volatile organic compounds (VOCs) by over 10 percent.

In October 2022, a revision of the Ambient Air Quality Directives is proposed. This revision aligns the air quality standards more closely with the recommendations of the World Health Organisation (WHO). For example, the annual limit value for fine particulate matter (PM_{2.5}) will be reduced by more than half (European Commission, 2022) [39].

South Korea introduced a National Action Plan on Air Pollution in 2019 to address fine particle matter (PM_{2.5}) pollution. The plan includes measures to reduce emissions from vehicles, industries, and power plants, as well as promoting clean energy and enhancing monitoring and enforcement efforts.

Also, there are many other countries and regions that have implemented policies and regulations to address air pollution and improve public health. As reported in the publication of Air pollution in Europe: 2023 reporting status under

the National Emission Reduction Commitments Directive, to fulfill their 2030 commitments the greatest challenge will be reduced NH_3 , NO_x and $\text{PM}_{2.5}$ emissions (European Environment Agency, 2023) [40]. While there is progress in some regions, global air pollution remains a significant challenge, especially in rapidly developing countries. The future will likely depend on stronger international cooperation, improved regulatory frameworks, and widespread adoption of cleaner technologies. Addressing air pollution is not only a health imperative but also essential for tackling broader environmental issues, including climate change.

2.2 Gas emission from marine diesel engine

2.2.1 Air pollutants from marine exhaust emissions

Marine diesel engines are a significant source of various air pollutants, including sulphur oxides (SO_x), nitrogen oxides (NO_x), particle matter (PM), carbon monoxide (CO), volatile organic compounds (VOCs), and greenhouse gases (GHGs) like carbon dioxide (CO_2) and methane (CH_4) [41–43]. These emissions can have adverse effects on both human health and the environment, especially in the regions of coastal areas and along shipping routes [44].

Sulphur oxides are generated from the sulphur content in marine fuels. The combustion process converts sulphur into SO_2 , which can further oxidize into SO_3 and contribute to the formation of acid rain. Studies such as those by Corbett and Wang [45] highlight that shipping contributes approximately 13% of global SO_x emissions, with significant implications for both human health and ecosystems.

NO_x emissions from marine vessels result from high-temperature combustion in ship engines. These pollutants contribute to the formation of ground-level ozone and photochemical smog, which are harmful to human health and vegetation. Research by Endresen et al. [2] indicates that NO_x from ships accounts for about 18-30% of global NO_x emissions, making it a major contributor to air pollution.

Particulate matter from marine vessels includes both primary particles (directly emitted) and secondary particles (formed in the atmosphere from SO_x and NO_x). PM is associated with adverse health effects, including respiratory and cardiovascular diseases. According to Eyring et al. [3], ships are responsible for a significant fraction of the fine particulate matter (PM_{2.5}) observed in coastal and port cities.

CO_2 is the primary greenhouse gas emitted by marine vessels. The International Maritime Organization (IMO) estimates that shipping contributes about 2-3% of global CO_2 emissions, a significant figure given the role of CO_2 in climate change. Studies like those by Buhaug et al. [46] emphasize the importance of addressing CO_2 emissions from shipping to meet global climate targets.

VOCs are released during fuel combustion and from cargo handling, particularly from oil tankers. These compounds contribute to the formation of ground-level ozone and secondary organic aerosols, both of which have significant environmental and health impacts [47].

The climate impact of CO_2 emissions from shipping is substantial, contributing to global warming and associated climate change effects such as rising sea levels and extreme weather events. Additionally, VOCs and NO_x emissions lead

to the formation of ground-level ozone, a pollutant with significant health impacts, including exacerbation of asthma and other respiratory conditions [4].

The pollutants emitted by marine vessels have far-reaching environmental and health consequences. Sulphur oxides and nitrogen oxides contribute to the acidification of oceans and terrestrial ecosystems, leading to biodiversity loss and the degradation of aquatic habitats [24]. Particulate matter, particularly PM_{2.5}, poses serious health risks, including respiratory and cardiovascular diseases, and has been linked to premature mortality in populations exposed to high concentrations, especially in port cities [27]. It is found that 94 200 (95% confidence interval: 84,800–103,000) premature deaths were associated with PM_{2.5} exposure due to maritime shipping in 2015 [48].

Historically, marine vessels have relied heavily on heavy fuel oil (HFO), a byproduct of crude oil refining with high sulphur content. The combustion of HFO in ship engines has been the primary source of SO_x emissions from the maritime sector. Data from the late 20th and early 21st centuries show that marine vessels were responsible for a significant percentage of global SO_x emissions, with estimates ranging from 10% to 15% of the total anthropogenic SO_x emissions [4]. Similarly, NO_x emissions from ships, resulting from high-temperature combustion processes, accounted for 18-30% of global NO_x emissions during this period [2].

In the early 2000s, the global fleet continued to grow, leading to an increase in overall emissions. For instance, Corbett et al. [27] reported that the global shipping fleet's CO₂ emissions were approximately 1,000 million tonnes per year, contributing around 2-3% of global CO₂ emissions. This period also saw a rise in particulate matter emissions, particularly PM_{2.5}, which posed significant health risks, especially in densely populated coastal areas.

The introduction of regulatory measures by the IMO has played a pivotal role in altering the emission conditions of marine vessels. The IMO's MARPOL Annex VI, adopted in 1997 and implemented in 2005, established the first international limits on SO_x and NO_x emissions from ships. Over the years, these regulations have been progressively tightened, with key milestones including the ECAs and the global sulphur cap.

One of the most significant regulatory changes was the implementation of the global sulphur cap on January 1, 2020, which reduced the permissible sulphur content in marine fuels from 3.5% to 0.5%. Data trends before and after this implementation reveal a substantial reduction in SO_x emissions. For instance, Johansson et al. [21] projected that the global sulphur cap would reduce SO_x emissions from shipping by 77% compared to pre-2020 levels. Indeed, preliminary studies conducted post-2020 indicate that SO_x emissions decreased by up to 70% compared to 2019 levels [49]. This substantial reduction reflects the direct impact of the sulphur cap on emission levels globally. In ECAs such as the Baltic Sea and North Sea, SO_x emissions decreased by over 80% between 2000 and 2020 [50].

NO_x emissions have also been significantly affected by regulatory measures, particularly through the establishment of Tier I, II, and III standards under MARPOL Annex VI. These regulations, especially the Tier III standards applied in ECAs to ships built after 2016, have led to notable changes in NO_x emissions data. Recent data indicate that NO_x emissions have stabilised or slightly decreased in regions with strict ECA regulations. For example, in the North Sea and Baltic Sea, where Tier III standards are enforced, NO_x emissions have shown significant reductions [50].

The trend in CO₂ emissions from shipping has been less responsive to reg-

ulatory measures, as CO₂ emissions are directly linked to fuel consumption, which has continued to increase with global trade growth. The Third IMO GHG Study [51] highlighted that CO₂ emissions from shipping continued to rise until around 2010. However, after 2010, CO₂ emissions began to stabilise, partly due to the gradual shift towards more energy-efficient ship designs and operational practices aimed at reducing fuel consumption. The introduction of the Energy Efficiency Design Index (EEDI) by the IMO, which mandates incremental improvements in the energy efficiency of new ships, is expected to contribute to further reductions in CO₂ emissions in the future [52].

Reducing the pollutants from marine gas emissions remains a long-term target, which is addressed in most countries in the world. According to reported data by Olaf MERK [53], in 2011, the shipping emissions were substantial and accounted for around 900 million tonnes of CO₂ emissions, 2 million tonnes of NO_x emissions, 10 million tonnes of SO_x emissions and 1.5 million tonnes of PM10 emissions. In 2015, maritime shipping was responsible for an estimated 866 million tonnes of CO₂ emissions, constituting 2.7% of the world's energy-related CO₂ emissions. In 2018, the amount of the CO₂ emissions grew to 1,056 million tonnes. Additionally, maritime shipping contributed 10.0 million tonnes of sulphur oxides (SO_x) emissions and 18.0 million tonnes of nitrogen oxide (NO_x) emissions. The share of shipping emissions in global anthropogenic emissions has increased from 2.76% in 2012 to 2.89% in 2018 [48].

2.2.2 PM emission status from marine vessels

PM emissions from marine vessels have exhibited a complex and nuanced trend over recent years. PM emissions primarily consist of primary particles emitted directly from ship exhausts and secondary particles formed from gaseous precursors such as SO_2 and NO_x . The reduction in SO_x emissions due to the switch to low-sulphur fuels, following the global sulphur cap regulation enforced by the IMO in 2020, has led to a significant decrease in the formation of secondary sulphate particles. As a result, regions with strict emission control regulations, such as ECAs in the Baltic Sea and North Sea, have observed substantial reductions in secondary PM levels, contributing to improved air quality and health outcomes.

However, the impact of low-sulphur fuels on primary PM emissions is more complex. Some studies, such as those by Lack et al. [54], have indicated that while low-sulphur fuels reduce secondary sulphate formation, they may also lead to an increase in the emission of primary particles. These primary particles include elemental carbon (black carbon) and organic carbon, which can vary significantly depending on the engine type, operating conditions, and fuel composition. In particular, the combustion of certain types of low-sulphur fuels, such as very low sulphur fuel oil (VLSFO) and marine gas oil (MGO), can produce higher levels of black carbon, a potent climate forcer and harmful air pollutant.

It is important to note that while regulations have been effective in reducing PM emissions in specific regions, there remains a concern regarding the global status of PM emissions. Areas outside ECAs, where less stringent regulations apply, continue to experience higher levels of PM emissions. Additionally, the variability in PM composition and the emerging evidence on the potential increase

in black carbon emissions necessitate further research and monitoring to better understand and mitigate the overall impact of shipping on air quality and climate change.

According to the dataset about the emissions to the atmosphere released as a result of production and consumption processes published by the Organisation for Economic Co-operation and Development (OECD), the emission amount of pollutants in specific areas could be concluded. Figure 2.1 indicates the contribution of water travel, which includes maritime and inland waterway transportation, to PM10 emissions across the European Union over a time period from 2008 to 2021. The over trend of this graph has decreased in nearly the decade years, followed

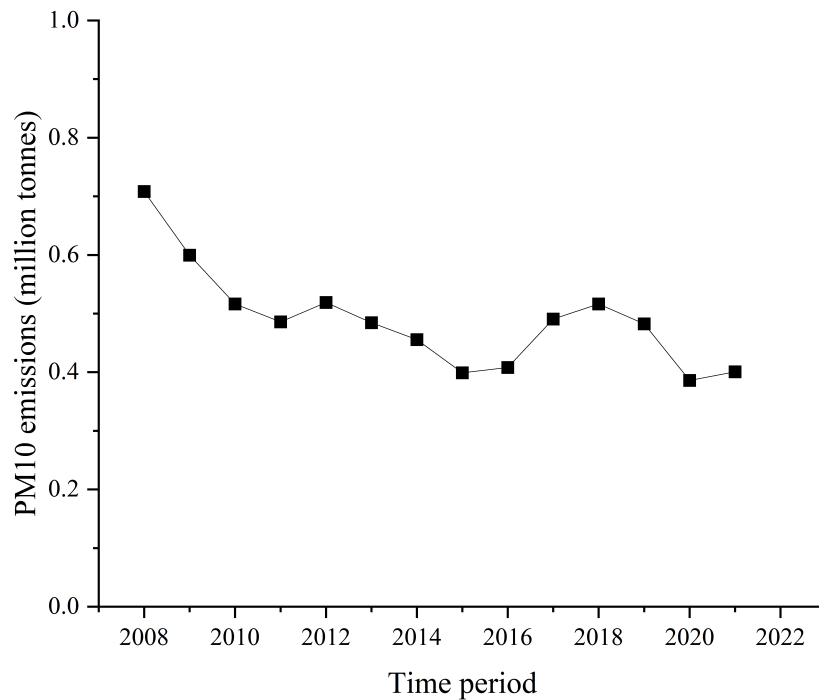


Figure 2.1: Annual PM10 emissions from water transportation in EU (2008-2022)(data from OECD).

by fluctuations but with a generally stable trend. The decrease from 2008 to 2011 could reflect the impact of the global financial crisis on trade and shipping ac-

tivities, resulting in reduced emissions. The slight decrease in shipping emissions around 2020 could be a combined effect of ongoing environmental policy efforts and the impact of the COVID-19 pandemic, which led to reduced economic activity, travel, and industrial output due to lockdowns and other restrictions. In summary, the graph shows that PM10 emissions from water travel in the EU have decreased since 2008, with some subsequent fluctuations. This trend could be influenced by economic factors, pandemic-related reductions in shipping activities, and the gradual implementation of stricter environmental regulations.

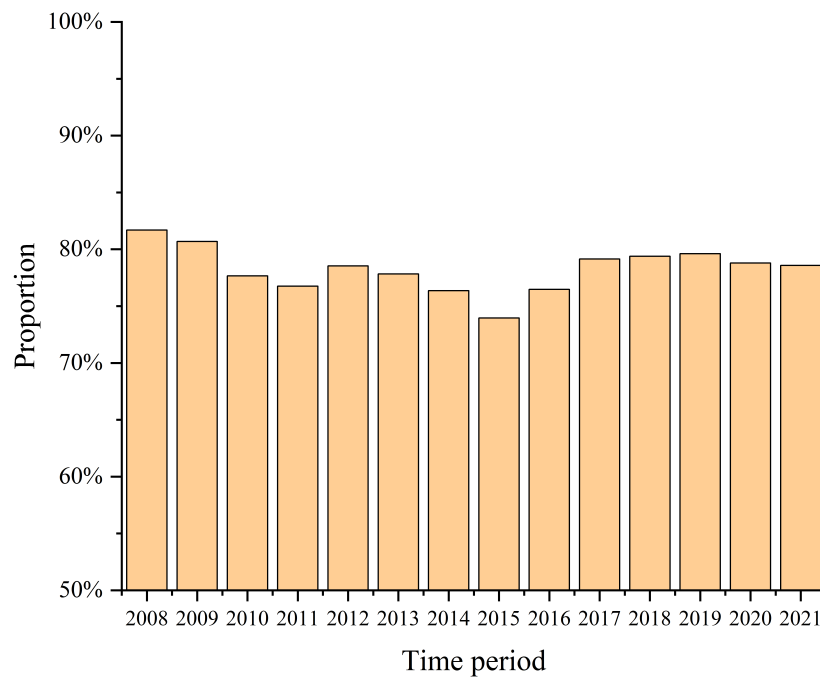


Figure 2.2: Proportion of PM10 emissions from water transportation to total emissions in EU transportation sector (2008-2021)(data from OECD).

Figure 2.2 shows the proportion of PM10 emissions from water transport relative to the total emissions from transportation over the time period from 2008 to 2021. The proportion seems quite stable, staying mostly between 70% to 80% throughout these years. The proportion suggests that shipping is a consistently significant contributor to PM emissions within the transportation sector in the

EU. The fact that the proportion never falls below 70% suggests that shipping is one of the largest sources of PM emissions in the transportation sector.

Figure 2.3 shows the trends in PM_{2.5} emissions from water transport in the EU from 2008 to 2021. Like the emission of PM₁₀, PM_{2.5} emissions also display a general downward trend over the years. It is notable that PM_{2.5} emissions are consistently lower than PM₁₀ emissions throughout the period. This may suggest that larger particulate matter (PM₁₀) is easier to reduce through filtration and other control technologies. Figure 2.4 depicts the proportion of PM_{2.5} emissions

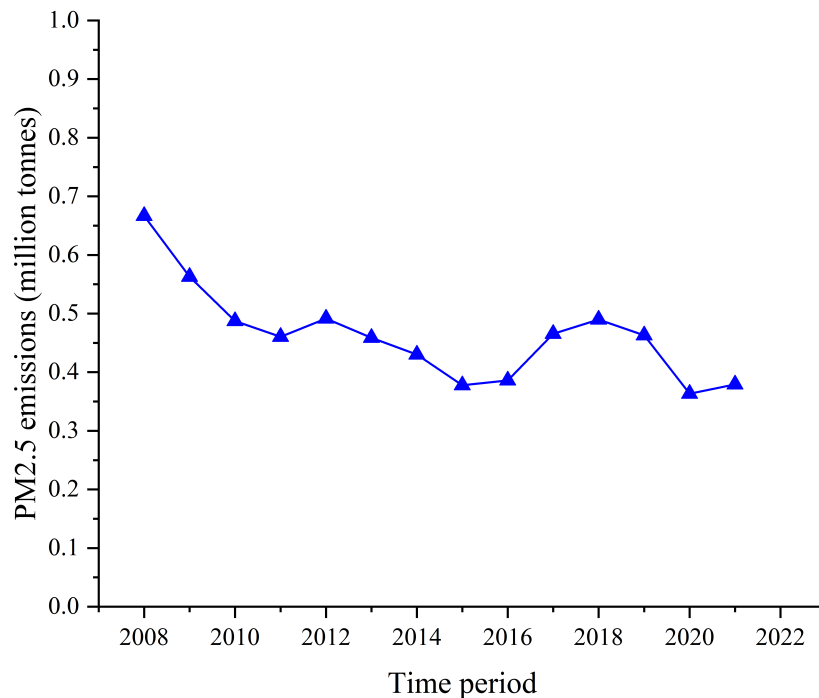


Figure 2.3: Annual PM_{2.5} emissions from water transportation in EU (2008-2022) (data from OECD).

from water transportation relative to the total emissions in the EU transportation sector from 2008 to 2021. The proportion of PM_{2.5} emissions from water transport is relatively stable, remaining within the 80-90% range throughout the entire time period. This stability suggests that, while absolute emissions of PM_{2.5} from

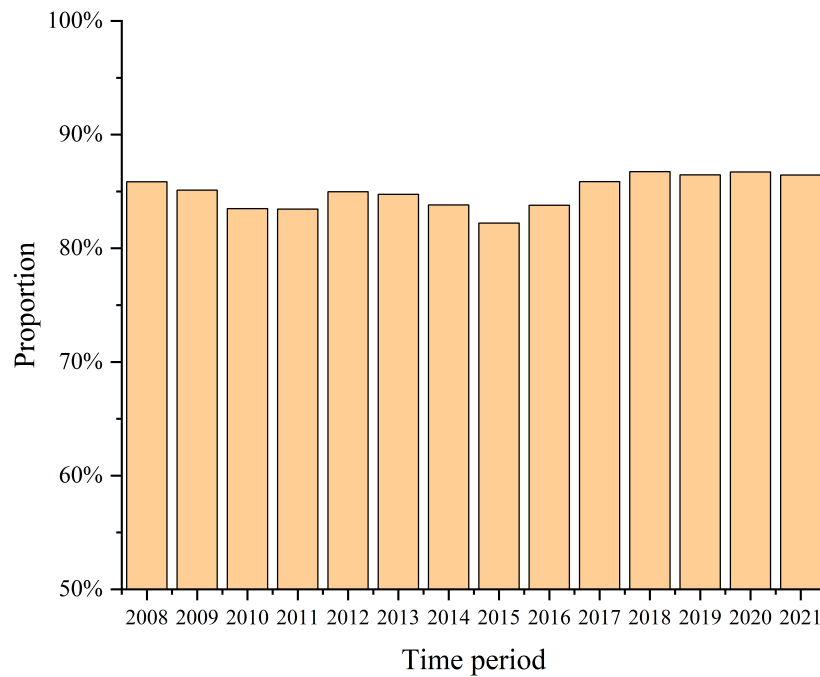


Figure 2.4: Proportion of PM_{2.5} emissions from water transportation to total emissions in EU transportation sector (2008-2021)(data from OECD).

water transport might have decreased (as seen in Fig. 2.3), the relative contribution of water transport to the total PM_{2.5} emissions within the transportation sector has not changed dramatically. The consistently high proportion could also reflect that water transport is a significant source of PM_{2.5} within the transportation sector. When comparing Fig. 2.2 and Fig. 2.4, it can be concluded that both PM_{2.5} and PM₁₀ proportions show remarkable stability over the years, indicating that water transport consistently contributes a substantial part of the total PM emissions within the transportation sector. The proportions for PM_{2.5} are slightly higher than those for PM₁₀ in most years. This could suggest that water transport is a relatively more significant source of finer particulate emissions (PM_{2.5}) than coarser particulate emissions (PM₁₀) within the transportation sector. In summary, despite absolute reductions in emissions, water transport remains a consistently dominant source of particulate matter emissions.

As of 2024, the shipping industry faces several challenges and changes concerning emissions and energy consumption. Global maritime container shipping emissions, particularly during cruising mode, form a significant part of the industry's total emissions. These emissions have shown notable changes in recent years, influenced by factors like geopolitical issues and international trade patterns. An increase in emissions per nautical mile during ocean cruising has been observed, attributed to shifts in trade structures and the efficiency of ships. Additionally, port operations have experienced fluctuations in hourly emissions, influenced by operational inefficiencies and the impact of the pandemic on shipping activities [7]. The international shipping industry is exploring alternative fuels like biofuels, methanol, hydrogen, and ammonia to reduce dependency on oil-based fuels. However, the adoption of these fuels faces challenges such as the need for technological development, infrastructure upgrades, and addressing safety hazards [55, 56]. In summary, the shipping industry is in a state of transition, grappling with the need to reduce emissions while facing external pressures from geopolitical developments and the need for technological innovation and infrastructure development.

2.2.3 Policies to limit the gas emission from marine diesel engine

To reduce the environmental footprint of shipping, protect public health, preserve marine ecosystems and contribute to the global effort against climate change, regulations for shipping emissions are essential. The regulations vary across different areas, because of the emissions control areas (ECAs), such as the Baltic Sea and North American areas are designated ECAs with more stringent

limits on SO_x , NO_x , and particulate matter. Besides, the regional environmental properties, technological feasibility and economic considerations may also cause variations in regulations. International agreements like MARPOL Annex VI set global standards, but individual countries or regions can impose stricter controls based on local legislation and environmental policies.

The International Maritime Organisation (IMO) has set specific emission standards for marine applications under MARPOL Annex VI. These standards aim to control air pollution from ships and include regulations for various pollutants. The first IMO emission regulation is initially targeted NO_x and SO_x . Then IMO Tier II and Tier III further reduced NO_x and SO_x emissions. The most significant regulation impacting PM emissions is in MARPOL Annex VI implemented on January 1, 2020. The global sulphur cap limits the sulphur content in fuel oil used on board ships operating outside designated ECAs to 0.50% m/m outside designated Emission Control Areas (ECAs). In ECAs, the sulphur content limit is even lower, at 0.10% m/m. While there are no specific numeric limits for PM emissions in the IMO regulations, the reduction in sulphur content in marine fuels indirectly leads to a decrease in PM emissions. Although current regulations focus on sulphur content in fuels as a means to control PM emissions, future regulations may address particulate matter more directly as technology and measurement techniques evolve.

China implemented the Emission Standards for Marine Engines in 2016. These standards became effective in 2018 (China I) and 2021 (China II). The standards set limits for pollutants such as carbon monoxides (CO), hydrocarbons plus nitrogen oxides (HC and NO_x), methane (CH_4 , applicable to natural gas engines), and particulate matter (PM). Marine engines complying with Stage 2 emission

regulations exhibit significant improvements in reducing emissions compared to Stage I. Specifically, there is a 19% reduction in hydrocarbons and nitrous oxides (HC and NO_x), limiting these emissions to 5.8 g/kWh. Methane (CH₄) emissions are reduced by 33%, with a new limit set at 1 g/kWh. Moreover, particulate matter (PM) emissions see a 40% reduction, leading to a new emission ceiling of 0.12 g/kWh.

The United States Environmental Protection Agency (EPA) has specific regulations for emissions from marine applications, primarily targeting marine diesel engines. The latest EPA Tier 4 standards, which are implemented in 2014, are applicable to new engines above 600 kW. These standards are the most stringent and require significant reductions in NO_x and PM emissions. Tier 4 regulations have introduced a further reduction in emissions of particulate matter, nitrous oxides and hydrocarbons compared to Tier 3 regulations. Engine manufacturers commonly use a separate exhaust aftertreatment technology to accomplish these emission reductions, such as selective catalytic reduction (SCR) and diesel particulate filters (DPF).

The EU regulations apply to diesel engines used in selected marine applications, particularly focusing on vessels operating in inland waterways. The EU regulations aim to reduce the emission of carbon monoxide (CO), hydrocarbons (HC), nitrous oxides (NO_x), and particulate matter (PM) from these engines. The latest one of these regulations is Stage V. Compared with Stage III A, the emission of nitrous oxides and hydrocarbons has a 70% reduction. And the reduction in the emission of particulate matter is 93%. Besides, the introduction of particulate number (PN) can further limit the emission of PM.

In addition to the mentioned emission regulations for marine applications,

vessels are also subject to specific national emission standards when operating within certain regions. The overarching goal of these diverse emission regulations is to minimise environmental pollution and protect public health. To meet these objectives, the shipping industry is increasingly adopting innovative strategies across various domains, including fuel composition, combustion methods, and emission aftertreatment technologies. Such advancements are essential for compliance with increasingly stringent regulations, as they collectively contribute to reducing harmful emissions and mitigating the environmental impact of maritime operations.

In conclusion, while regulatory measures have led to significant reductions in PM emissions in controlled regions, the status of PM emissions globally requires ongoing attention. Future policies may need to address not only sulphur content but also other components of PM, such as black carbon, to achieve comprehensive improvements in air quality and public health outcomes associated with marine vessel emissions.

2.3 Method to reduce PM emission from marine diesel engines

2.3.1 Technologies for reducing PM emission from marine diesel engines

PM emissions from marine diesel engines are a significant environmental concern, accounting for a substantial share of emissions in the transportation sector.

These emissions contribute to air pollution and have multiple environmental and health effects [57–59]. Black carbon, a major component of PM, absorbs sunlight and heats the atmosphere, accelerating the melting of snow and ice in polar regions and contributing to sea-level rise [60]. PM emissions are also recognized as the second most significant human-made contributor to global warming, after carbon dioxide (CO₂). Strategies to achieve this include adopting cleaner fuels, enhancing engine efficiency, and implementing emissions treatment technologies.

One of the primary methods to reduce the PM emissions from shipping is switching to cleaner fuels. Low-sulphur fuels and alternative fuels like Liquefied Natural Gas (LNG) and biofuels produce fewer PM emissions. Even as the maritime industry moves towards more sustainable options, diesel continues to be the primary fuel choice, mainly due to its abundant availability and the well-established support infrastructure [7, 8]. Besides, the global supply chain for diesel is robust and well-established. Transitioning to alternative fuels requires significant changes in the supply chain, which takes time to develop. Even with a strong push towards greener alternatives, the transition away from diesel is a gradual process. Current ships have long operational lifespans, and the switch to alternative fuels will occur over several years or decades [61].

The method of using Diesel Particle Filter (DPF) to reduce PM emissions has been widely used for decades connected with high-speed diesel engines, such as small engines in vehicles, inland ships and luxury yachts. The core of the DPF is typically made from a ceramic material with a honeycomb structure. As exhaust gases pass through this structure, the soot particles are physically captured on the walls of the honeycomb cells. Over time, these trapped particles accumulate and are eliminated in regular intervals through a process called regeneration. Re-

generation involves burning off the trapped soot, usually at high temperatures, to prevent the filter from becoming clogged. This process can be initiated either passively, by the heat in the exhaust system, or actively, by additional heating elements or catalysts within the filter [62, 63]. But for large marine diesel engines, the volume of filter tends to be rather oversized. This may cause high requirements for production and technical methods [64]. Besides, DPFs require regular maintenance to function effectively. The accumulation of soot can lead to clogging. Sometimes, the added back pressure from a DPF can impact engine performance and efficiency.

Wet scrubbers equipped with marine engines are effective for sulphur dioxide abatement. The scrubber also can reduce the emissions of PM [33, 65]. It works by spraying water or a water-based solution into the exhaust stream. As the exhaust gases pass through this mist, particles are captured by the water droplets due to collision. The resulting mixture of water and particulate matter is then removed from the exhaust stream. Fridell and Salo [66] studied the particle emissions from a marine engine equipped with an open-loop wet scrubber using seawater. They found that there's a 92% reduction in total particle number and a 75% decrease in particulate mass suggesting the scrubber is effective, particularly against soluble and large particles. However, the less significant reduction (48%) in smaller, solid particles like black carbon (BC) indicates a limitation in the scrubber's effectiveness for these types of particles [67]. The efficiency in reducing PM can be influenced by several conditions, such the type of PM, scrubbing liquid properties, flow rate of exhaust gas, and design and operation of scrubber [68, 69].

Electrostatic precipitators (ESP) work by charging the particles in the exhaust stream electrically and then using an electric field to attract and collect

them onto plates or other collection devices [70, 71]. While effective in capturing fine particles, ESPs in marine applications face challenges such as handling the high volume and variable nature of ship exhausts, coping with space constraints on vessels, and dealing with the corrosive marine environment, which can affect the durability and maintenance requirements of the system. Thus, though electrostatic precipitation is a widely used method for particle removal, it is not currently used in combination with marine engines.

There are studies about the method consisting of a scrubber and a Wet Electrostatic Precipitator (WESP) in series to reduce the PM emissions for marine applications [72–74]. Their studies showed that the combination of a scrubber and a WESP is a potential aftertreatment system for large marine engines running with HFO, leading to significantly lower emissions than the use of scrubbers only. However, considering the space and energy constraints, this method is not an ideal approach since it requires a large installation space and regular cleaning and maintenance.

2.3.2 Comparison of methods on reducing PM emission from marine applications

According to Sobczyk et al. [69], electrohydrodynamic methods, notably the water electrified spray technique, are effective for particulate matter (PM) removal from marine diesel engines, achieving high efficiency even with very small particles. This method is utilised in vessel wet electrostatic scrubbers (WES), which show promise in reducing emissions. An experimental work made by Di Natale et al. [76] demonstrated that this technology is more effective in removing

Table 2.1: Comparison of methods applied for marine vessel diesel PM emission. [69, 75]

Method applied in marine vessels	Reduction of PM emission	Limitation
Fuel borne additive	35%	Lowest reduction efficiency among those methods
Venturi scrubber	Over 90%	High pressure drops
Diesel particle filter (DPF)	<70% for submicron particle	Regular maintenance to avoid clogging; Increased back pressure on engine
Wet scrubber	85%-95%	Affected by many factors in scrubber
Electrostatic precipitator	70-99% for >pm1.0	Re-entrainment of particles after a certain time operation
Electrified water spray	About 50% for <pm1.0	Operational characteristics are not yet fully understood
	80%-93%	
	Capture efficiency over 95% (<pm0.4)	

SO₂ and PM than conventional wet scrubbers, highlighting its potential in marine applications. Table 2.1 compares different methods applied to reduce particulate matter (PM) emissions from marine vessel diesel engines.

Among these methods, the electrified water spray shows the highest reduction

efficiency for very small particles. The Venturi scrubber is highly effective but has the downside of creating high-pressure drops. The wet scrubber is quite effective, especially for larger particles, but its performance can be inconsistent due to variable factors. The electrostatic precipitator offers a good balance between efficiency and operational consistency but can suffer from particle re-entrainment over time. Finally, the fuel-borne additive provides the least reduction in PM emissions, making it the least desirable option based on this data alone. Confronted with the detrimental effects of particulate matter emissions on environmental and human health, alongside the tightening emission standards for marine applications, the future maritime industry necessitates the development of more effective and practical particulate matter removal techniques.

When considering the use of WES for controlling PM emissions from marine vessels, several specific research gaps need to be addressed. These gaps relate to the unique conditions of marine environments, the nature of marine PM emissions, and the technical and operational challenges associated with deploying WES systems on ships. There is a research gap in understanding the effectiveness of WES systems in capturing fine particles and nanoparticles emitted from marine engines. These smaller particles are more challenging to capture due to their low mass and high mobility. Research could focus on optimizing the electrostatic field strength, droplet size, and water flow rate to enhance the capture of these fine particles. Thus, this research work is focused on the characteristics and optimization of WES for marine PM capture.

2.4 Research progress on WES technology

Recent research into the performance of WES has been conducted. Studies show that WES can be significantly effective under droplet and particle charging conditions. Numerical and experimental techniques are both employed to investigate the elimination of particles in wet electrostatic scrubbers [77–81]. Jaworek et al. [82, 83] did detailed theoretical and simulated work about both charged particle-droplet. In their theoretical work, they described the coordinate motion of the droplet-particle system by Newton’s vector differential equations, in which aerodynamic drag and image-charge effects were considered. Then Krupa et al. [84] proposed a theoretical basis for the electro-hydrodynamics of submicron particles, which can describe the droplet-particle intersection movement in a wet electrical scrubber, but without derivation and analysis. Through a wet electrostatic scrubber experiment tests the results of high sulphur heavy fuel oil and marine gas oil, in his research, they analysed PM removal efficiency of charged or not and different engine loads. The results showed that PM is efficiently removed from diesel engine exhaust by using a wet electrostatic scrubber system. An experiment study was made by Lipeng Su et al. [85], which is about wet electrostatic scrubbing on capturing submicron particles like fly ash and black carbon from small-scale industrial boilers. Droplet charging was found to be effective on capturing the pollutants, suggesting a promising avenue for enhancing traditional wet scrubber performance. The research indicated that this method could be especially beneficial for improving air quality by targeting pollutants that are challenging to capture.

D’addio et al. [86] conducted an experimental study under the background of marine diesel engine emission control. They highlighted the advantages of a

wet electrostatic scrubber compared to other PM removal methods. their results showed that particle abatement efficiency increases dramatically when spray and particles are both charged with opposite polarities. if either the spray or the particles are not charged, the abatement efficiency does not change significantly. Tests were carried out in various conditions, which are wet scrubber, charged droplet and opposite polarities charged droplet and particles respectively [10]. Besides, Hirotsugu Fujita and his team [78] investigated the diesel particulate matter (DPM) emission control of marine diesel engines and conducted experiments on electrostatic water-spraying scrubber, using both fresh water and seawater. Based on the numerical and experimental results, it can be concluded that the efficiency of particle removal is significantly higher when both particles and droplets carry opposite charges. However, it may be difficult to generalise the results due to variations in operating conditions and scrubber gas characteristics used in the experiments.

The basic mechanism of a WES is capturing these small-size particles, even micron particles, by spraying charged droplets and applying electric forces to attract oppositely charged particles. Then, the droplets and settled particles are removed from the scrubber through a process of drainage or flushing. Diesel particles are mainly solid carbon (41%), unburned lubricant (25%), sulphate/water (14%) and other ash and unburned contents, which account for less than 20% of the DPM [30–32]. Zhou et al. [87,88] investigated the influence of fuel properties and particle size distributions on particle emissions from marine diesel engines. These investigations found that different types of diesel fuel oil influence the specific emissions of total PM and its composition. Additionally, droplet size was found to be a critical parameter influencing the efficiency of particle capture.

However, in the current body of literature, there exists a noticeable paucity of comprehensive and rigorous scientific elucidations regarding the phenomena of charged particles being captured by charged droplets within a gaseous flow field. This gap is primarily due to an underdeveloped comprehension of the intricate interplay among the governing parameters of this process. Consequently, the primary objective of this research is to clarify the mechanism underlying the movement of charged particles that are captured by charged droplets, and to develop a comprehensive scientific framework for the WES technology. Since the shipping industry significantly contributes to global emissions and with the introduction of stricter regulations on ship emissions, it is vital to understand how WES technology can be adapted for marine use. Optimising this technology for maritime applications is crucial for effective PM emission control. Additionally, this research can help ensure operational efficiency in the face of unique challenges presented by marine environments, such as high humidity and limited space, which can affect the performance of WES.

Chapter 3

Adopted approach and innovations

3.1 Approach adopted in this work

The chapter briefly describes the approach adopted to achieve the aims and objectives of this research work. The mind map of the complete approach is given in Fig. 3.1, which broadly comprises of three main flows. Those approaches were adopted to help study the movement mechanism of charged particles captured by charged droplets. The first one is to learn the theoretical mechanism of the particle motion process. A connection between the electrostatic field and the flow field could be established in theory to describe the particle motion process. The second one is to develop a numerical system to describe the particle motion process when captured by a droplet under the existence of an electrostatic field. The third one is to develop an experiment to watch the particle movement before

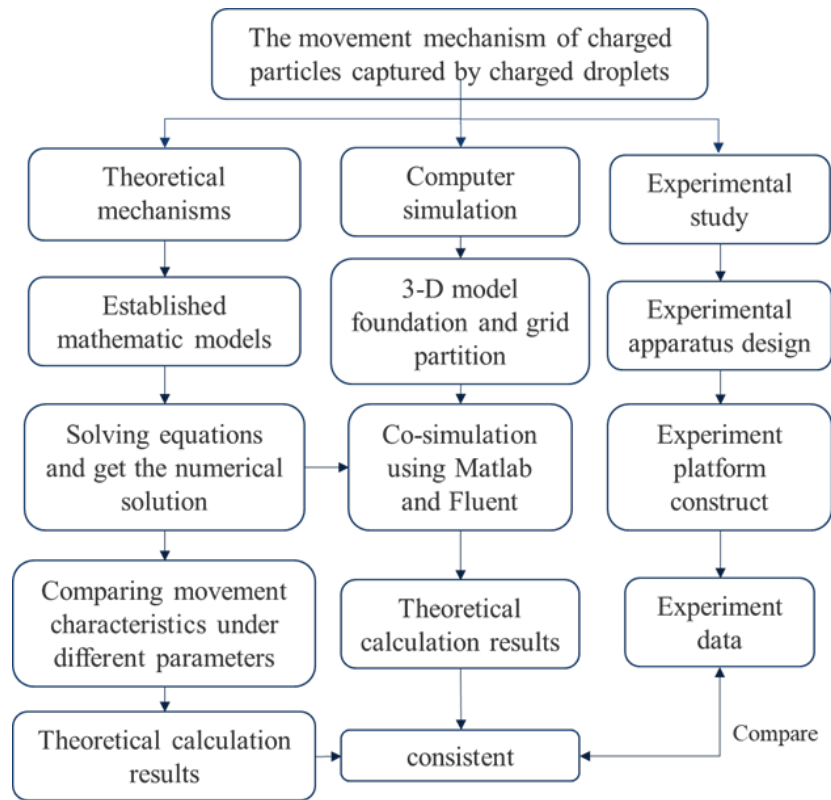


Figure 3.1: Mind map of the approach adopted.

when arriving at the droplet under the electrostatic field.

3.2 Innovations of this work

Compared to previous work reviewed in chapter 2, the innovations of this work can be outlined as follows:

- Developed a novel approach that combines electric and fluid flow fields to effectively address complex two-phase flow problems, particularly in scenarios involving charged particles and droplets.
- Provided a comprehensive and novel mathematical model describing the

mechanism of charged particle motion and capture by a charged droplet within a gas flow field, enhancing understanding of particle-droplet interactions under electrostatic forces.

- Developed an integrated numerical co-simulation model combining ANSYS Fluent and MATLAB, specifically designed to simulate and analyze the particle motion process in a gas flow field around a droplet under the influence of an electrostatic field, enabling more accurate predictions of particle behavior.
- Designed a novel experimental setup to observe and quantify the particle motion process upon approaching the droplet surface in a gas flow field under the influence of an electrostatic field, providing empirical validation for the theoretical and simulation models.

3.3 The advantages of WES technology

The WES is an advanced technology designed to remove fine particulate matter, aerosols, and gaseous pollutants from industrial exhaust streams and emissions. This system combines the features of a wet scrubber and an electrostatic precipitator to enhance pollutant removal efficiency. Compared to other technologies, the WES presents a balanced solution that effectively captures particles while optimising energy and water usage, minimising pressure drop, and conserving space [89].

Figure 3.2 gives an overview of the process flow and the basic components of a WES, illustrating how it cleans the exhaust gases. In this type of scrubber,

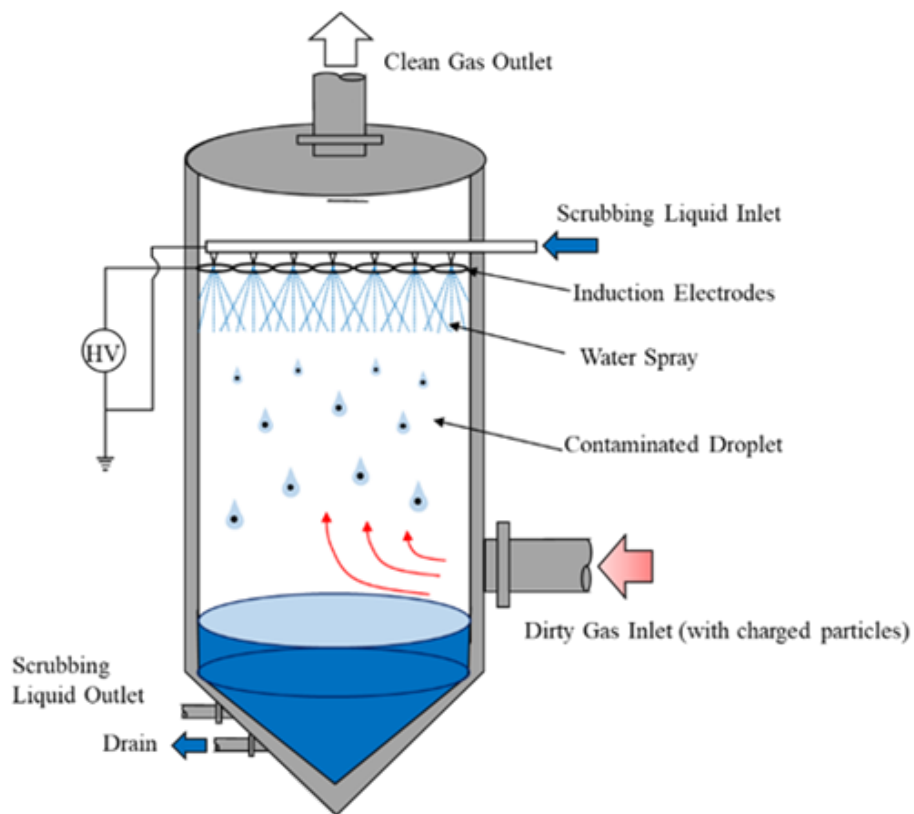


Figure 3.2: An example of WES with counter-current gas flow.

the gas stream flows through a scrubber tower that contains a liquid film or droplets that are charged with high voltage electrodes. Before the polluted gas stream enters the scrubber, it passes through an area with charged electrodes. These electrodes impart a charge to the particulate matter within the stream. As the gas stream passes through the WES, the charged liquid droplets attract the oppositely charged particles in the gas stream due to electrostatic forces. The electrostatic force plays a crucial role in the particle capturing efficiency of the vessel WES, as it increases the capture efficiency of the scrubber by attracting more particles to the charged liquid droplets. Researchers have made diligent efforts to apply this technology to shipping exhaust.

Not only the highly efficient at capturing fine particles, but WES also has

several advantages when it comes to removing fine PM and aerosols from marine applications. The system can handle a variety of pollutants, including both PM and gaseous pollutants in one step, which can be more cost-effective than using separate systems. Besides, the system operates with a relatively low pressure drop across the system, which can lead to energy savings. They often require less space than other control systems with similar capacities. These benefits make WES a valuable tool for maritime industries seeking to comply with emission regulations and improve air quality. However, they do require careful design and operation to ensure optimal performance and handling of the resultant wastewater.

Chapter 4

Mathematical model development

4.1 Introduction

To reduce PM emissions from marine diesel engines that cannot be removed using conventional methods efficiency, a wet electrostatic scrubber appears to be highly effective. The efficiency of WES largely hinges on the intricate motion of particles within the scrubbing process. Understanding how these particles interact with electric fields and liquid droplets is key to enhancing the efficacy of pollutant removal. Establishing the mathematical model describing particle motion in WES presents unique challenges, such as accurately representing the interactions between charged particles, electric fields, and fluid dynamics within the scrubbing medium.

This chapter aims to outline the development of a comprehensive mathe-

mathematical model that captures the complex dynamics of particle motion in WES, addressing both theoretical and practical aspects. Firstly, the moving model of a particle in a gas flow field is illustrated. In this section, the effect of electrostatic force is combined into the function. Then consider about the gas flow field distribution around droplets, the gas flow velocity distribution around the droplet is clarified. At last, through combing the effect of electrostatic field, the particle movement and the specific flow field around droplets, the defined mathematical model to describe the particle movement in WES could be conducted and solved. This study explores the fundamental principles governing particle behaviour in WES, establishing a mathematical model contains multi field and multiphase that describe these processes. Developing an advanced mathematical model for particle motion in WES not only contributes to learning the particle's motion characteristics but also contributes to more effective air pollution control strategies.

4.2 Theoretical model assumptions

Before implementing this technology on boats, a thorough understanding of the theoretical mechanism of particle and droplet transport is essential. Electrohydrodynamics are utilised in the mechanics study of particle capture by charged droplets. For the theoretical model, there are some assumptions:

- Ideal steady incompressible viscous flow field.
- Laminar flow field.
- Black carbon particle and droplet are both single solid spherical particles.

- The droplet is static in the flow field, the movement of particle in the flow field around the liquid droplet are the main target considered in this study.
- The direction of gas flow and particle movement is vertical upward.

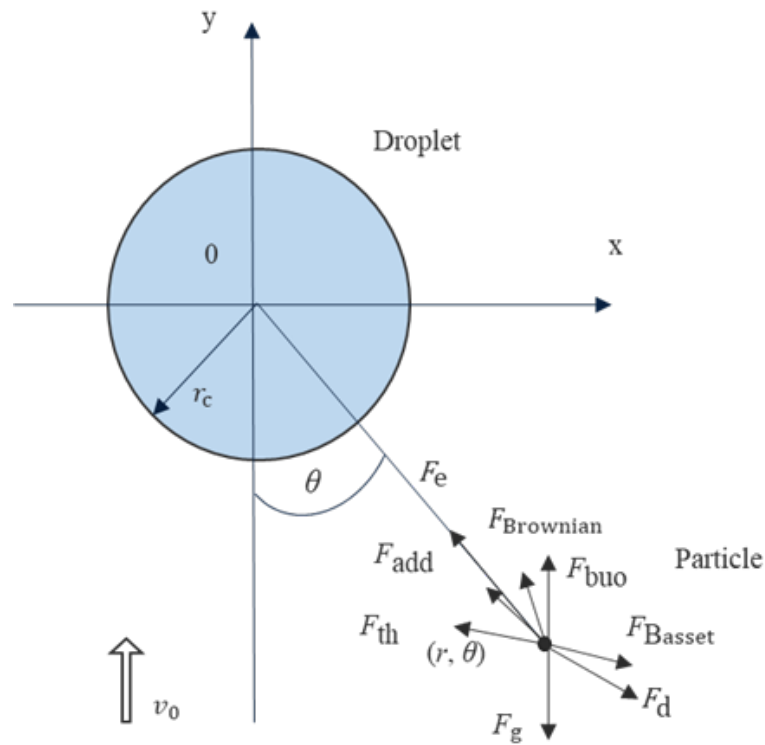


Figure 4.1: Forces acting on the particle and flow field near the droplet.

Analysing the forces acting on charged particles captured by charged droplets is a necessary step to understanding their movement characteristics. This preliminary analysis is crucial before establishing the equations that govern their motion. Figure 4.1 shows the analysing work that conducted about forces acting on the particle and flow field near the droplet. For this part, an investigation is conducted under the setting of the particle moving in the vertical direction. Without considering about the motion of droplet, the particle moves upwards with the gas in the vertical direction and as shown in Fig. 4.1 the direction of

gravity is vertically downwards.

4.3 Particle motion mechanism

For a particle in fluid, gravity, added mass force, Basset force, thermophoresis, drag force, and Brownian force should be all taken into consideration, as shown in Fig. 4.1. Besides these common forces, because the particle and droplet are both electrified, electric force is the dominant force that exists in this research condition. The electronic force considered here is the Coulomb force, since it has much more effect than particle image force when the particle and droplet are both charged [86]. Therefore, a vector differential equation can be used to describe the motion of a small-scale particle in an electric fluid field.

$$m_p \frac{dv_p}{dt} = F_g + F_{buo} + F_{add} + F_d + F_{Basset} + F_{th} + F_{Brownian} + F_e \quad (4.1)$$

where m_p is the mass of a particle, v_p is the velocity of a particle, F_g , F_{buo} , F_{add} , F_d , F_{Basset} , F_{th} , $F_{Brownian}$, F_e are the gravity, buoyancy, added mass force, drag force, Basset force, thermophoresis force, Brownian force and Electrostatic force, respectively. Particles are suspended and move with the gas flow at the same velocity by default when there is no additional force. Thus, gravity and buoyancy can be ignored simultaneously.

The added mass force in Eq. 4.1 is given by the following:

$$F_{add} = \frac{1}{2} \rho_f V_p \left(\frac{du}{dt} - \frac{dv_p}{dt} \right) \quad (4.2)$$

where ρ_f is the density of gas fluid, V_p is the volume of particle, and u is the velocity of flow field. In this study, the magnitude of density ratio of gas and particle is 10^{-3} approximately, as shown in Tbl. 5.1. Their velocity magnitudes are in the same order in this research. Thus, the impact of added mass force is not considered.

The drag force in the Eq. 4.1 can be written in the following form:

$$F_d = 3\pi\mu d_p \left(1 + \frac{3}{16}Re\right)(u_f - v_p) \quad (4.3)$$

in which μ is fluid viscosity, d_p is the diameter of particle, ρ_p is the density of the particle, $Re = \frac{\rho_f d_p (u_f - u_p)}{\mu}$ is the Reynold number. The Basset force exists when the particle moves in an unstable flow field, which is not the condition in this model assumption. Thus, this force is not considered in this study. The force can be described as follows:

$$F_{Basset} = \frac{3}{2}d_p^2(\pi\rho_f\mu)^{1/2} \int_{t_0}^t (t-t')^{1/2} \left(\frac{du_f}{dt} - \frac{du_p}{dt}\right) dt' \quad (4.4)$$

in which t is the time period of the particle moving.

The thermophoresis force can be written in the form as follows [90]:

$$F_{th} = 1.15 \frac{K_n}{4\sqrt{2}\alpha(1 + \frac{\pi_1}{2}K_n)} \left[1 - \exp\left(-\frac{\alpha}{K_n}\right)\right] \left(\frac{4}{3\pi}\phi\pi_1 K_n\right)^{1/2} \cdot \frac{k}{d_p^2} \nabla T d^2 \quad (4.5)$$

where $K_n = 2\lambda/d$ is the Knudsen number, k is the Boltzmann constant, and

$$\phi = 0.25(9\gamma - 5) \frac{C_v}{R} \quad (4.6)$$

in which $R = 287$ J/kgK, where R is the fluid constant. $C_v = 718 + 0.1167\rho_f$

J/kgK, where C_v is the constant volume specific heat. $\gamma=1.4$, where γ is the specific heat ratio.

$$\alpha = 0.22 \left[\frac{\frac{\pi}{6} \Phi}{1 + \frac{\pi_1}{2} K_n} \right]^{(1/2)} \quad (4.7)$$

and

$$\pi_1 = 0.18 \frac{\frac{36}{\pi}}{(2 - S_n + S_t) \frac{4}{\pi} + S_n} \quad (4.8)$$

where S_n and S_t are the normal and tangential movement accommodation coefficients. This thermophoresis force exists when the temperature difference exists between the gas flow field and the droplet.

The Brownian force effect is quite negligible when compared with the electrical force and drag force effect.

The electrostatic force can be given out in the form proposed by A. Jaworek [91]:

$$F_e = \frac{Q_p Q_c}{4\pi\epsilon_0 r^2} + \frac{r_p Q_c^2}{4\pi\epsilon_0 r^3} (r^4 / (r^2 - r_p^2)^2 - 1) + \frac{r_c Q_p^2}{4\pi\epsilon_0 r^3} (1 - \frac{r^4}{(r^2 - r_c^2)^2}) \quad (4.9)$$

where Q_p and Q_c are the charges on the aerosol particle and droplet, respectively, r is the distance between the particle and the droplet centre, and ϵ_0 is the permittivity of the free space. The first term on the left in the equation represents the Coulomb force and the other two terms represent Image force. The main electrostatic force considered here is Coulomb force, since it has much more effect than particle image force when the particle and droplet have opposite charges [86].

The expression of the particle movement can be concluded as follows:

$$\begin{aligned}
m_p \frac{dv_p}{dt} = & 3\pi\mu d_p \left(1 + \frac{3}{16} Re\right) (u_f - v_p) \\
& + 1.15 \frac{K_n}{4\sqrt{2} \alpha \left(1 + \frac{\pi_1}{2} K_n\right)} \left[1 - \exp\left(-\frac{\alpha}{K_n}\right)\right] \left(\frac{4}{3\pi} \phi \pi_1 K_n\right)^{1/2} \frac{k}{d_p^2} \nabla T d^2 \\
& + \frac{Q_p Q_c}{4\pi\epsilon_0 r^2} + \frac{r_p Q_c^2}{4\pi\epsilon_0 r^3} \left(\frac{r^4}{(r^2 - r_p^2)^2} - 1\right) + \frac{r_c Q_p^2}{4\pi\epsilon_0 r^3} \left(1 - \frac{r^4}{(r^2 - r_c^2)^2}\right)
\end{aligned} \tag{4.10}$$

This function can be used to describe the particle motion process when the flow field, electrostatic field, and temperature field exist.

4.4 Air flow field distribution

According to the analysis of forces on the particle motion, as shown in Fig. 4.1, particle moving characteristic is affected by the surrounding gas flow field distribution. This motion mechanism coupled particle velocity, gas flow field velocity, particle position, and also the electrostatic field strength in our research. Thus, a coupled mathematical model is needed to describe the particle-droplet intersection motion characteristics under the condition of an electrostatic field. In this study, the stream function φ is utilised to obtain the velocity distribution around a sphere droplet. The equations are as follows:

$$\begin{cases} \nabla^2 \varphi = 0 & (\text{in flow field}) \\ \frac{\partial \varphi}{\partial r} = 0 & (\text{on the surface of droplet}) \\ \frac{\partial \varphi}{\partial r} = v_0 \cos \theta, \frac{\partial \varphi}{r \partial \theta} = -v_0 \sin \theta & (\text{at infinity}) \end{cases} \quad (4.11)$$

After derivation, the velocity distribution can be described as follows:

$$v_r = \frac{\partial \varphi}{\partial r} = v_0 \cos \theta \left(1 - \frac{r_c^2}{r^2}\right) \quad (4.12)$$

$$v_\theta = \frac{1}{r} \frac{\partial \varphi}{\partial \theta} = -v_0 \sin \theta \left(1 + \frac{r_c^2}{r^2}\right) \quad (4.13)$$

The function 4.12 and 4.13 describes the gas flow velocity distribution around a sphere, where v_r represents the radial velocity component and v_θ represents the angular velocity component. For the research work of this article, the value of θ is set to 0.

4.5 Derived Mathematical Model for particle motion in WES

The velocity of the gas flow field surrounding a particle can be determined based on the distance between the particle and the droplet. Using simultaneous equations of the air velocity distribution around the droplet and the particle motion equation, a mathematical model can be obtained to describe the motion of a charged particle around an oppositely charged droplet in a gas flow field. The

mathematical model is presented in Eqs. 4.14 to 4.16. By determining the motion characteristics of particles in the flow field around the droplet, the mechanism behind the capture of small-scale particles by electrostatic liquid droplets can be explained in detail.

For this study, the temperature parameters were selected at a fixed temperature of 80°C. Therefore, the effect of thermophoresis force resulting from temperature variations was not taken into consideration in this research. Thus, this study firstly mainly considers the drag force, F_D , and the electrostatic force, F_E , specifically the Coulomb force, as the predominant forces acting on the particle based on the theoretical model proposed in this thesis.

$$m_p \frac{du_p}{dt} = -3\pi\mu d_p \left(1 + \frac{3}{16} Re\right) (u_f - u_p) + \frac{Q_p Q_c}{4\pi\epsilon_0 r^2} \quad (4.14)$$

$$u_f = u_0 \cos\theta \left(1 - \frac{r_c^2}{r^2}\right) \text{ (Gas flow field around sphere droplet)} \quad (4.15)$$

Relationship of a particle or a droplet saturation charge Q with E and d :

$$Q = \frac{3\epsilon_r}{\epsilon_r + 2} \pi\epsilon_0 d^2 E \quad (4.16)$$

where d is diameter, ϵ_r is the relative dielectric constant, ϵ_0 is the dielectric constant of vacuum whose value is 8.8510^{-12} F/m, and E is electric field strength, which value is ranged from 10 kV to 30 kV according to the ESP utilisation [92].

The ultimate charge of a liquid droplet is known as Rayleigh limit [93]:

$$Q_{dc} = 8\pi(\varepsilon_0\sigma_c r_c^3)^{(1/2)} \quad (4.17)$$

where σ_c is surface tension of droplet, which value is $71.95 \times 10^{-3}\text{N}$. For the condition shown in Tbl. 5.1, the value of Q_{dc} is 6.342×10^{-10} . When the electrostatic field strength is 10 kV, the droplet charge Q is 3.256×10^{-12} , which is much less than the value of Q_{dc} . The value Reynolds number of the particle in the gas flow field is:

$$Re = \frac{\rho_f d_p (u_f - u_p)}{\mu} = 0 - 5.23 \quad (4.18)$$

4.6 Summary

A mathematical model, describing the particle motion process in the gas flow field in one WES, is developed in this chapter. In the mathematical model, the electrostatic effects are introduced into the equations of particle motion in the fluid, and then coupled with the flow field distribution characteristics around the spherical droplet for a combined solution.

The description of particle motion is based on the classic BBO (Boussinesq-Basset-Oseen) equation, which is used for describing the motion of a small spherical particle in a viscous fluid [94–96]. Through force analysis, the electrostatic force is added into the particle motion equation. The electric field strength is considered into the model which is directly adapted to practical application. In

the particle motion equation, the fluid factors are relative to the particle position in the flow field around the droplet. The flow field distribution is affected by the droplet features.

Thus, the mathematical model is coupled with the particle motion equation and the flow field distribution equations around a spherical droplet. During the solving process, the fluid factors around the particle is dependent on the particle position, while the position of the particle is associated with the particle motion process. Thus, the mathematical model is solved by iterative calculations with the method of 4-th order Runge-Kutta method.

Chapter 5

Characteristics of particle motion process

5.1 Introduction

Through the analysis of the mathematical model in chapter 4, especially considering Eq. 4.14 which describes the particle motion process combined with the effect of an electrostatic field, there are varied conditions that could influence the particle motion. This chapter aims to systematically investigate the influences on the particle capture process.

In this chapter, parametrisation research of Eq. 4.14 is conducted, enabling a comprehensive analysis under varied conditions. Specifically, we focus on examining the impact of electric field strength, particle size, and droplet size on the behaviour of charged particles. This approach allows us to gain detailed insights into the characteristics of particle movement influenced by different factors. The

complexities of these interactions between gas flow field, electrostatic field and particle movement are addressed through computational analysis, employing the 4th order Runge-Kutta method for solving the Eqs. 4.14 to 4.16. This methodical examination promises to deepen our understanding of the electrostatic effects on particle dynamics in the given context. Parameters chosen when solving the equations are listed in Table 5.1. The angle (θ) of the particle moving towards the droplet is set to 0 to simplify the equation solving.

Table 5.1: Model properties.

Droplet radius/ r_c	0.1 mm, 0.5 mm, 1 mm, 2 mm
Particle radius/ r_p	5 μm , 10 μm , 20 μm , 50 μm
Density of particle/ ρ_p	$1.05 \times 10^3 \text{ kg/m}^3$
Density of gas fluid/ ρ_f	1.019 kg/m^3
Dynamic viscosity of gas fluid/ μ	$1.948 \times 10^{-5} \text{ Pa} \cdot \text{s}$
Inlet velocity of flow field/ u_0	5 m/s
Vacuum dielectric constant/ ε_0	$8.85 \times 10^{-12} \text{ F/m}$
Relative dielectric constant (particle)/ ε_{rp}	30
Relative dielectric constant (droplet)/ ε_{rc}	81.5

5.2 Effect of electrostatic field strength

Firstly, particle moving characteristics are compared when electric force exists or not. In the process of the theoretical calculation, the particle was defined as moving towards the vertical axis of the droplet. In this research, collision and rebound were not considered. The droplet radius (r_c) was 1 mm. When the distance between a particle and the centre of a droplet is less than 1mm, it is

considered that the particle has been captured by the droplet theoretically. The initial distance between a particle and the centre of a droplet is set to 6 mm here, which means the distance between the particle and the surface of the droplet is 5 mm.

The distance in the figures represents the distance between the particle and the droplet surface. When $t=0$ ms, the distance represents the initial distance of the particle in the flow field around the droplet. When the distance is equal to 0 mm, that represents the particle reaches the droplet surface. The initial particle velocity equals the flow velocity of the particle initial position in the flow field. The trends of distance between the particle and droplet surface, with and without an electric field, are shown in Fig. 5.1. The Y-axis represents the distance from the particle to the droplet surface. It can be seen from the figures that the changing trend of the two curves is generally similar when the electric field exists or not. That means the times of particles reaching the droplet were almost the same under these two conditions, whose value is approximately 1.05 ms as shown in Fig. 5.1.

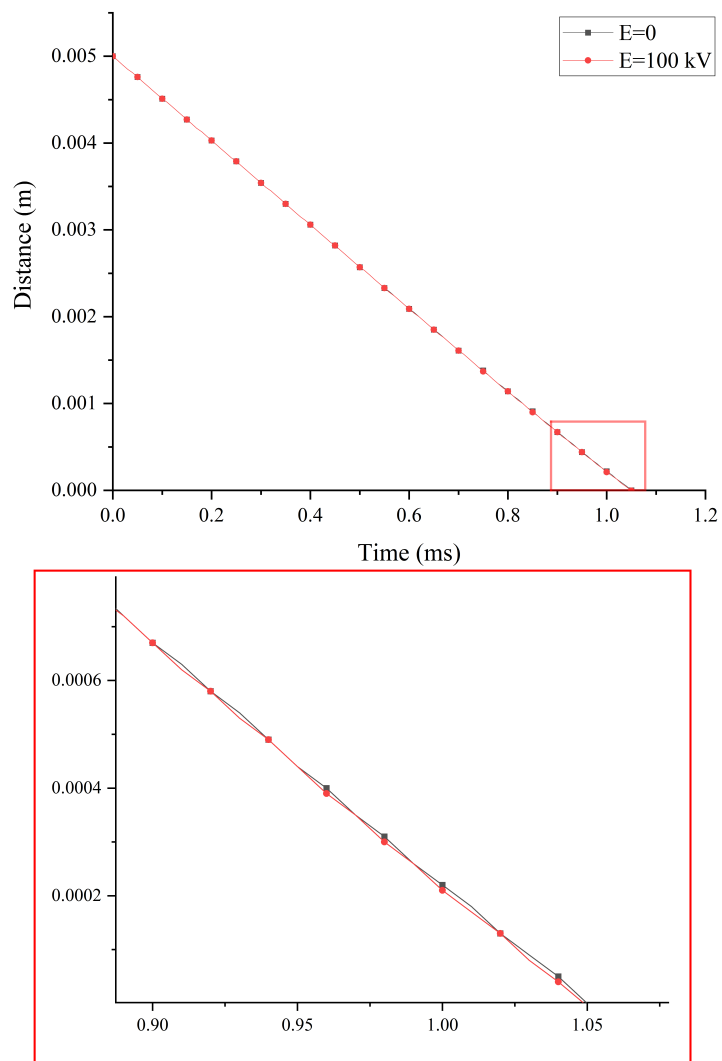


Figure 5.1: Trend of distance change with and without electric force when droplet radius is 1 mm and particle radius is 10 μm .

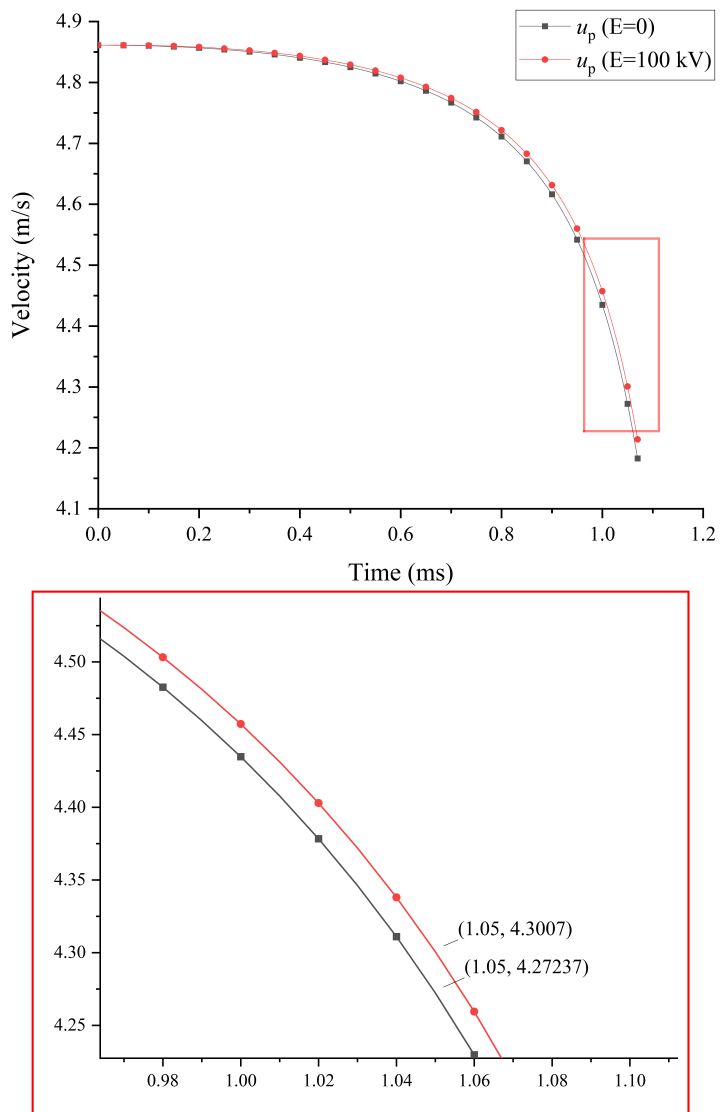


Figure 5.2: Trend of velocity change with and without electric force when droplet radius is 1 mm and particle radius is $10 \mu\text{m}$.

As for the trend of the particle velocity, it can be illustrated from Fig. 5.2 that the electrostatic force can help increase the velocity of particle when it moves close to the droplet. The velocity difference was 0.028 m/s or 28 mm/s before the particle was captured by the droplet.

To verify the influence trend and extent of each factor, different electric field strengths, droplet radii and particle radii are defined when solving the equations. Thus, a series of trend changes in distance and velocity can be concluded.

It can be seen from Fig. 5.3, that the particle starts 5 mm away from the droplet, with an initial velocity of approximately 4.85 m/s. The different lines (0 kV, 30 kV, 50 kV, 100 kV) show that stronger electric fields result in a greater velocity, particularly as the particle approaches the droplet. Focusing on the final approach, just before the particle approaches the droplet surface, under different electric fields, the velocity at 1.05 ms varies slightly depending on the electric field applied. With a strong electric field (cyan line, $E=100$ kV), the velocity remains higher at 4.3007m/s. Without a field (red line, $E=0$ kV), the velocity is reduced to 4.27237 m/s. The difference between these different electric field strengths is 2.57 mm/s, 4.5 mm/s, and 21.28 mm/s respectively. In summary, this figure shows that although the drag force is the dominant factor over the 5 mm distance, the electrostatic field reduces particle deceleration, particularly in the final stage of its motion (close to the droplet surface). This subtle but significant effect becomes more apparent as the electric field strength increases.

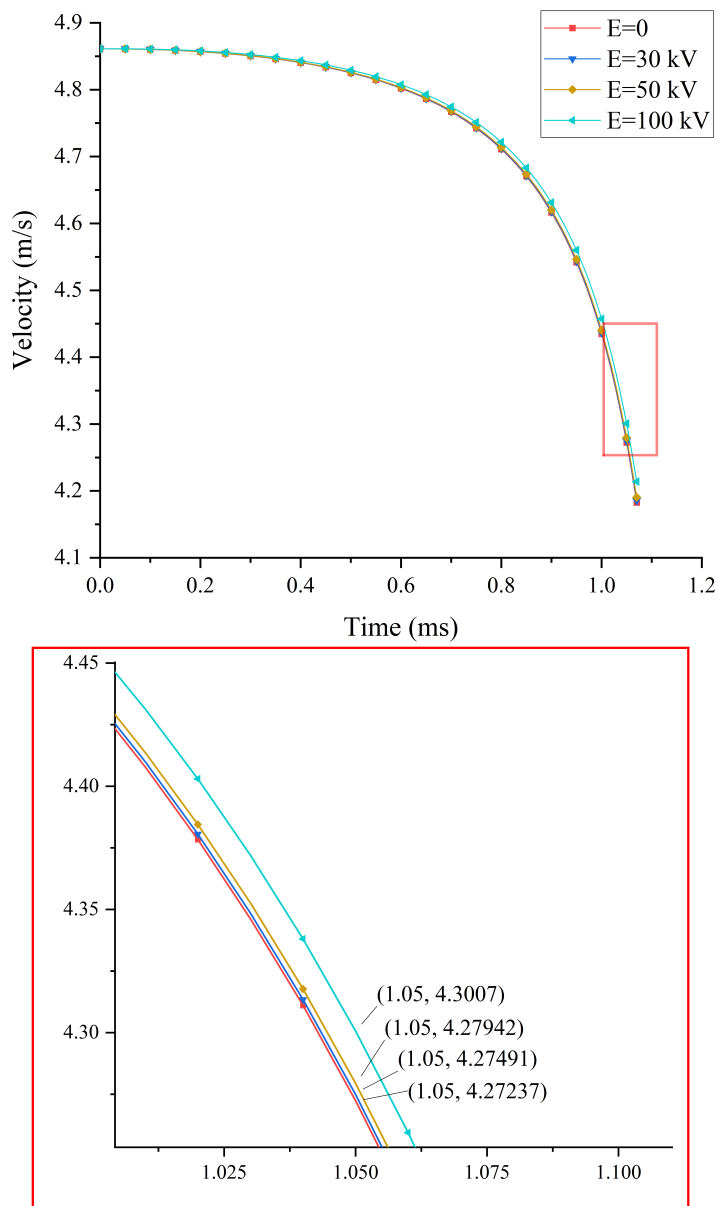


Figure 5.3: Trends of velocity under different electric field strength when droplet radius is 1 mm and particle radius is 10 μm .

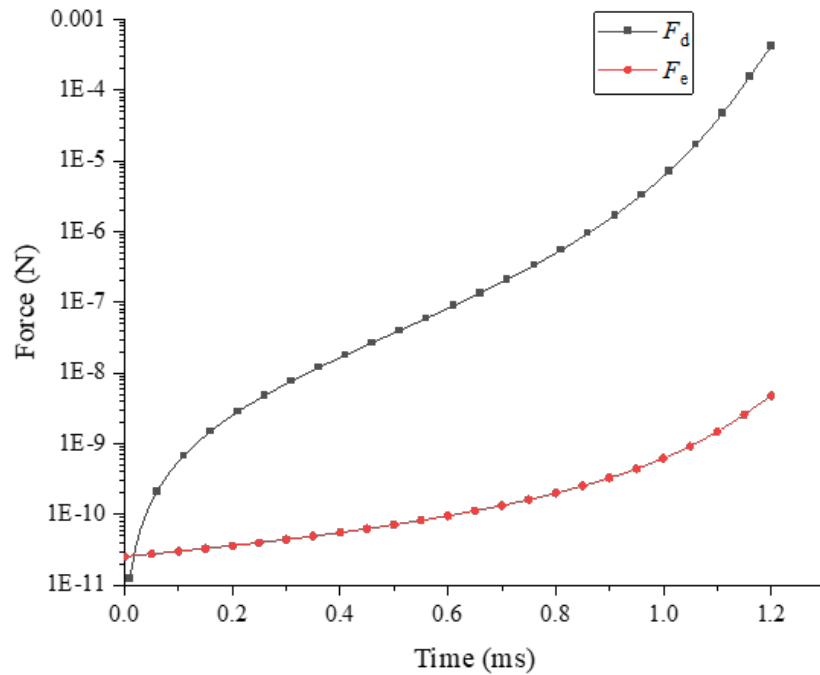


Figure 5.4: Magnitude comparison of drag force and electric force when droplet radius is 1 mm and particle radius is 10 μm .

Then the magnitude of drag force F_d and electrical force F_e was compared in Fig. 5.4, when the electric field strength was 100 kV. The magnitudes are presented using a logarithmic scale to show their magnitudes more clearly. It can be seen that the magnitude of the electric force was far less than that of the drag force even though the electric field strength was 100 kV. Therefore, simply improving the electrostatic field strength will not influence the particle motion process obviously. Even though the drag force is much larger than the electric force, the particle still moves toward the droplet because the electric force is attractive and acts continuously over time. The drag force, while resisting motion, does not push the particle away but only slows it down. Hence, the electric force is still effective in guiding the particles toward the droplet despite the larger drag force.

5.3 Effect of particle size

Figures 5.5 and 5.6 depicts the time history curve of particle displacement of particles of different sizes ($5\ \mu\text{m}$, $10\ \mu\text{m}$, $20\ \mu\text{m}$, and $50\ \mu\text{m}$) under identical electric field strength ($20\ \text{kV}$). The result indicates that larger particles are easier to capture by the droplet. In Fig. 5.5, the $50\ \mu\text{m}$ particle reaches the droplet's surface more rapidly than other particles. The capture time of the $50\ \mu\text{m}$ particle is $1.028\ \text{ms}$ approximately, while the capture time of the $20\ \mu\text{m}$ particle is $1.035\ \text{ms}$, of $10\ \mu\text{m}$ is $1.051\ \text{ms}$, and of $5\ \mu\text{m}$ is $1.103\ \text{ms}$. From this figure, it can be concluded that when the particle of $50\ \mu\text{m}$ radius reaches the droplet surface, the particle of $5\ \mu\text{m}$ radius is $0.25\ \text{mm}$ away from the droplet surface.

In Fig. 5.6, the velocity of particles decreases with time as the particles move closer to the droplet. Before the particles were captured, the particle velocity of $50\ \mu\text{m}$ is much greater than that of $5\ \mu\text{m}$. It is annotated in Fig. 5.6, and the difference in particle velocities of different sizes is obvious. For the particle size below $10\ \mu\text{m}$, when the particle radius decreases by 50%, from $10\ \mu\text{m}$ to $5\ \mu\text{m}$, the particle velocity of reaching the droplet surface decreases by 30.28%. For particle sizes beyond $10\ \mu\text{m}$, the velocity is still over $4\ \text{m/s}$ before arriving at the droplet surface. When particle radius decreases from $20\ \mu\text{m}$ to $10\ \mu\text{m}$, the change in radius is large, but the particle velocity reaching the droplet surface only decreases by 9.01%. Under this condition, particles can maintain their high velocity upon reaching the surface of the droplet, thereby significantly enhancing the efficiency of particle capture [97]. This indicates that under the electrostatic field condition, for particle size beyond $10\ \mu\text{m}$, the influence of particle size is not obvious. Thus, the electrostatic effect was much greater for larger particles.

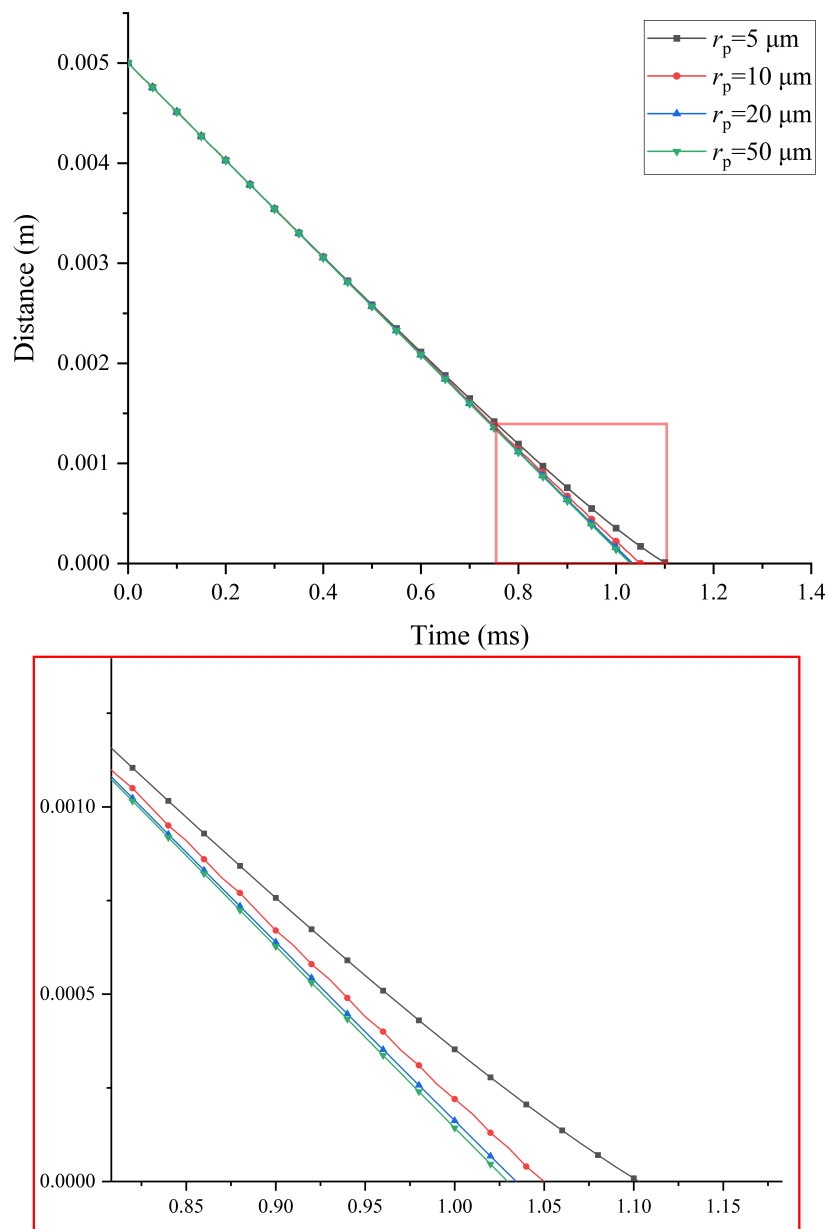


Figure 5.5: Trends of distance change under different particle diameters when droplet radius is 1 mm and electric field strength is 20 kV.

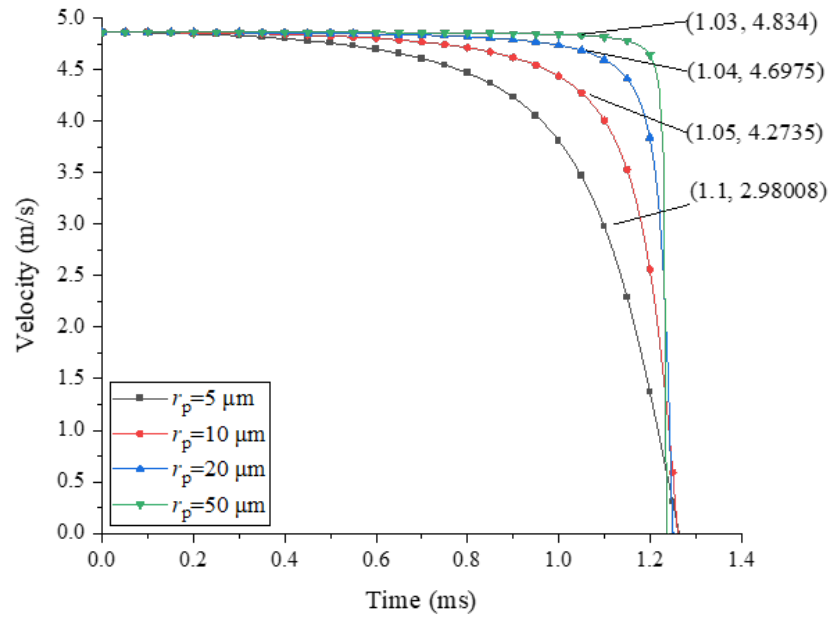


Figure 5.6: particle velocity changes with time under different particle diameters when droplet radius is 1 mm and the electric field strength is 20 kV.

5.4 Effect of droplet size

Figures 5.7 and 5.8 present the results of particles' movement with different droplet sizes (0.1 mm, 0.5 mm, 1 mm, and 2 mm) under identical electric field strength (20 kV). The time when these particles arrive at the droplet surface are 1.021 ms, 1.031 ms, 1.051 ms, and 1.097 ms, respectively. Comparing the results in Fig. 5.7, the distance between the particle and the droplet decreases over time for all droplet diameters. The curves are linear initially, indicating a constant velocity, but then they start to curve as the distance decreases, indicating a reduction in velocity.

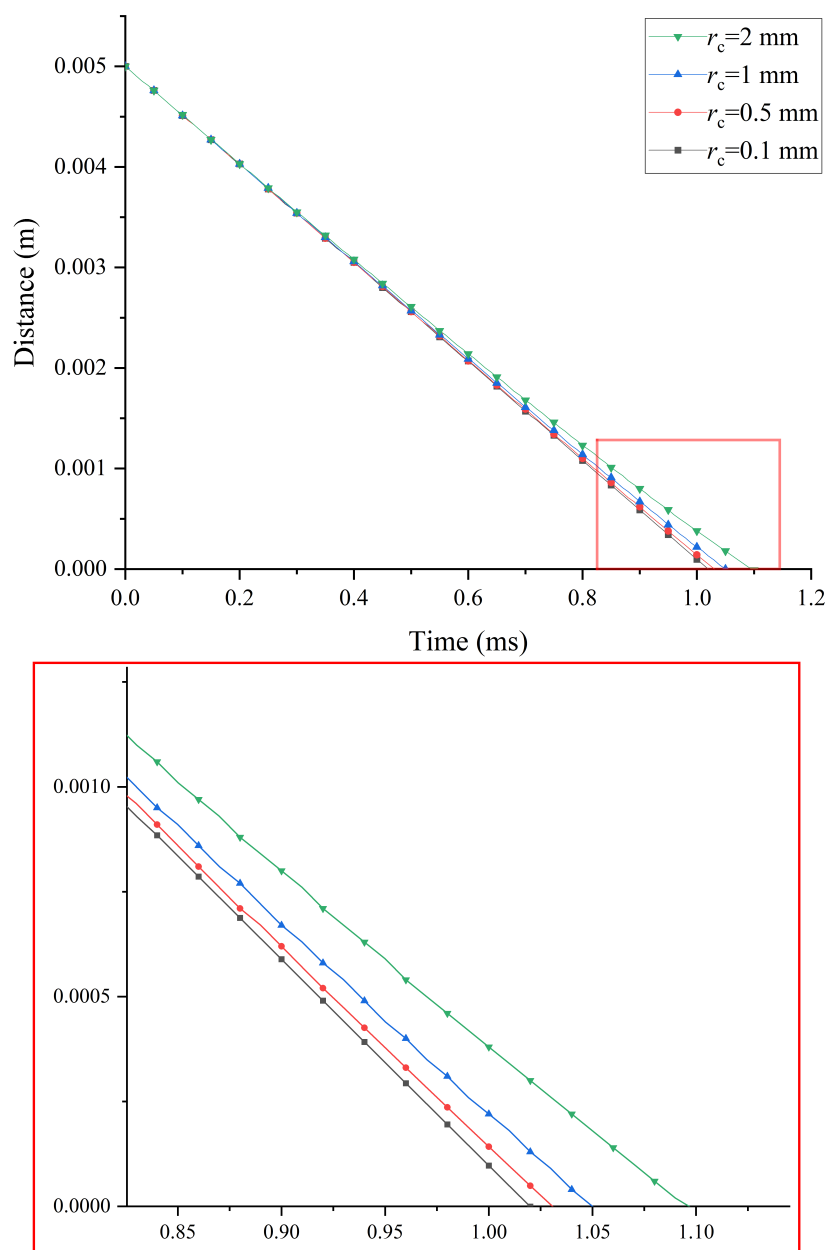


Figure 5.7: Distance between particle to the droplet surface changes with time under different droplet diameters when particle radius is $10 \mu\text{m}$ and electric field strength is 20 kV.

As shown in 5.7, when the distance is 0 m, that means the particle reaches the droplet surface. For larger droplets ($r_c=2\text{mm}$ and $r_c=1\text{mm}$), the distance decreases more gradually compared to smaller droplets ($r_c=0.5\text{mm}$ and $r_c=0.1\text{mm}$). This implies that particles approaching larger droplets slow down earlier and more gradually than those approaching smaller droplets. From this figure, it can be found that when a particle reaches the droplet surface of 0.1 mm radius, the particle is 0.3 mm away from the droplet surface of 2 mm radius. It can be concluded that smaller droplets can attract the particle more quickly.

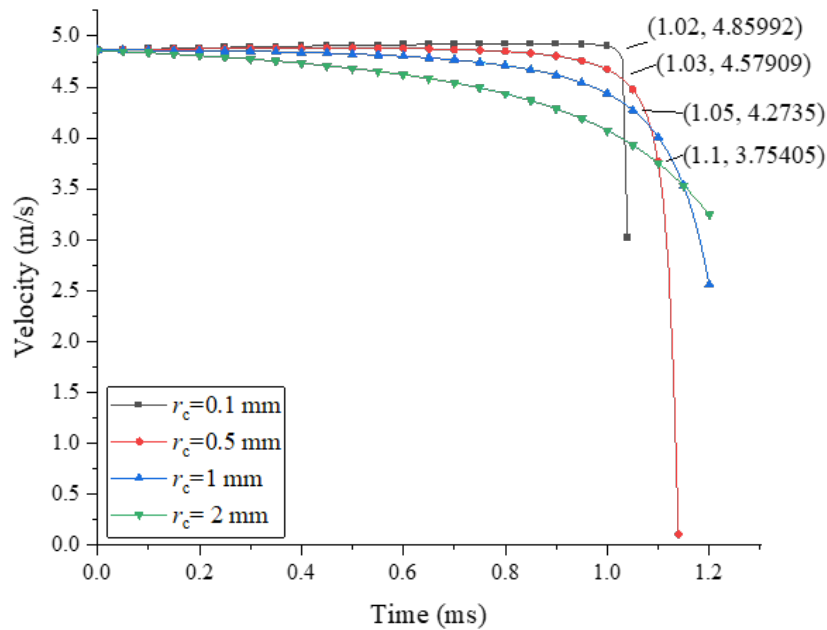


Figure 5.8: Particle velocity changes with time under different droplet diameters when particle radius is $10\ \mu\text{m}$ and electric field strength is 20 kV.

Figure 5.8 shows that the size of droplets has a significant impact on particle velocity. When the droplet size is small (radius is 0.1 mm), the particle keeps moving at a relatively high speed before arriving at the droplet surface. As shown in Fig. 5.8, at the moment attracted by the droplet, the particle velocities are 4.86 m/s, 4.58 m/s, 4.27 m/s, and 3.75 m/s respectively when droplet radii are

0.1 mm, 0.5 mm, 1 mm, and 2 mm. This implies that when droplet size decreases by 50% from 2 mm to 1 mm, the final particle velocity increases by 13.85%. When droplet size decreases by 50% from 1 mm to 0.5 mm, the final particle velocity increases by 7.26%. The increase in final particle velocity is significant with the decrease in droplet size. Figure 5.9 illustrates the ratio of drag force to electrostatic force acting on a particle in the present research work. This figure helps explain the results analysed regarding the relationship between the F_D/F_E and r_c/r_p . The four cases presented correspond to the same position ($r = 0.0001$ mm) near the droplet surface. The results suggest that droplet size has an influence on the velocity distribution of the gas flow field around the droplet. Simultaneously reducing the droplet size can lead to a diminished impact of the drag force. While this reduction also lessens the influence of the electrostatic force, it's important to note that the drag force plays a more dominant role in the particle motion process as shown in section 5.2. Consequently, a decrease in droplet size can effectively facilitate the accelerated capture of particles.

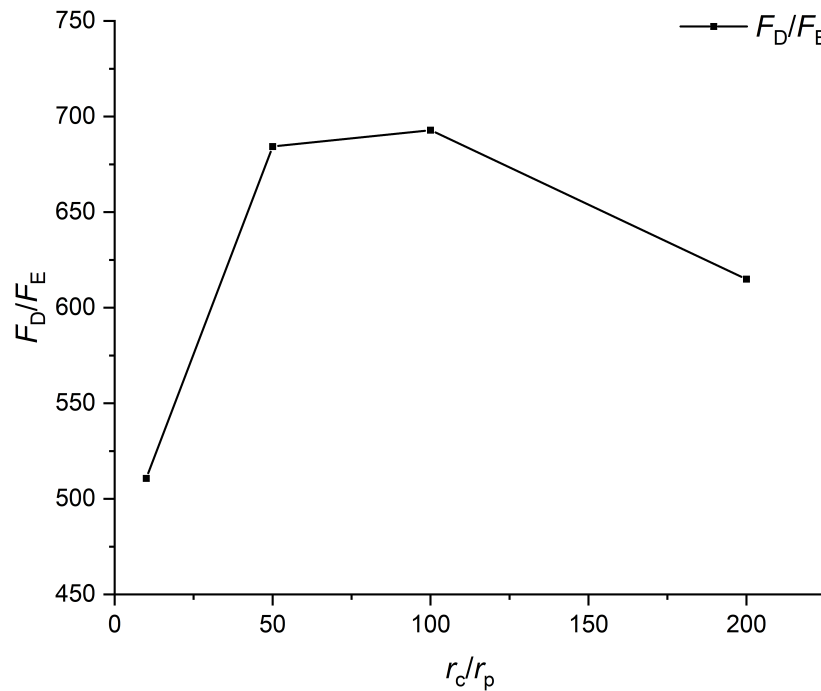


Figure 5.9: Drag Force to Electrostatic Force Ratio (F_D/F_E) as a Function of Droplet to Particle Size Ratio (r_c/r_p)

5.5 Effect of particle density

The specific particle density emitted from marine diesel engines can vary widely depending on the type of engine, the fuel used, operating conditions, and the presence of emission control technologies. The true density of carbon particles is approximately between 1.7 and 1.9 $\text{g}\cdot\text{cm}^{-3}$. But normally the carbon particles emitted from marine diesel engines may form agglomerated structures. The carbon particles often have a high porosity because of the air spaces between the particles. Thus, the bulk density of the emitted particles is much lower than their true density, potentially a few hundred kilograms per cubic meter (kg/m^3) [98,99].

This parameter may play a crucial role on the particle motion process in the WES. Taking the particle density in the range of 0.1 $\text{g}\cdot\text{cm}^{-3}$ to 1.5 $\text{g}\cdot\text{cm}^{-3}$ as

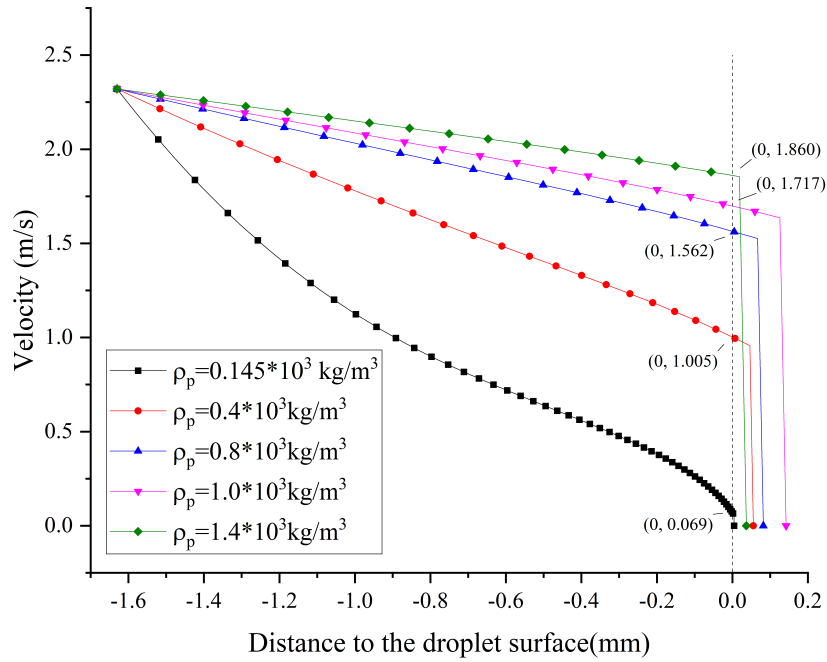


Figure 5.10: Particle velocity distribution of different particle densities.

an example, the variations in their motion characteristics under different particle densities are compared. It's noticeable in Fig. 5.10 that for all particle densities, the velocity decreases as the particles approach the droplet surface. The final velocities of the particles at the droplet surface are shown on the graph by the points at the vertical axis (0, Velocity). The particles with the highest density ($1.4 \times 10^3 \text{ kg/m}^3$) decelerate to a velocity of approximately 0.069 m/s, while the lowest density particles ($0.145 \times 10^3 \text{ kg/m}^3$) come to a near stop at the droplet surface with a final velocity closest to zero. The trend indicates that despite starting at higher velocities, heavier particles (higher density) slow down more significantly than lighter ones as they reach the droplet surface. This could be due to the increased momentum of the heavier particles making them more susceptible to the electrostatic force. This analysis suggests that particle density has a direct correlation with the ability of particles to retain their velocity as they approach the droplet surface. This is crucial for applications where particle

capture efficiency is important.

In practical applications, the density of particles emitted under actual operating conditions can be determined by effective measurement methods [98]. This parameter can then be used to accurately calculate and simulate the movement of particles in a WES.

5.6 Summary

There are several key factors that can affect the particle motion process under the presented fields. To evaluate the effectiveness of those factors, the motion characteristics were calculated by solving the mathematical model by changing one of those factors. Four factors were mainly considered in this thesis research. They are electrostatic field strength, particle size, droplet size, and particle density.

To evaluate the effect of electrostatic field strength, particle movement characteristics are calculated when electrostatic field exists and not and also several electrostatic field strengths. The results show that the movement of particles could be affected when there is an electrostatic field, and the velocity when the particle arrives the droplet is increased. But when changing the electrostatic field strength, the change in particle movement is not obvious, since the drag force is still dominant in the particle motion process. Thus, a proper electrostatic field strength range is supposed to be defined in follow-up research work.

When comes to the effect of particle size and droplet size, the results showed that the electrostatic effect is much greater for larger particles. The effect of

particle size is different for the range of particle radius. Under the electrostatic field condition (20 kV), for particle size beyond $10\mu\text{m}$, when particle radius decreases by 50%, the particle velocity of reaching the droplet surface decreases by 9.01%. While the particle radius is below $10\mu\text{m}$, the particle velocity of reaching the droplet surface decreases by 30.28% when particle size decreases by 50%. Besides, the droplet size has a great influence on the particle motion characteristics. Results in this thesis show that when droplet size decreases by 50%, the particle velocity at the droplet surface increases by 7.26% to 13.85%. Thus, decreasing the droplet size can help improve the collection effect. Thus, the larger particle and the smaller droplet can help increase the particle movement when particles moving to the droplet under the effect of electrostatic field.

Besides, when studying about the effect of particle density, the efficiency of particles capturing under the electrostatic field condition can be determined by the characteristics of the PM emission. Thus, it would be accurately when calculating and simulating the movement of particles in a WES with the accurate PM emission parameters.

Chapter 6

Co-simulation of Ansys fluent and MATLAB for particle motion around a sphere droplet

6.1 Introduction

In the ever-evolving landscape of computational fluid dynamics (CFD), the integration of robust simulation tools like Ansys Fluent with powerful computational platforms such as MATLAB presents unparalleled opportunities for advanced analyses. This chapter delves into the intricate world of particle motion, specifically around spherical droplets under the condition of the electrostatic field, through the lens of co-simulation using Ansys Fluent and MATLAB. This synergy of software tools opens up new avenues for precision, efficiency, and depth in understanding particle dynamics. The simulation results can provide a much

more intuitive understanding of the motion characteristics of particles around droplets under the influence of the electrostatic field.

Ansys Fluent, renowned for its detailed CFD capabilities, offers a comprehensive framework for simulating fluid flow and interactions with particles. When coupled with MATLAB's extensive data analysis, the combined power of these tools enhances our ability to investigate complex physical phenomena with greater accuracy.

This chapter first introduces the process framework of the simulation. In Fluent, conditions are set and initialised for the flow field around the droplet. Then, in MATLAB, a connection with Fluent is established through code. This allows for the calculation of particle motion using the flow characteristics around the particle, and the results are then fed back into Fluent for simulation. The entire process involves iterative calculations until the particles reach the surface of the droplet. Then, the development of the model within Fluent is presented in this part, including the generation of overset meshing. Finally, the chapter concludes with an analysis of the simulation results, comparing them with theoretical solutions to validate and contextualise the findings in this work.

6.2 Co-simulation mechanism

For the simulation of the particle moving process, in this study, a co-simulation approach using ANSYS Fluent and MATLAB is employed to realise a coupled simulation of the flow field and electrostatic field. The flow field distribution around the particle and the droplet obtained from the ANSYS Fluent simulation

is combined with particle movement models that take the presence of electrostatic fields into account.

The flow chart of the computational procedures for the co-simulation approach is shown in Fig. 6.1. As shown in this figure, running the command code in MATLAB realises the initialisation of Fluent, and reading data from the monitoring points. The monitoring points are points chosen around the particle and move with the overset system. Overset meshing involves creating multiple, overlapping meshes that cover different parts of the computational domain. These meshes are allowed to overlap with each other, and the solution is interpolated between the meshes in the overlapping regions. This approach is particularly useful for modeling moving parts within a fixed background mesh without the need for re-meshing and allowing localized mesh refinement by using finer meshes in regions of interest without affecting the global mesh. In the computational procedures, the velocity of the monitoring point, which represents the flow field velocity at the particle's position, is read into MATLAB for the calculation of particle movement in MATLAB. While solving the particle movement equation, besides basic movement laws of sphere particles in a flow field, the function of electrostatic force was added to the computational process. Then a description of particle motion at this moment in a gas flow field under the action of a charged droplet in an electrostatic field was obtained. A user-defined function (UDF) is employed to incorporate the effects of electrostatic fields into the simulation procedure. However, the MATLAB solution needs to be converted to C language, which could be recognised by Fluent, before being written into the UDF file. Then the motion UDF was compiled in Fluent software to complete the particle moving simulation. The next step is judging whether the particle is captured by the droplet after simulating under a given time step size. If not, the updated flow

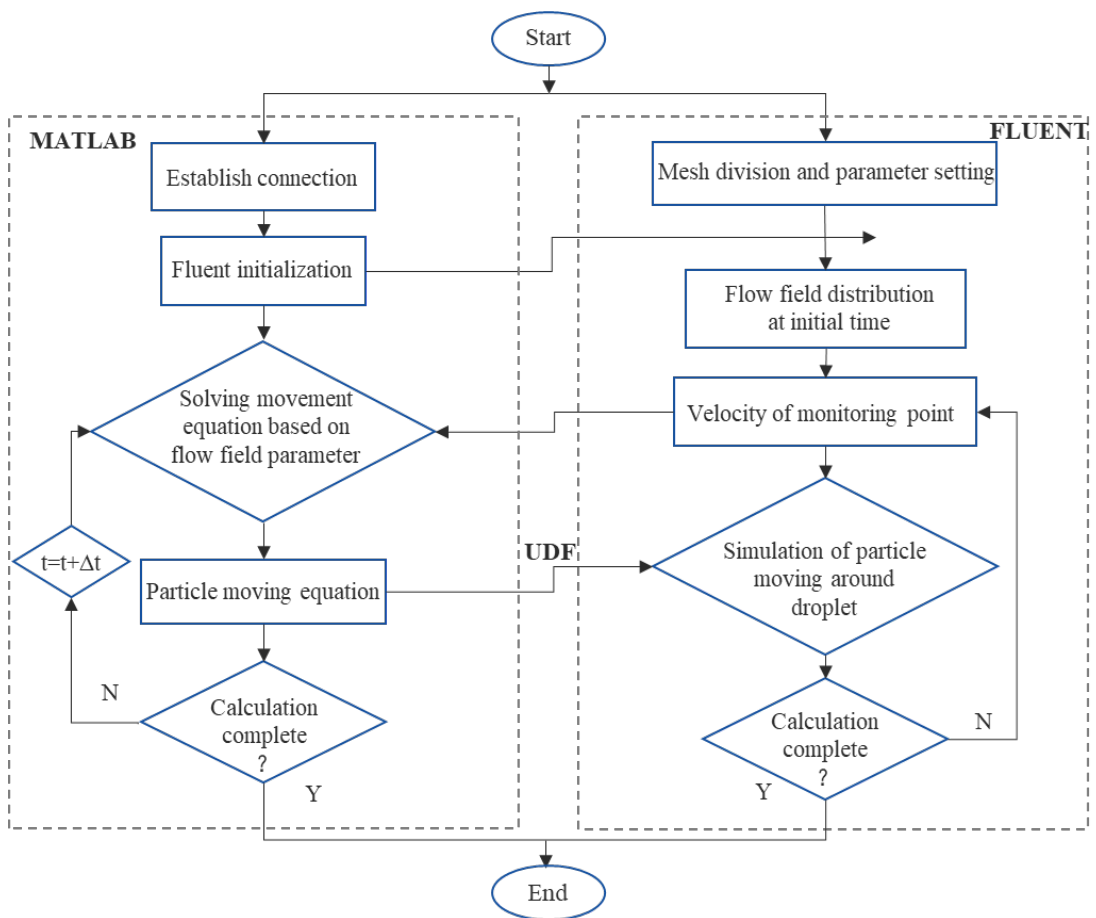


Figure 6.1: Flow chart of the computational procedures for the co-simulation approach.

field data of the monitoring points were rewritten into MATLAB to complete the next iteration. Iterative computation was finished when the particle arrived at the droplet surface. Thus, the simulation of a particle moving towards to droplet under the acting of an electrostatic field was obtained.

6.3 3-D model development

The particle moving numerical model in a wet electrostatic scrubber is shown in Fig. 6.2. The model consists of a cylindrical flue gas channel ($100\text{mm} \times \varnothing 50\text{mm}$), a flue gas inlet and an outlet at both ends of round-through. Detailed design parameters of the model are presented as the properties in Tbl. 5.1. Gravity direction is the opposite direction of X -axis. During the simulation, it was found that the effect of electrostatic force is not obvious when the particle was far from the droplet. Thus, the initial distance between droplet and particle was defined as 6 mm in this simulation model.

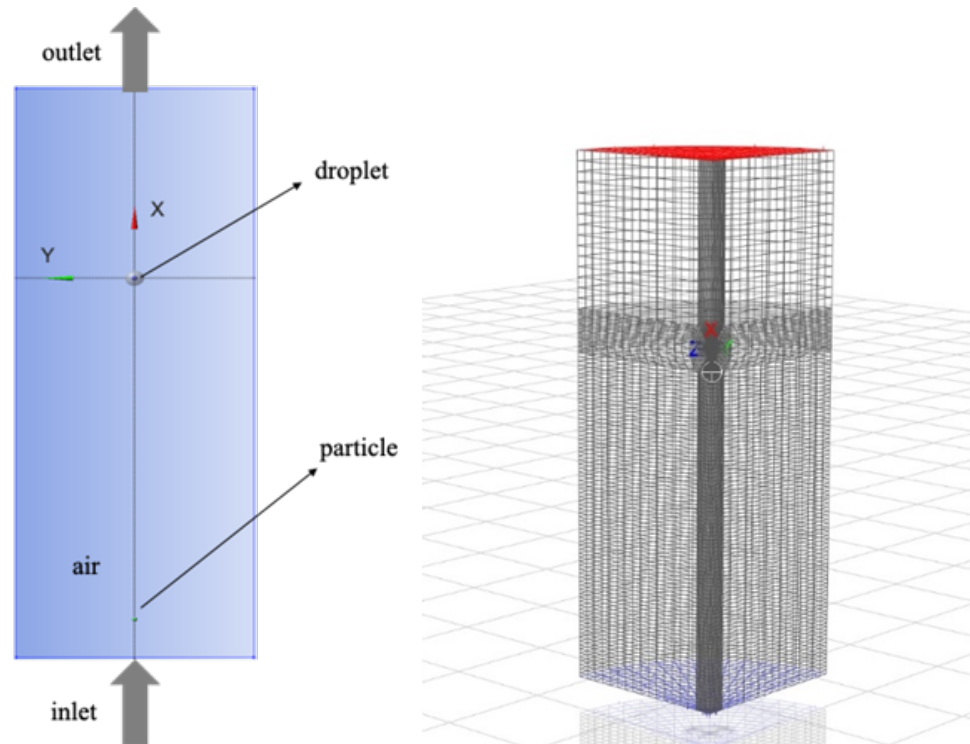


Figure 6.2: Coupled motion model of particle and droplet for simulation.

Figure 6.2 shows the general configurations of the boundary conditions. The inlet velocity was set at the upstream inlet boundary, the below surface of the

tube. Here the fluid material that fully filled the tube was air, whose parameter is the same as flue gas, as shown in Tbl. 5.1. Material of droplet is defined as solid without considering its movement and deformation.

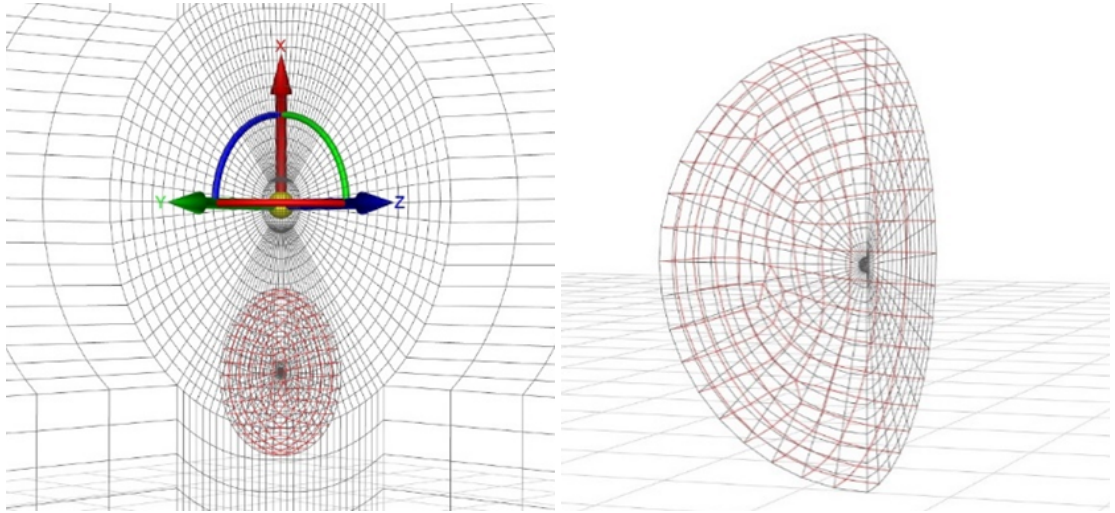


Figure 6.3: Illustration of the particle overset mesh.

Since the model is a rotationally symmetrical structure, to improve the calculation accuracy and operation efficiency, only a quarter of the model is considered in the simulation. According to the mainstream and flow field distribution, the model mesh was divided into several parts and locally refined as well, as shown in Fig. 6.2. The particle moving simulation is based on an advanced overset moving grid method that accurately considers the local and global motion of a three-dimensional wet electrostatic scrubber. The overset mesh system consists of the background mesh, which is the whole computational fluid domain, and the refined overlapping meshes. In the present study, as shown in Fig. 6.3 a sphere overset mesh was designed outside the particle to compute the flow field distribution around the moving particle.

6.4 Co-simulation results

In the co-simulation of flow field distribution in the cylindrical flue gas channel around a solid sphere, the model used is the standard k-epsilon viscous model. The kinetic energy and turbulent dissipation rate equations are both first-order upwind. The particle movement is simulated by adding the motion function on the overset mesh. The motion function, which takes the electrostatic force into consideration, is solved in MATLAB and then written into a UDF file. Figure 6.4 shows a contour plot of the velocity magnitude when the particle is approaching the droplet. It can be seen in this figure, under the presence of electrostatic effect, the velocity of the particle is much greater than that of the surrounding flow field when the particle approaches the droplet surface. Through changing certain model parameters and electrostatic field strengths, simulation results of particle moving characteristics under some features were concluded.

Through the method of co-simulation of ANSYS Fluent and MATLAB, the entire process of a charged particle moving towards the charged droplet in a fuel gas flow field under the effect of electrostatic force can be described. In the meanwhile, the influence of some features on the movement characteristic can be observed by changing the corresponding parameters during simulation.

Referring to the theoretical results, moving processes of different particle sizes and droplet sizes under electrostatic field strength of 20 kV were simulated in this section. Fig. 6.5 demonstrates the velocity change trend with the time of different particle radii (10 μm , 20 μm , 50 μm). Comparing with the mathematical result, a consistent conclusion is obtained that the larger the particle, the greater its velocity will be before being captured. Meanwhile, the velocity of particle is zero

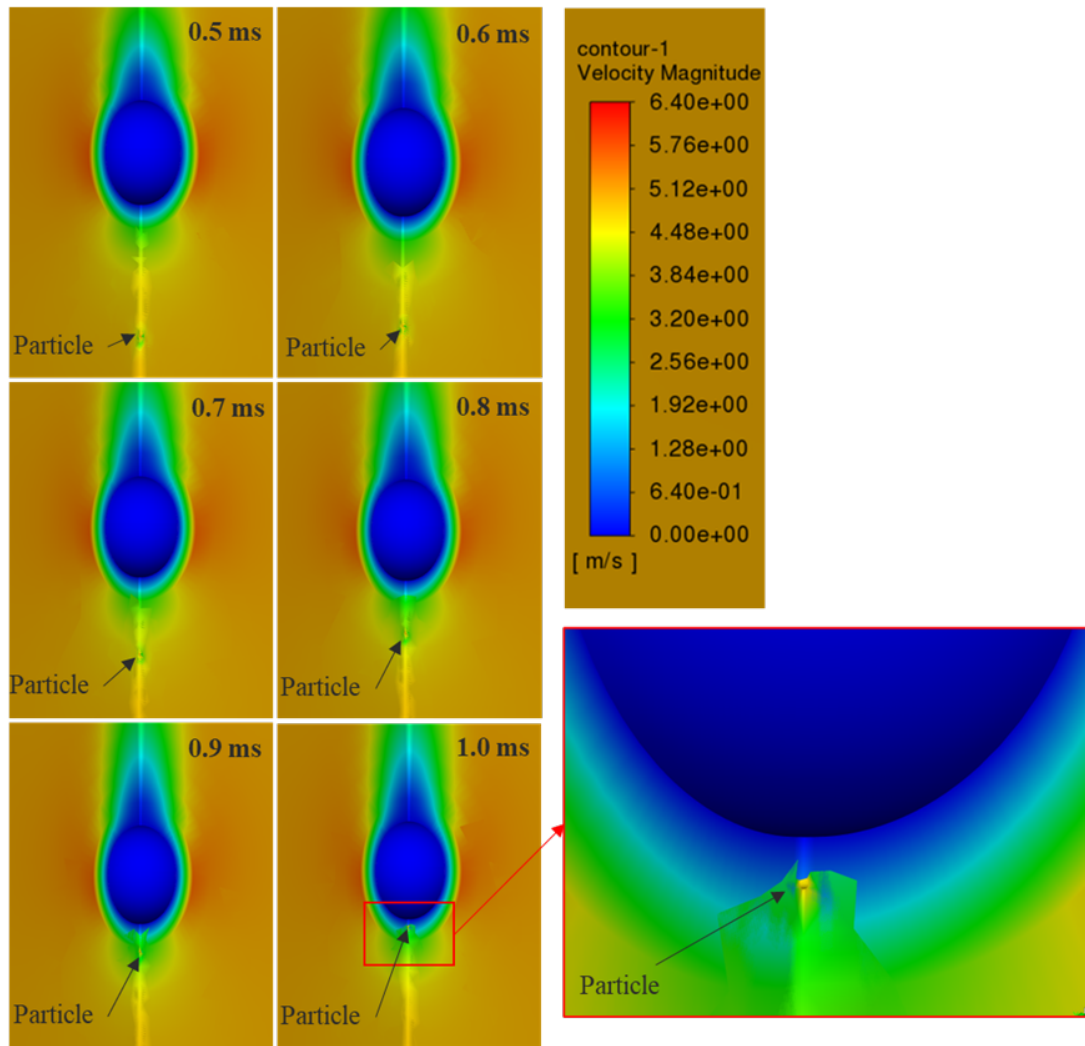


Figure 6.4: Contour plot of the velocity magnitude when the particle is approaching the droplet when droplet radius is 1mm and particle radius is $10\ \mu\text{m}$ and electric field strength is 20kV.

when it arrives at the droplet surface in simulation. Thus, the time when velocity equals zero means the particle arrives at the droplet surface. In Fig. 6.5, under the same movement conditions, for particles with radii of $10\ \mu\text{m}$, $20\ \mu\text{m}$, and $50\ \mu\text{m}$, the lengths of time for them to reach the surface are 1.079 ms, 1.031 ms, and 1.010 ms respectively. The results show that the larger particles are captured faster than the smaller ones under the effect of electrostatic force.

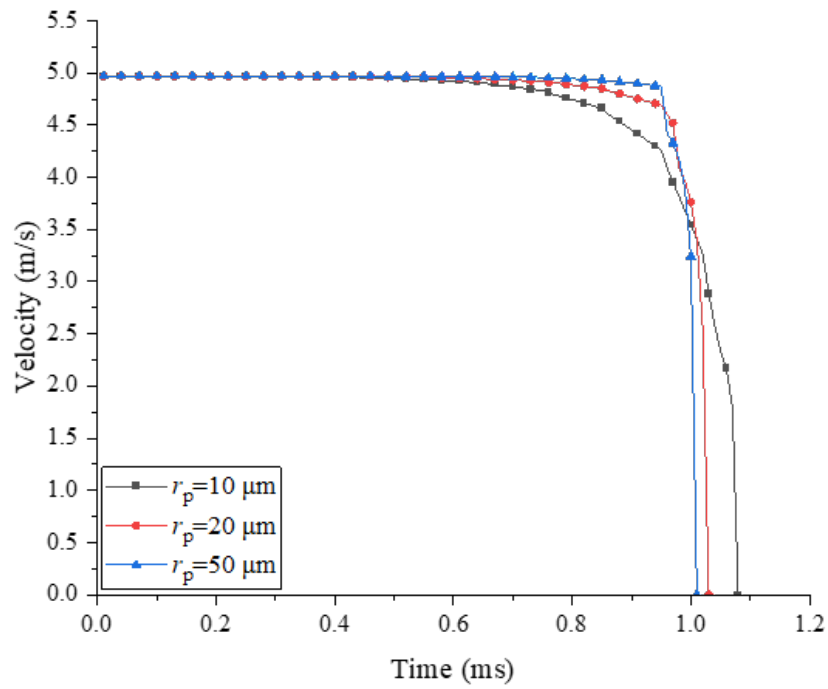


Figure 6.5: Comparison of the velocities of particles with different particle radii when droplet radius is 1 mm.

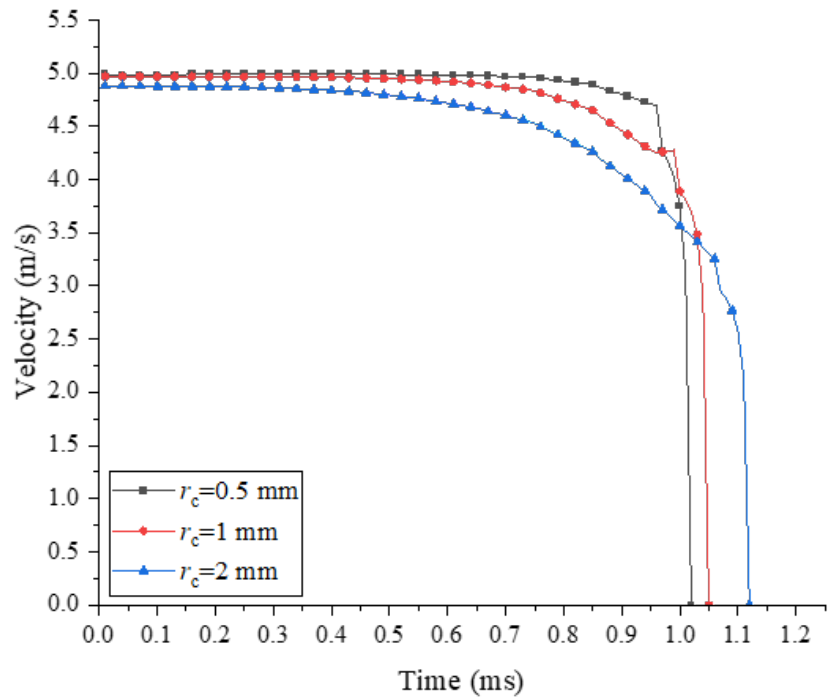


Figure 6.6: Comparison of the velocities of particles with different droplet radii when particle radius is $10 \mu\text{m}$.

As for different droplet sizes, the co-simulation results of velocity change trends are shown in Fig. 6.6. The velocity change tendency of three droplet sizes (0.5 mm, 1 mm, 2 mm) are basically the same as in Fig. 5.8. The tendency indicates that smaller droplet shows a better capture effect. For droplet radii of 0.5 mm, 1 mm, and 2 mm, the time for particles to reach the droplet surface is 1.018 ms, 1.052 ms, and 1.121 ms respectively. Meanwhile, the flow field distribution around the droplet is affected by the droplet size. The increase of droplet size decreases the effect of drag force and increases the effect of electrostatic force. Thus, the velocity of particle around smaller droplets is greater than that around larger droplet. Then, the velocity distributions of particle and flow field during particle motion are conducted when particle sizes are 10 μm and 20 μm . The change in velocity distribution of the flow field along the particle motion path during the particle motion process is obtained in simulation. Figure 6.7 shows the velocity distribution of 0.2 ms, 0.4 ms, 0.6 ms, and 0.8 ms of particle size 10 μm and 20 μm , respectively. The horizontal coordinate represents the position on the motion path. Zero on the horizontal coordinate is the spherical centre of the liquid droplet, whose radius is 1 mm. It can be seen in this figure, during the particle moving process, the velocity difference between the particle and the gas flow field is increasing as the particle approaches the droplet. Comparing the velocity distribution of gas flow field of size 10 μm and size 20 μm particles, it is found that the larger particle has a greater impact on the flow field around it. This impact is mainly manifested in the reduction of flow field velocity in the area where the particles pass through.

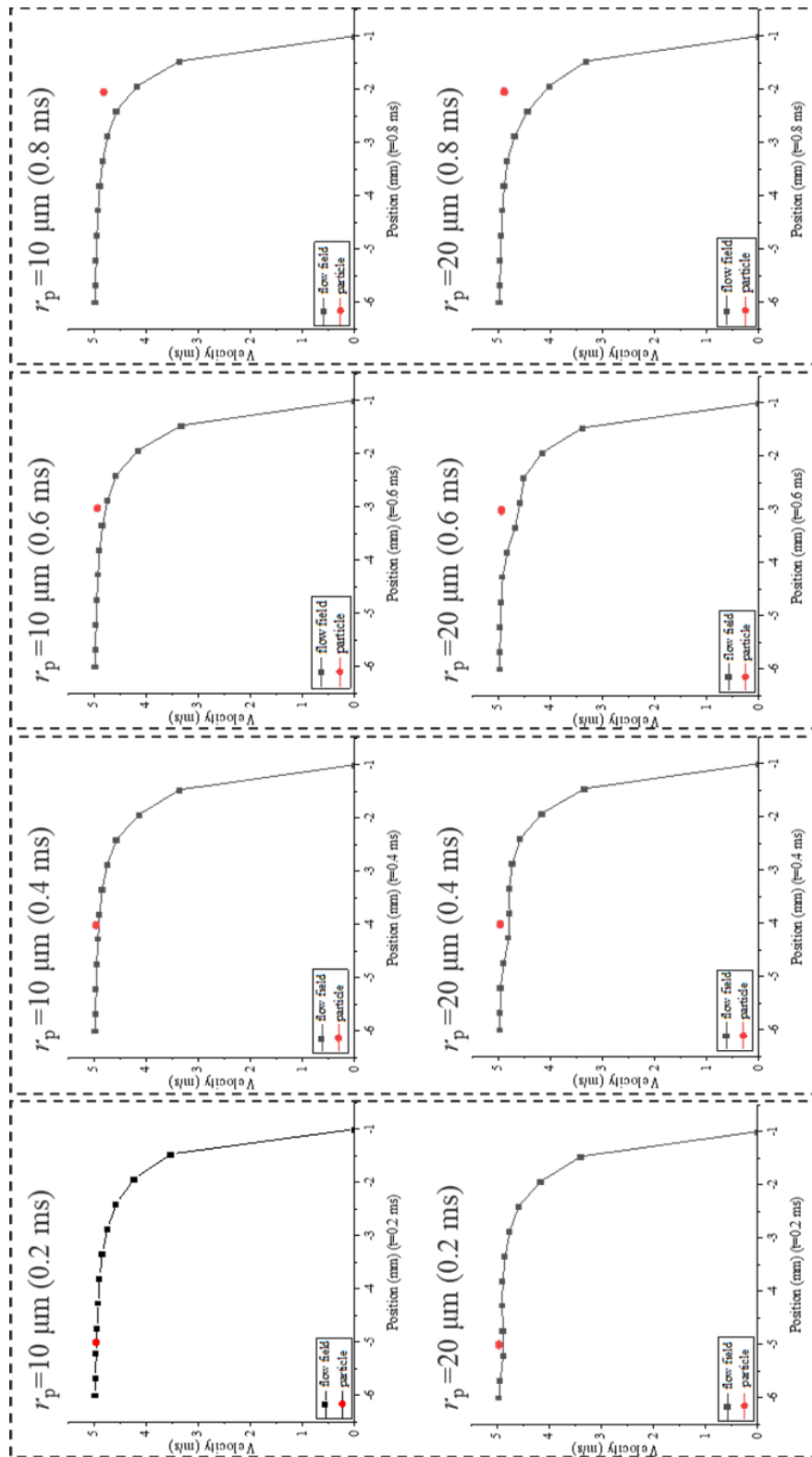


Figure 6.7: Instantaneous velocity distribution plots of particle and flow field when droplet radius is 1 mm and electric field strength is 20 kV.

6.5 Comparison of simulation and theoretical results

Comparing the particle velocity change trend in mathematical and simulation results in Fig. 6.8, the changing tendencies of particle velocity solved in simulation and mathematical model are compared under the electrostatic field strength of 20 kV. The changing trends in these two results show general consistency. The difference between these two results in the last part of Fig. 6.8 is mainly because the influence of the droplet surface on the flow field is ignored in the mathematical calculation, while the droplet surface is regarded as the wall surface in simulation. As a result, the velocity is zero when the particle reaches the droplet surface in simulation, which is not the case in the mathematical calculation. Besides, the velocity change curve in the theoretical results is slightly lower than that of the simulation curve. That is because the surrounding gas flow field velocity is affected by the moving particle, which is ignored in theoretical calculation.

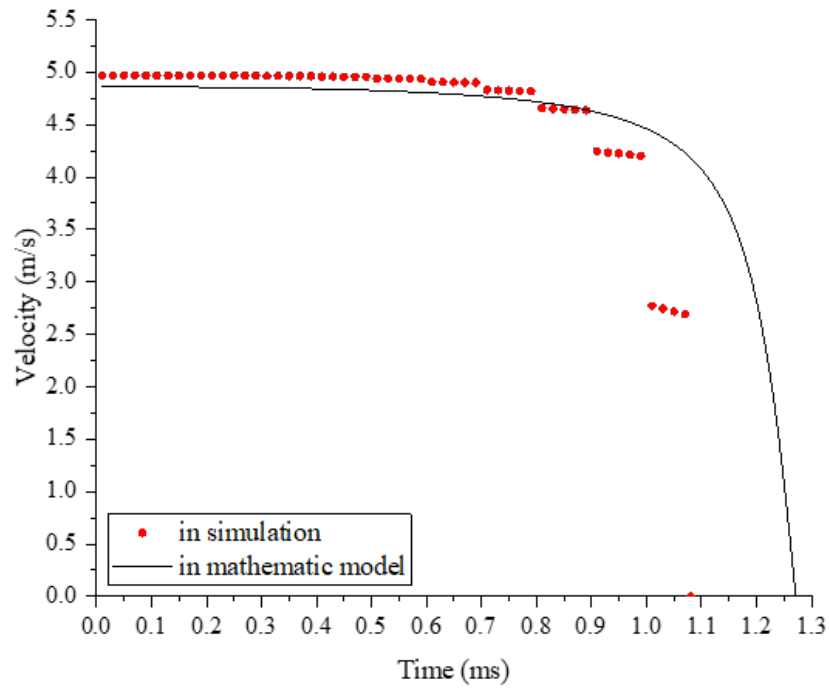


Figure 6.8: Comparison of simulation and theoretical results under the electric field strength of 20 kV.

Figure 6.9 shows the velocity distribution around the droplet and moving particle. It can be seen in this figure that the flow field around the particles is affected by moving particles. The velocity of particles on the windward side increases and the velocity on the leeward side decreases. However, in this simulation condition, the affected area is not large when compared with the droplet size.

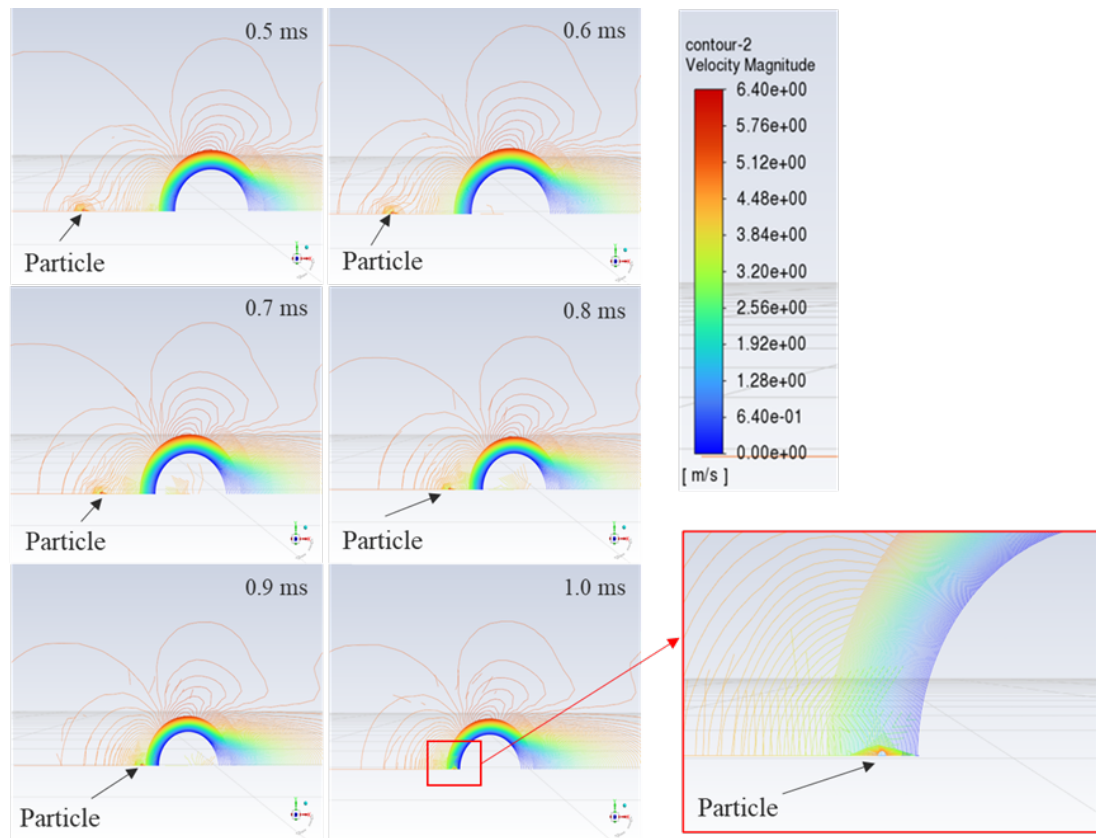


Figure 6.9: Side view of instantaneous velocity magnitude profiles when droplet radius is 1mm and particle radius is $10 \mu\text{m}$ and electric field strength is 20 kV.

The mathematical calculation and simulation results under the condition of 20 kV electrostatic field strength are summarised in Tbl. 6.1 and Tbl. 6.2. Comparing the particle movement characteristics under different particle sizes and droplet sizes, the conclusions obtained from the previous analysis in this thesis are more apparent in this table. Besides, the results for the time it takes for particles to reach the droplet surface in this table are compared in mathematical calculation and in simulation under the same conditions. The relative error ranges from 0.4% to 2.6%, and the average error is 1.5%.

Table 6.1: Results of mathematical calculation and simulation of different particle sizes when droplet radio is 1 mm.

	r_p (μm)	t (ms)	$\Delta\epsilon$
In theory	10	1.051	2.6%
In simulation		1.079	
In theory	20	1.035	0.4%
In simulation		1.031	
In theory	50	1.028	1.8%
In simulation		1.010	

Table 6.2: Results of mathematical calculation and simulation of different droplet sizes when particle radio is 10 μm .

	r_c (mm)	t (ms)	$\Delta\epsilon$
In theory	0.5	1.031	1.3%
In simulation		1.018	
In theory	1	1.051	0.9%
In simulation		1.052	
In theory	2	1.097	2.1%
In simulation		1.121	

These results indicate that co-simulation results and mathematical calculation results are basically consistent, which can be used to describe the charged particle moving characteristics when approaching the oppositely charged droplet in a gas flow field under the effect of electrostatic effect. Also, particle sizes and droplet sizes have a significant influence on the particle motion characteristics.

6.6 Summary

To realise the utilisation of WES on marine vessels, the definition and verification of the theoretical mechanism of this technology are very essential in the research of this field. This chapter established a co-simulation method to simulate the particle motion process towards a droplet in the gas flow field with the electrostatic effect. Through co-simulation of ANSYS Fluent and MATLAB, the simulation of the particle motion being captured by droplet is performed, which verifies the reliability of the mathematical model. Also, the particle motion processes of different particle size and droplet size are simulated separately. Meanwhile, the flow field distribution around the particle during the particle movement can be performed.

The mathematical calculation results and co-simulation results are basically consistent, which indicates that the two methods are both reliable in describing the process of a charged particle moving in gas flow field when attracted by charged droplet. The existence of an electrostatic field can improve the particle velocity when it approaches the droplet, making the velocity greater than that of the surrounding flow field. Meanwhile, this effect is much more obvious with the particle approaching the droplet. Besides, simulation results show that the

moving particle can affect the surrounding velocity of the gas flow field, which is ignored in theoretical calculation. This effect becomes more apparent as the particle size increases.

Chapter 7

Experiment on particle capture process

7.1 Introduction

This chapter integrates an experimental approach to validate the reliability of the mathematical models and simulations used to understand charged particle motion towards a charged droplet. An experiment is designed and detailed, aiming to observe this phenomenon while taking into account variables such as electrostatic field strength. The designed experiment allows for the separate charging of droplets and particulate matter. The droplets remain suspended, while the particles move towards the droplets under the influence of a gaseous flow field and are captured by the droplets under the action of electrostatic forces. In the experiment, parameters such as wind speed and electric field strength can be adjusted through the input device.

The experimental methodology involves monitoring particle motion around the droplet and capturing video footage of particles with clear trajectories. This visual data is then analysed using TRACKER software to extract detailed information on the trajectories and velocities of the particles. At last, the experimental results are analysed and compared with the theoretical results. This approach not only reinforces the theoretical predictions but also provides empirical evidence for a deeper understanding of particle-droplet interactions.

7.2 Experimental set up

Considering the properties of particle emission from marine diesel, the particle used in the experiment are carbon. The standard radius particles are obtained through the process shown in Fig. 7.1. In this process, irregular large carbon particles are ground in a mortar to small size particles. Then by 300 mesh and 2300 mesh stainless steel mesh filter, standard particle radius from $2.5 \mu\text{m}$ to $25 \mu\text{m}$ are obtained. Besides, the liquid of the droplet is water. And the temperature of the condition is $20 \text{ }^\circ\text{C}$. The temperature difference of gas and droplet is not considered in this experiment.

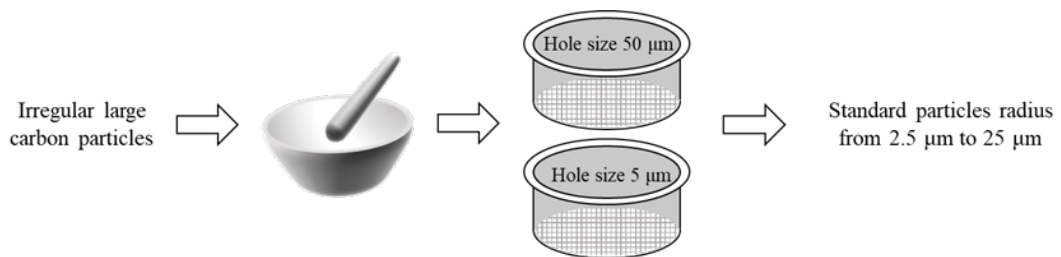
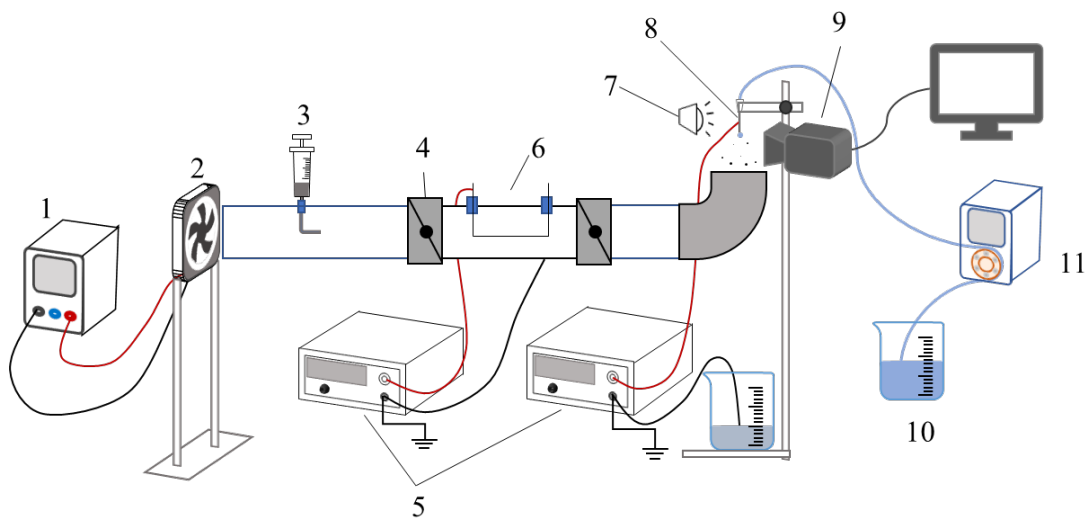


Figure 7.1: Particles production process



- | | |
|---|-----------------------------|
| 1. DC power supply | 6. Particle charging device |
| 2. Fan | 7. Light sources |
| 3. Particle injection | 8. Steel flat ended needle |
| 4. Air valve | 9. High speed camera |
| 5. High voltage electrostatic generator | 10. Water tank |
| | 11. Peristaltic pump |

Figure 7.2: Schematic diagram of the experimental system

The experimental system, as shown in Fig. 7.2, is mainly consist of four parts. The first part is the gas flow field and particle injection section. In this section, gas flow field is generated through a fan blowing wind towards the gas flow pipe. The flow velocity of the wind is controlled by adjusting the voltage of the DC power supply. Then the particles are injected into the mainstream region from a 90-degree tube linked with a syringe. The second part is the particle charging section. In this part, particles moving with the flow gas are charged by metal wire high voltage corona discharge. The third part is the droplet generated section. In this part, a droplet is generated through a peristaltic pump extracting liquid from the water tank to a steel flat-ended needle and hovering at the needle. The droplet is charged through a high voltage electrostatic generator linked to the steel

needle. The fourth part is the particle and droplet intersection section. In this part, high speed camera perpendicular to the particle motion path watches and records the particle motion process to the droplet surface. Relative parameters in the experiment are shown in Tbl. 7.1. The experimental equipment information is shown in Tbl. 7.2.

Table 7.1: Results of mathematical calculation and simulation of different droplet sizes when particle radio is $10\ \mu\text{m}$.

Droplet radius	1 mm
Particle radius	$2.5\ \mu\text{m} - 25\ \mu\text{m}$
Density of particle	$0.145 \times 10^3\ \text{kg/m}^3$
Density of gas fluid	$1.205\ \text{kg/m}^3$
Dynamic viscosity of gas fluid	$1.79 \times 10^{-5}\ \text{Pa}\cdot\text{s}$
Velocity of gas flow field	0.8 m/s
Electric field strength	0 - 8 kV

In the experiment, the velocities of the gas flow at the outlet of the pipeline are 0.8 m/s and 1.5 m/s when the voltage of the fan's power supply is 4 V and 5 V respectively. In the whole flow field, the material of the pipes is PVC in spite of the particle charging device part, which is a stainless steel pipe. Those two high voltage electrostatic generators are one positive high voltage and one negative high voltage respectively. In this experiment, the particles are negative charging, while the droplet is positive charging. The Reynolds number of the particle in the gas flow field is:

$$Re = \frac{\rho_f d_p (u_f - u_p)}{\mu} = 0 - 2.69 \quad (7.1)$$

Table 7.2: Results of mathematical calculation and simulation of different droplet sizes when particle radio is 10 μm .

Equipment Name	Manufacturer	Model Number	Specifications	Function
High-Speed Camera	Optronis	CP80-3-M-540	540 fps, 196×1710 p resolution	Capturing particles motion
High voltage electrostatic generator	GLOW	GLOW28720	0-20 kV	Charging particles and the droplet
Peristaltic pump	Kamoer	KSP-F01A	AC 100-240V, 50-60Hz, 1.01A max	Extract liquid and generate one droplet
DC power supply	WANPTEK	GPS3010D	Input: AC230V, Output: 0-32V	Provide continuously adjustable voltage for the fan

7.3 Data processing of particle moving towards the droplet

In the experiment, a high-speed camera is used to record the particle motion process when it approaches the droplet surface. A microlens is linked to the high-speed camera to zoom in on the watching zone. The camera focuses on the lower surface of the droplet to record the particles moving with the gas flow field upwards to the lower surface of the droplet. A light source behind the droplet and opposite and on the same horizontal line as the lens. During the experiment, the window size of the high-speed camera is 512×512 (resolution ratio). The frame rate is 4000 frames per second. Start running the experimental system until motion particles appear in the camera and start recording the video.

Those recorded videos then are processed by the software TRACKER. In this software, the particle of clear trajectory is chosen to be tracked. Fig. 7.3 shows an example of particle trajectory processed by the software. The red points in the picture represent the particle position of each frame. The black sphere is the droplet. The gas fluid field flows upwards in the vertical direction. It can be seen in this figure, that on the seventh frame, the particle reaches the droplet surface at last. In this figure, the particle's trajectory is tracked. The final position of the particle reaching the surface of the droplet is set as the coordinate origin. Then a coordinate system is established. And according to the position of the particle per frame, the velocity of the particle can be obtained.

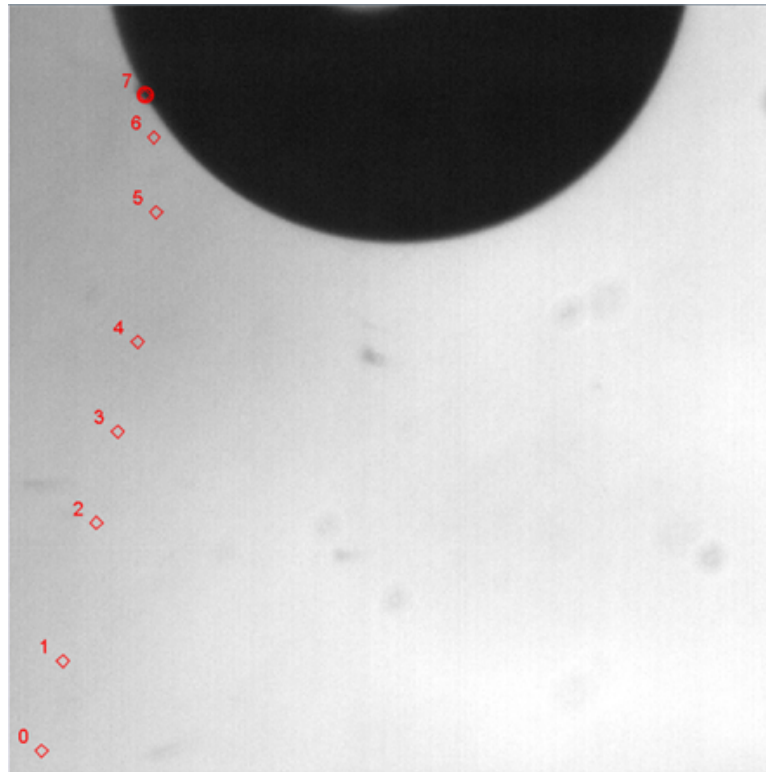


Figure 7.3: An example of particle trajectory processed by the software.

7.4 Particle motion behaviour of different conditions

Particles moving to the droplet under different electrostatic field strengths were recorded in the experiment. During the experiment process, adjusting the electric field strength generated by the high-voltage electrostatic generator to change the charge of particles and droplets. Then the electric force between the particles and the droplet is changed. The charge on the particles is achieved by their contact with stainless steel wires connected to a high-voltage electrostatic generator in the particle charging device as shown in Fig. 7.2. The charge on the droplet is achieved by the steel flat ended needle connected with a high-voltage

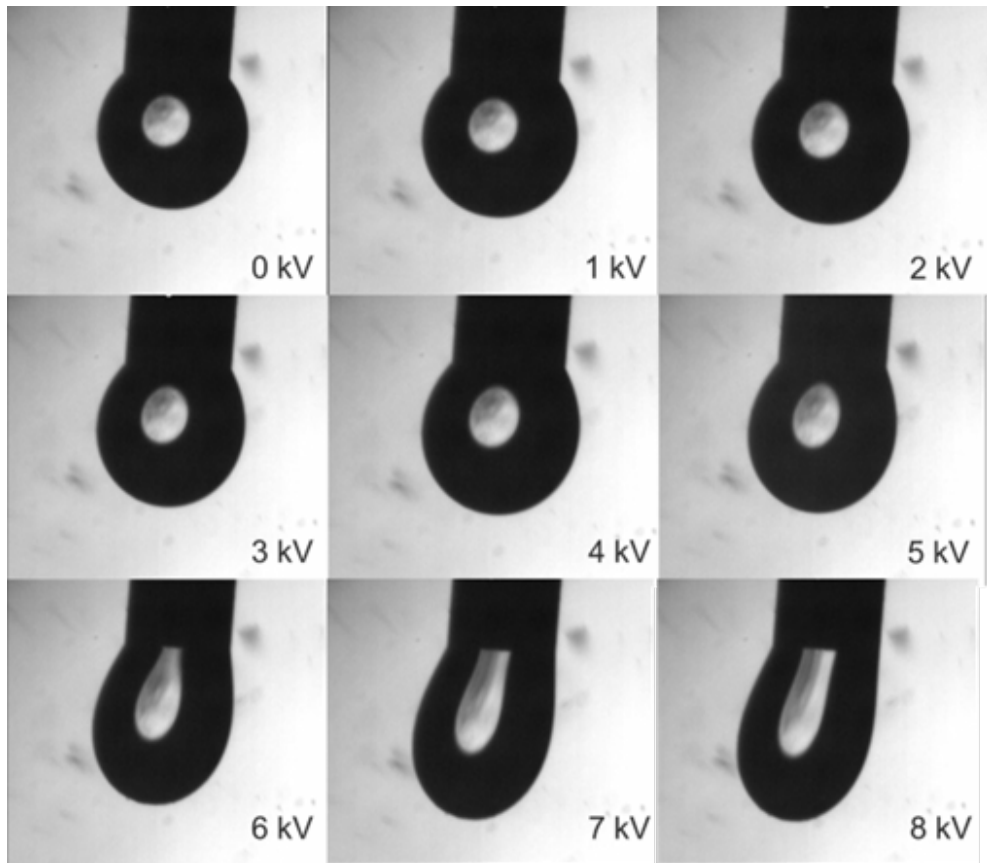


Figure 7.4: Droplet deformation with the electric field strength increases.

electrostatic generator, which also is shown in Fig. 7.2. In the experiment, the electrodes of the two high-voltage electrostatic generators, which are used to charge particles and the droplet respectively, are opposite. And the electric field strengths of them are same in value. During the experiment, open the fan and start injecting particles when the electrostatic generator reaches a stable output state, and then begin recording.

The value range of electric field strength in the experiment is from 0 kV to 8 kV. When the electric field strength is beyond the range, the droplet will deform and fall off the needle. Fig. 7.4 shows the change of droplet shape when the electric field strength increases from 0 kV to 8 kV. As shown in Fig. 7.5, an

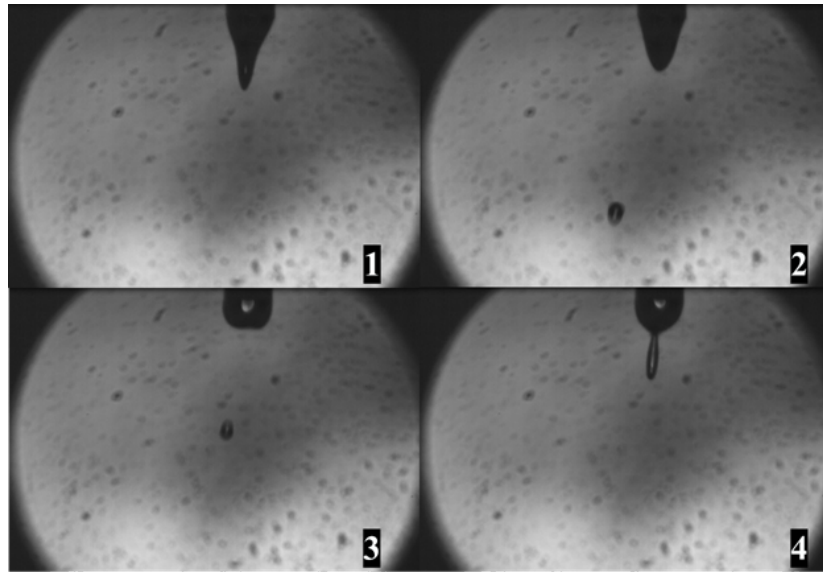


Figure 7.5: Droplet deform and fall off when the electric field strength is 10 kV.

example of a droplet deforms and falls off from the needle when the electric field strength is 10 kV. The number 1 to 4 in this figure shows four frames of images captured from a video sequence. Thus, in the experiment, watching the particles movement around a static droplet, the droplet is expected to be kept stationary at the end of the tube. The electric field strength is chosen between the range of 0 kV to 8 kV.

As shown in Fig. 7.6, a series particle motion trajectory was obtained under the electric field strengths of 0 kV, 2 kV, 4 kV, and 5 kV when the gas flow field velocity is 0.8 m/s and the droplet size is 1 mm in radius. The right part of this figure shows four images representing particle motion trajectories obtained in the experiment of four electric field strengths respectively.

It can be concluded from the figure that for all electrostatic field strength the particle velocity decreases as the distances to the droplet surface approaches 0 mm. When the electrostatic field strength is zero, the velocity remains relatively

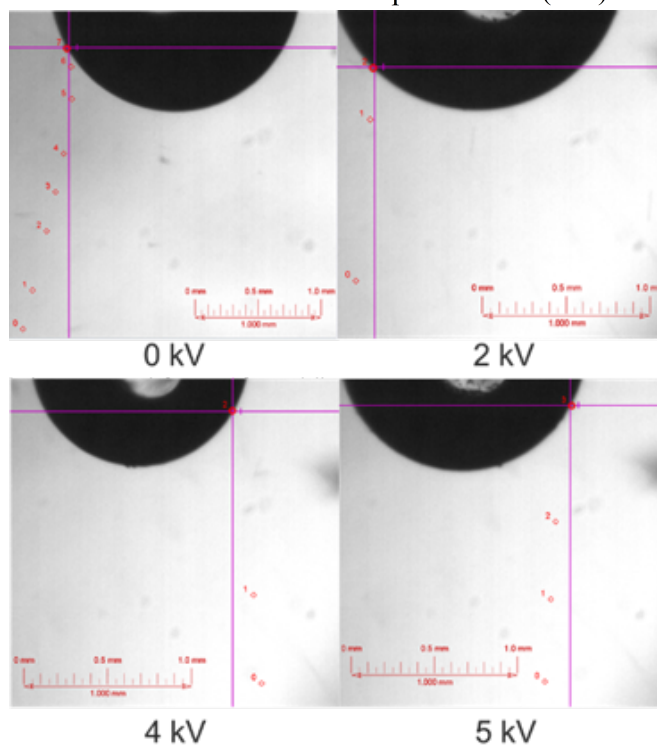
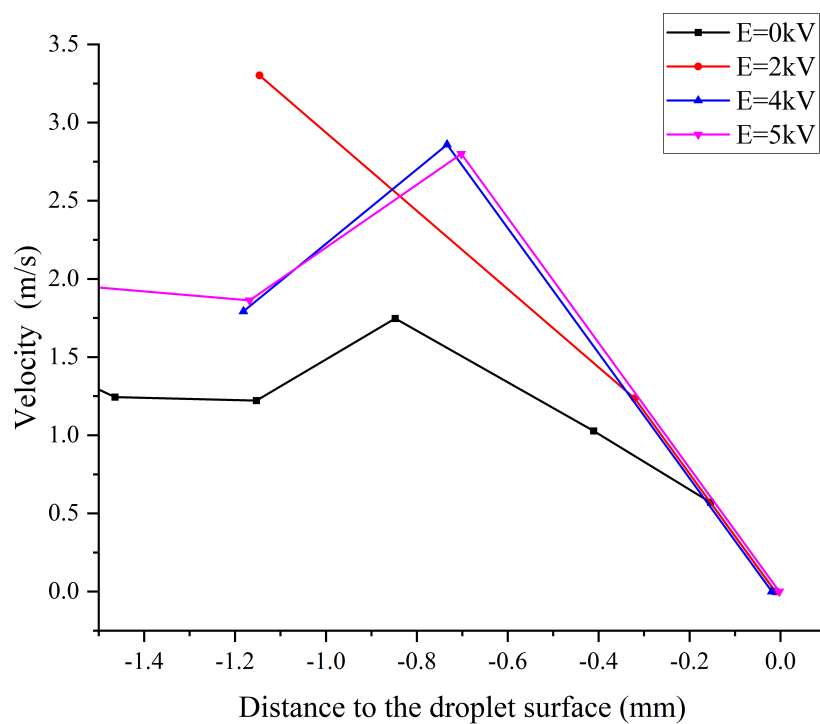


Figure 7.6: Velocity distribution before arriving at the droplet surface under different electrostatic field strengths in lab condition.

constant across the range of distances, with a slight fluctuation as it gets closer to the droplet surface. The exist of an electrostatic field helps increase the particle motion velocity before arriving at the droplet surface when compared with the condition of without the electrostatic field. At $E=2$ kV, the velocity decreases steadily as the distance to the droplet surface decreases. $E=4$ kV and $E=5$ kV show similar behaviour, they both have a slight increase before declining sharply towards 0 m/s at the droplet surface. The presence of an electric field (values greater than 0 kV) influences the velocity of particles. The higher the electric field strength, the more pronounced the variation in velocity as one approaches the droplet surface. In summary, this graph indicates that the electric field strength has a significant effect on the velocity profile as one approaches the droplet surface.

7.5 Experimental results

Taking the condition of a 4-kilovolt electric field strength as an example, compare the particle motion characteristics in experimental and theoretical results. To avoid the influence of randomness during the experimental process as much as possible, an average of six sets of experimental data under the same lab condition was obtained. Fig. 7.7 shows a comparison of particle velocity distribution on the distance to the droplet surface between the velocity from the theoretical calculation and the average velocity observed in a lab experiment.

The black line with white square markers represents the theoretical velocities. The red line with circular markers represents the average velocities of data 1 to 6 observed in lab experiments. Both the theoretical and experimental data show that particle velocity decreases as the distance to the droplet surface gets

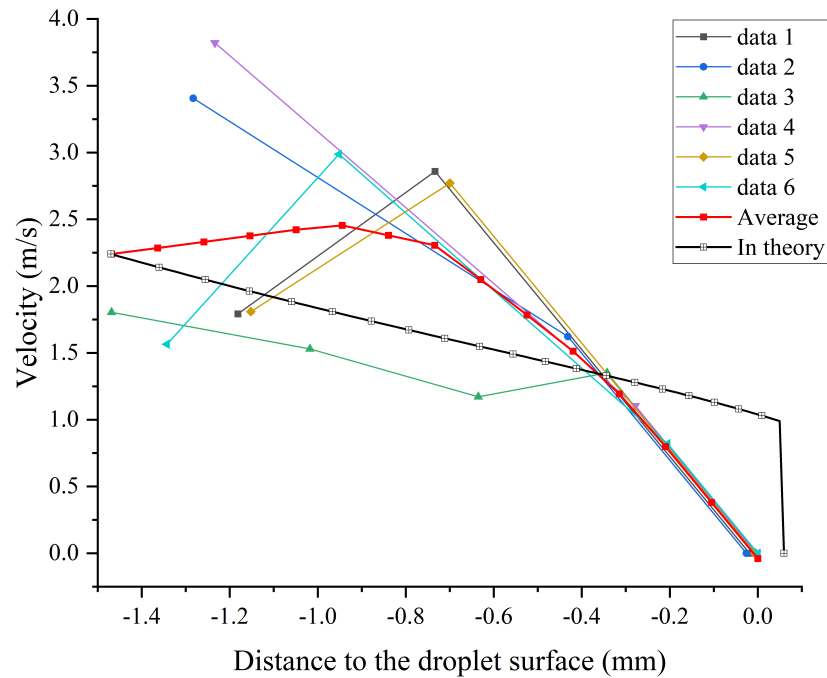


Figure 7.7: Comparison of particle velocity distribution before arriving at the droplet between the theoretical result and experimental test data.

closer to 0 mm. There is a fluctuation in the lab measured velocity and the lab measurements show a more rapid decrease in velocity, reaching zero well before the droplet surface, while the theoretical model predicts a more gradual decline until it hits the droplet surface. The discrepancy is mainly caused by simplifications in the theoretical model, where the flow field is steady, and the influence of the droplet boundary layer is ignored. Meanwhile, the gas flow distribution around the particle could be influenced by the moving particle, which is found in the co-simulation research work. This affection is not considered in the theoretical calculation and may also cause the difference between the theoretical result and experimental test data.

Standard deviation is a measure of the dispersion or variability of a set of data points around the mean. A lower standard deviation indicates that the data

points are close to the mean, while a higher standard deviation suggests greater spread or variability [100–102]. The equation for standard deviation (σ) is as follows:

$$\sigma = \sqrt{\frac{1}{N} \sum_{i=1}^N (x_i - \bar{x})^2} \quad (7.2)$$

where: σ is the population standard deviation. N is the total number of data points. x_i represents each data point. \bar{x} is the population mean.

In this experiment, the standard deviation was used to quantify the variability in particle motion velocities, providing insight into the consistency of the results under different conditions. A smaller standard deviation suggests that the measurements were consistent across trials, whereas a larger standard deviation indicates greater variability. A result of the standard deviation calculated from the experiment data from Fig. 7.7 could be found in Fig. 7.8. The figure illustrates the standard deviation (σ) of six experimental data sets plotted against the distance to the droplet surface (in mm). The standard deviation (σ) gradually decreases as the distance to the droplet surface reduces, approaching zero at the surface (0 mm). The decreasing trend in the standard deviation suggests that the variability of the measured parameter diminishes as the measurements are taken closer to the droplet surface. This indicates more uniform conditions near the droplet surface. Thus, the experimental results around the droplet surface are much more reliable.

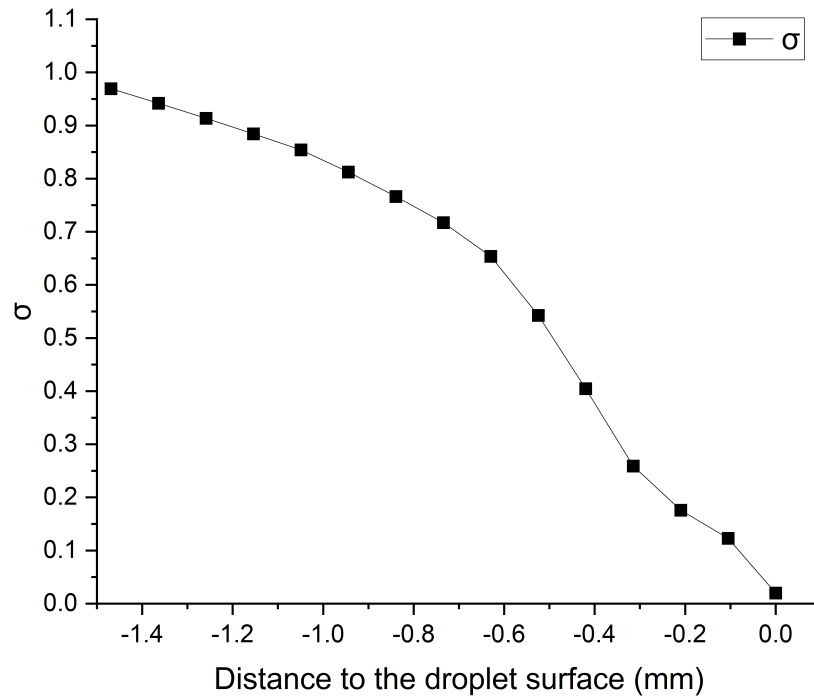


Figure 7.8: Standard deviation for six sets of experimental data

The theoretical model describes the motion process of charged particles being captured by a charged droplet due to the influence of electric field forces when an electrostatic field is present. Although the impact of the electrostatic forces on the collection efficiency cannot be intuitively determined from the results of this theoretical model, the effect of the electric field strength on the collection outcome can be observed by examining the adhesion of particles to the droplet surface under different electric field intensities during the experimental process.

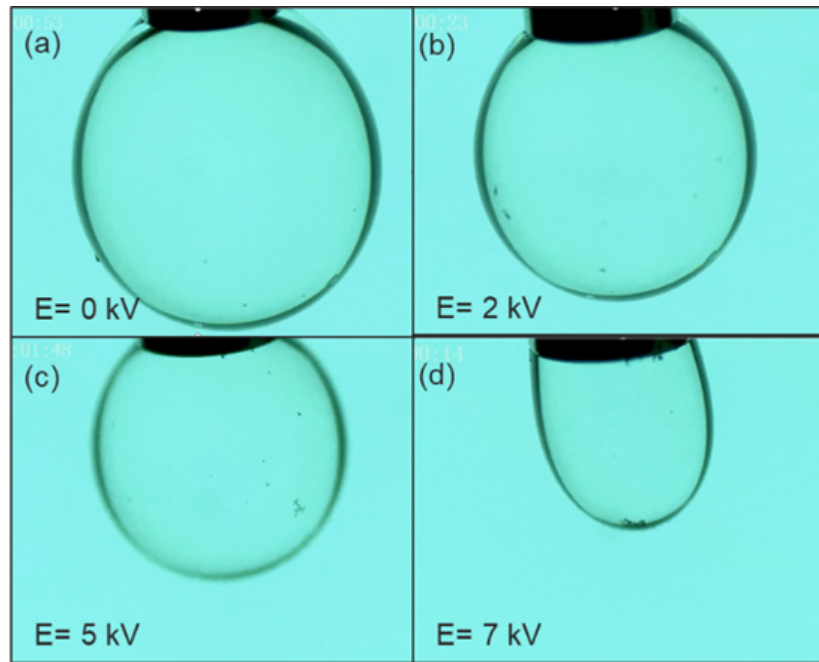


Figure 7.9: Four photographs taken during an experiment involving particle adhesion on a droplet under varying electric field strengths.

Figure 7.8 shows four photographs taken during an experiment involving particle adhesion on a droplet under varying electric field strengths. In this figure, (a) shows the electrostatic field strength is 0 kV indicating no electric field is applied. The droplet appears clear with minimal to no visible particles attached to it. Image (b) shows a condition when electrostatic field strength is 2 kV indicating a low electric field strength is applied. There are a few particles visible, slightly more than in image (a). Image (c) shows a condition when electrostatic field strength is 5 kV indicating a moderated electric field strength. There is a noticeable increase in the number of particles attached to the bottom of the droplet. Image (d) shows a condition when electrostatic field strength is 7 kV indicating a high electric field strength. Here, the accumulation of particles is much greater, especially at the bottom of the droplet, which appears to be heavily coated by the particles.

The experiment visually demonstrates the effect of electric field strength on the adhesion of particles to the droplet surface. As the electric field strength increases, the number of particles adhering to the droplet surface also increases. This suggests that electrostatic forces are indeed influencing the capture efficiency of the droplet, capturing more particles as the field strength rises. The theoretical model introduced in this thesis shows that electric field strength affects the motion process of charged particles before capture by the oppositely charged droplet. The particle velocity increases before arrives at the droplet surface when a high electric field strength is applied, which may have a relationship with the collection efficiency of the particles captured by the droplet. To learn the relationship between them, further research may be needed on the interaction between particles and droplet surfaces, which is expected to be conducted in future research.

7.6 Summary

Firstly, this chapter introduces the design and construction of the test bench, detailing the equipment used and the settings of experimental parameters. Additionally, a comprehensive overview of the experimental process is provided, including the methodologies for data collection and analysis. In the experiment, particle movement towards a droplet under various electrostatic field strengths, ranging from 0 kV to 8 kV, was observed. The charge of particles and droplets was manipulated using a high-voltage electrostatic generator. The experiment showed that particle velocity decreases as it gets closer to the droplet surface, with the decrease becoming more pronounced at higher electric field strengths. Observations also included the deformation and detachment of droplets at higher

field strengths, particularly at 10 kV. The study underscores the significant impact of electric field strength on particle movement behaviour near the droplet surface.

This chapter presents a comparison between the theoretical calculations and experimental observations of particle movement as they approach a droplet under the influence of a 4-kilovolt electric field. An average of six sets of experimental data were obtained under controlled lab conditions to minimise randomness. The comparison of theoretical and experimental particle velocities as they approach the droplet surface is illustrated, highlighting differences like the more rapid velocity decrease observed in the lab. This discrepancy could stem from various factors, such as experimental errors or oversimplifications in the model. Additionally, the effect of the moving particle on the surrounding gas flow, found in co-simulation research but not included in the theoretical calculations, might contribute to these differences. It is also explored in this chapter that the influence of electric field strength on particle adhesion to the droplet surface is visually demonstrated through photographs under varying field intensities. This visual evidence supports the idea that increasing electrostatic forces enhance particle capture efficiency, a concept backed by the theoretical model. This leads to the suggestion that further research is necessary to understand the detailed interaction between particles and the droplet surface.

Chapter 8

Conclusions and future work

8.1 Conclusions

The mechanism of the particle motion towards a droplet under the effect of an electrostatic field is studied in this work. In this condition, particles suspended in the gas are attracted by a droplet under the effect of both the gas flow field and the electrostatic field. In this work, a mathematical model is established, which describes the particle motion in the flow field around a sphere and also adds the electric field effect. Besides, the thermodynamic effect is considered in the model, which caused because of the temperature difference between the gas and the droplet.

To simulate the particle motion process and watch the surrounding flow condition, a method of co-simulation of Ansys Fluent and Matlab is utilized in this research, which combines the electric force into the particle movement in the gas flow field.

Besides, an experiment is laid out to watch and record the particle motion process around the droplet surface under different electrostatic field conditions. Meanwhile, the phenomenon of particle adhesion on the droplet surface under an electrostatic field is watched in this experiment. Through analysing the research results obtained from these three approaches, several conclusions could be concluded as follows:

1. A theoretical framework has been developed to describe the motion of particles in a flow field when captured by electrostatic droplets. The analytical solution considers both thermodynamics and electrohydrodynamics, providing a comprehensive description of particle motion in a Water Electrostatic Sprayer (WES) where both particles and droplets are charged.
2. The theoretical analysis and simulation results reveal that an electrostatic field enhances the velocity of particles as they approach the droplet surface. However, the increase in particle velocity prior to reaching the droplet surface is not pronounced, due to the relatively weaker electrical forces compared to drag forces. The relative error between mathematical calculation and in simulation ranges from 0.4% to 2.6%, and the average error is 1.5%. Additionally, the study shows that the electrostatic effect is more significant for larger particles. The droplet size also plays a crucial role, with smaller droplets improving particle collection efficiency.
3. Co-simulation studies indicate that the gas flow around a moving particle can be influenced by the particle itself, a phenomenon not accounted for in the theoretical models. This interaction may partly explain the discrepancies observed between the theoretical predictions, co-simulation results, and experimental data.

4. Experimental observations show that beyond a certain threshold of electrostatic field strength, spherical droplets undergo shape deformation. This deformation can hinder the observation of particle motion near the droplet surface. Consequently, the applied electrostatic field strength in experiments is maintained within a specific range to prevent such deformation and ensure accurate measurement.
5. The experimental results not only corroborate the theoretical findings but also provide visual evidence that charged droplets effectively capture charged particles. The adhesion of particles to the droplet surface increases with higher electric field strengths, significantly enhancing particle capture efficiency.

According to the presented work, the main objectives of the subject have been achieved which provide a theoretical method to describe the particle movement behaviour in WES and can be considered as a theoretical foundation of charged particles captured by charged droplets in the flow field for further study in the relative field.

8.2 Recommendations for future research

Due to the complexity of the research topic and the time constraints. There are several things that need further study in order to make a better analysis of the WES on particles captured before actual application.

Firstly, this study mainly focuses on the particle motion process before arriving at the droplet surface. The effect of an electrostatic field on one particle

movement when captured by a droplet in a gas flow field is mainly considered in this research. However, as a complete process of particles captured by a droplet, the particle behaviour after arriving at the droplet surface is also crucial. The particle droplet interaction is important in particle capturing process. Further research should focus on the interaction on the droplet surface based upon the research in this work with considering about the effect made by the electrostatic field. By analysing the particle behaviour on the droplet surface, the effectiveness of particle captured by the droplet under an electrostatic field could be obtained. Further identify the range of electric field intensities that can efficiently capture particles, considering various characteristics of emission gases and operating environments.

Secondly, in this study, the motion characteristics of individual charged particle were considered in the gas flow field around the charged droplet. The charged particle moves in the gas flow field on the same axis as the charged droplet. The drag force and the electrostatic force, that acting on the particle are on the same vertical axis. There are no external forces in the other directions. In subsequent research, the number of particles can be increased while considering the effects between charged particles. The force analysis may be more complicated.

Finally, in the present research work, the droplet is the sphere and is considered to be static in the gas flow field. In the theoretical model, the gas flow field distribution around the droplet is considered as the flow distribution around a sphere. But in the practical condition, the shape of the droplet may change in the flow or because of the electrostatic field effect. Thus, there may be some differences between the theoretical results and the reality phenomenon. Further research may should take this feature into consideration.

Bibliography

- [1] James J. Corbett, Paul S. Fischbeck, and Spyros N. Pandis. Global nitrogen and sulfur inventories for oceangoing ships. *Journal of Geophysical Research Atmospheres*, 104(D3):3457–3470, 2 1999.
- [2] Øyvind Endresen, Eirik Sørgård, Jostein K. Sundet, Stig B. Dalsøren, Ivar S.A. Isaksen, Tore F. Berglen, and Gjermund Gravir. Emission from international sea transportation and environmental impact. *Journal of Geophysical Research: Atmospheres*, 108(17), 9 2003.
- [3] V. Eyring, Ivar S.A. Isaksen, Terje Berntsen, William J. Collins, James J. Corbett, Oyvind Endresen, Roy G. Grainger, Jana Moldanova, Hans Schlager, and David S. Stevenson. Transport impacts on atmosphere and climate: Shipping. *Atmospheric Environment*, 44(37):4735–4771, 12 2010.
- [4] V. Eyring, H. W. Köhler, J. Van Aardenne, and A. Lauer. Emissions from international shipping: 1. The last 50 years, 9 2005.
- [5] Cristina B.B. Guerreiro, Valentin Foltescu, and Frank de Leeuw. Air quality status and trends in Europe. *Atmospheric Environment*, 98:376–384, 12 2014.
- [6] *ITF Transport Outlook 2019*. ITF Transport Outlook. OECD, 5 2019.

- [7] Bo Lu, Xi Ming, Hongman Lu, Deyang Chen, and Hongbo Duan. Challenges of decarbonizing global maritime container shipping toward net-zero emissions. *npj Ocean Sustainability*, 2(1), 8 2023.
- [8] Chin Ko Yeh, Chitsan Lin, Hsueh Chen Shen, Nicholas Kiprotich Cheruiyot, Duy Hieu Nguyen, and Chi Chung Chang. Real-time energy consumption and air pollution emission during the transpacific crossing of a container ship. *Scientific Reports*, 12(1), 12 2022.
- [9] T. C. Bond, S. J. Doherty, D. W. Fahey, P. M. Forster, T. Berntsen, B. J. Deangelo, M. G. Flanner, S. Ghan, B. Kärcher, D. Koch, S. Kinne, Y. Kondo, P. K. Quinn, M. C. Sarofim, M. G. Schultz, M. Schulz, C. Venkataraman, H. Zhang, S. Zhang, N. Bellouin, S. K. Guttikunda, P. K. Hopke, M. Z. Jacobson, J. W. Kaiser, Z. Klimont, U. Lohmann, J. P. Schwarz, D. Shindell, T. Storelvmo, S. G. Warren, and C. S. Zender. Bounding the role of black carbon in the climate system: A scientific assessment. *Journal of Geophysical Research Atmospheres*, 118(11):5380–5552, 6 2013.
- [10] Francesco Di Natale and Claudia Carotenuto. Particulate matter in marine diesel engines exhausts: Emissions and control strategies. *Transportation Research Part D: Transport and Environment*, 40:166–191, 2015.
- [11] V Eyring, D S Stevenson, A Lauer, F J Dentener, T Butler, W J Collins, K Ellingsen, M Gauss, D A Hauglustaine, I S A Isaksen, M G Lawrence, A Richter, J M Rodriguez, M Sanderson, S E Strahan, K Sudo, S Szopa, T P C Van Noije, and O Wild. Atmospheric Chemistry and Physics Multi-model simulations of the impact of international shipping on Atmospheric Chemistry and Climate in 2000 and 2030. Technical report, 2007.

- [12] Harshit Agrawal, William A. Welch, J. Wayne Miller, and David R. Cocker. Emission measurements from a crude oil tanker at sea. *Environmental Science and Technology*, 42(19):7098–7103, 10 2008.
- [13] Harshit Agrawal, Quentin G.J. Malloy, William A. Welch, J. Wayne Miller, and David R. Cocker. In-use gaseous and particulate matter emissions from a modern ocean going container vessel. *Atmospheric Environment*, 42(21):5504–5510, 7 2008.
- [14] Robert M. Healy, Ian P. O’Connor, Stig Hellebust, Arnaud Allanic, John R. Sodeau, and John C. Wenger. Characterisation of single particles from in-port ship emissions. *Atmospheric Environment*, 43(40):6408–6414, 2009.
- [15] L. Johansson, J. P. Jalkanen, J. Kalli, and J. Kukkonen. The evolution of shipping emissions and the costs of recent and forthcoming emission regulations in the northern european emission control area. *Atmospheric Chemistry and Physics*, 13(6):16113–16150, 2013.
- [16] Shanem Murphy, Harshit Agrawal, Armin Sorooshian, Luz T. Padró, Harmony Gates, Scott Hersey, W. A. Welch, H. Jung, J. W. Miller, David R. Cocker, Athanasios Nenes, Hafliði H. Jonsson, Richard C. Flagan, and John H. Seinfeld. Comprehensive simultaneous shipboard and airborne characterization of exhaust from a modern container ship at sea. *Environmental Science and Technology*, 43(13):4626–4640, 7 2009.
- [17] L. Ntziachristos, E. Saukko, K. Lehtoranta, T. Rönkkö, H. Timonen, P. Simonen, P. Karjalainen, and J. Keskinen. Particle emissions characterization from a medium-speed marine diesel engine with two fuels at different sampling conditions. *Fuel*, 186:456–465, 12 2016.

- [18] Mar Viana, Fulvio Amato, Andrés Alastuey, Xavier Querol, Teresa Moreno, Saúl García Dos Santos, María Dolores Herce, and Rosalía Fernández-Patier. Chemical tracers of particulate emissions from commercial shipping. *Environmental Science and Technology*, 43(19):7472–7477, 10 2009.
- [19] R WHO. Review of evidence on health aspects of air pollution—REVIHAAP Project. *Technical Report*, 2013.
- [20] Mar Viana, Pieter Hammingh, Augustin Colette, Xavier Querol, Bart Degraeuwe, Ina de Vlieger, and John van Aardenne. Impact of maritime transport emissions on coastal air quality in Europe, 2014.
- [21] Lasse Johansson, Jukka Pekka Jalkanen, and Jaakko Kukkonen. Global assessment of shipping emissions in 2015 on a high spatial and temporal resolution. *Atmospheric Environment*, 167:403–415, 2017.
- [22] Alexandra Monteiro, Michael Russo, Carla Gama, and Carlos Borrego. Shipping emissions and their impact on air quality in urban coastal areas: Present and future scenarios. In *WIT Transactions on the Built Environment*, volume 186, pages 145–151. WITPress, 2019.
- [23] Huan Liu, Xinxin Jin, Luolin Wu, Xuemei Wang, Mingliang Fu, Zhaofeng Lv, Lidia Morawska, Feifan Huang, and Kebin He. The impact of marine shipping and its DECA control on air quality in the Pearl River Delta, China. *Science of the Total Environment*, 625:1476–1485, 6 2018.
- [24] Mikhail Sofiev, James J. Winebrake, Lasse Johansson, Edward W. Carr, Marje Prank, Joana Soares, Julius Vira, Rostislav Kouznetsov, Jukka Pekka Jalkanen, and James J. Corbett. Cleaner fuels for ships provide public

- health benefits with climate tradeoffs. *Nature Communications*, 9(1), 12 2018.
- [25] John Van Aardenne. The impact of international shipping on European air quality and climate forcing.
- [26] A. Aulinger, V. Matthias, M. Zeretzke, J. Bieser, M. Quante, and A. Backes. The impact of shipping emissions on air pollution in the greater North Sea region - Part 1: Current emissions and concentrations. *Atmospheric Chemistry and Physics*, 16(2):739–758, 1 2016.
- [27] James J. Corbett, James J. Winebrake, Erin H. Green, Prasad Kasibhatla, Veronika Eyring, and Axel Lauer. Mortality from ship emissions: A global assessment. *Environmental Science and Technology*, 41(24):8512–8518, 12 2007.
- [28] H Abida and J Moreno-Gutiérrez. USING EMISSIONS OF PRECURSOR POLLUTANTS BY SHIPS IN DIFFERENT REGIONS TO CALCULATE YEARLY MORTALITY ATTRIBUTABLE TO MARITIME TRANSPORT: CASE FOR THE IMO TO DESIGNATE THE STRAIT OF GIBRALTAR AN ECA ZONE. Technical Report 3, 2021.
- [29] J. J. Winebrake, J. J. Corbett, E. H. Green, A. Lauer, and V. Eyring. Mitigating the health impacts of pollution from oceangoing shipping: An assessment of low-sulfur fuel mandates, 7 2009.
- [30] R. Prasad and Venkateswara Rao Bella. A review on diesel soot emission, its effect and control, 2010.
- [31] M. Matti Maricq. Chemical characterization of particulate emissions from diesel engines: A review, 2007.

- [32] H. Burtscher. Physical characterization of particulate emissions from diesel engines: A review. *Journal of Aerosol Science*, 36(7):896–932, 2005.
- [33] Kati Lehtoranta, Päivi Aakko-Saksa, Timo Murtonen, Hannu Vesala, Leonidas Ntziachristos, Topi Rönkkö, Panu Karjalainen, Niina Kuittinen, and Hilikka Timonen. Particulate Mass and Nonvolatile Particle Number Emissions from Marine Engines Using Low-Sulfur Fuels, Natural Gas, or Scrubbers. *Environmental Science and Technology*, 53(6):3315–3322, 3 2019.
- [34] European Union. Regulation (EU) 2016/1628 of the European Parliament and of the Council of 14 September 2016 on requirements relating to gaseous and particulate pollutant emission limits and type-approval for internal combustion engines for non-road mobile machinery. *Official Journal of the European Union*, L(252):1–86, 2016.
- [35] International Maritime Organization. MARPOL Annex VI: Regulations for the Prevention of Air Pollution from Ships. *International Maritime Organization*, 2020.
- [36] World Health Organization (WHO). Ambient (outdoor) air pollution. 12 2022.
- [37] Eloise Scotford, Delphine Misonne, and Alastair Lewis. Guide on Ambient Air Quality Legislation-Air Pollution Series. 2023.
- [38] CONVENTION ON LONG-RANGE TRANSBOUNDARY AIR POLLUTION. Technical report, 1979.

- [39] European Commission. Proposal for a Directive of the European Parliament and of the Council on ambient air quality and cleaner air for Europe (recast) (COM(2022) 542 final/2). Technical report, Brussels, Belgium., 2022.
- [40] European Environment Agency. Air pollution in Europe: 2023 reporting status under the National Emission reduction Commitments Directive. Technical report, 2023.
- [41] Anca Cristea, David Hummels, Laura Puzzello, and Misak Avetisyan. Trade and the greenhouse gas emissions from international freight transport. *Journal of Environmental Economics and Management*, 65(1):153–173, 1 2013.
- [42] Philip Linné and Erik Svensson. Regulating pollution from ships. In *Shipping and the Environment: Improving Environmental Performance in Marine Transportation*, pages 75–121. Springer Berlin Heidelberg, 1 2016.
- [43] USEPA. Overview of greenhouse gases. 2017.
- [44] Tony R. Walker, Olubukola Adebambo, Monica C. Del Aguila Feijoo, Elias Elhaimer, Tahazzud Hossain, Stuart Johnston Edwards, Courtney E. Morrison, Jessica Romo, Nameeta Sharma, Stephanie Taylor, and Sanam Zomorodi. Environmental effects of marine transportation. In *World Seas: An Environmental Evaluation Volume III: Ecological Issues and Environmental Impacts*, pages 505–530. Elsevier, 1 2018.
- [45] Chengfeng Wang and James J Corbett. The costs and benefits of reducing SO₂ emissions from ships in the US West Coastal waters. *Transportation Research Part D: Transport and Environment*, 12(8):577–588, 2007.

- [46] Øyvind Buhaug, J J Corbett, O Endresen, V Eyring, J Faber, S Hanayama, David Lee, H Lindstad, A Mjelde, and C Palsson. Second IMO greenhouse gas study. *International Maritime Organization, London*, 2009.
- [47] Mingliang Fu, Yan Ding, Yunshan Ge, Linxiao Yu, Hang Yin, Wentao Ye, and Bin Liang. Real-world emissions of inland ships on the Grand Canal, China. *Atmospheric Environment*, 81:222–229, 12 2013.
- [48] Yiqi Zhang, Sebastian D. Eastham, Alexis K.H. Lau, Jimmy C.H. Fung, and Noelle E. Selin. Global air quality and health impacts of domestic and international shipping. *Environmental Research Letters*, 16(8), 8 2021.
- [49] I M O Sulphur. Cutting Sulphur Oxide Emissions, 2020.
- [50] Jan Eiof Jonson, Michael Gauss, Michael Schulz, Jukka-Pekka Jalkanen, and Hilde Fagerli. Effects of global ship emissions on European air pollution levels. *Atmospheric Chemistry and Physics*, 20(19):11399–11422, 2020.
- [51] Tristan W P Smith, J P Jalkanen, B A Anderson, J J Corbett, J Faber, S Hanayama, E O’keeffe, S Parker, L Johansson, and L Aldous. Third IMO greenhouse gas study 2014. 2015.
- [52] Maria Polakis, Panos Zachariadis, and Jan Otto de Kat. The energy efficiency design index (EEDI). *Sustainable Shipping: A Cross-Disciplinary View*, pages 93–135, 2019.
- [53] Olaf Merk. Shipping Emissions in Ports. *International Transport Forum, Paris, France*, 2014.
- [54] D. A. Lack and J. J. Corbett. Black carbon from ships: A review of the effects of ship speed, fuel quality and exhaust gas scrubbing, 2012.

- [55] IEA. Tracking Clean Energy Progress 2023. Technical report, IEA, Paris, 2023.
- [56] By Juan Garcia Valencia. The Shipping Industry Won't Meet its Decarbonization Goals without Investing More in Low-carbon Fuels. Technical report, 2023.
- [57] OP. Brunila, T. Inkinen, V. Kunnaala-Hyrkki, E. Hämäläinen, and K. Alarämi. Black Carbon, Maritime Traffic and the Arctic. In: Pongrácz, E., Pavlov, V., Hänninen, N. (eds) Arctic Marine Sustainability. *Springer Polar Sciences. Springer, Cham.*, 2020.
- [58] B. Comer. Maritime Shipping: Black Carbon Issues at the International Maritime Organization. In: Brewer, T. (eds) Transportation Air Pollutants. *SpringerBriefs in Applied Sciences and Technology. Springer, Cham.*, 2021.
- [59] Mark G. Flanner, Charles S. Zender, James T. Randerson, and Philip J. Rasch. Present-day climate forcing and response from black carbon in snow. *Journal of Geophysical Research Atmospheres*, 112(11), 6 2007.
- [60] Naya Olmer, Bryan Comer, Biswajoy Roy, Xiaoli Mao, and Dan Rutherford. Greenhouse gas emissions from global shipping, 2013–2015: Detailed methodology. *International Council on Clean Transportation: Washington, DC, USA*, pages 1–38, 2017.
- [61] Konstantinos Kouzelis, Koos Frouws, and Edwin van Hassel. Maritime fuels of the future: what is the impact of alternative fuels on the optimal economic speed of large container vessels. *Journal of Shipping and Trade*, 7(1), 10 2022.

- [62] Shuzhan Bai, Jiao Tang, Guihua Wang, and Guoxiang Li. Soot loading estimation model and passive regeneration characteristics of DPF system for heavy-duty engine. *Applied Thermal Engineering*, 100:1292–1298, 5 2016.
- [63] W. Addy Majewski. Diesel Particulate Filters. *DieselNet, Ecopoint Inc, Brampton, ON, Canada.*, 2001.
- [64] Antiopi Malvina Stamatellou and Anastassios Stamatelos. Overview of Diesel particulate filter systems sizing approaches, 2017.
- [65] Kati Lehtoranta, Päivi Aakko-Saksa, and Hannu Vesala. Reducing particle emissions from marine engines-fuel choices and technology pathways. Technical report, 2023.
- [66] Erik Fridell and Kent Salo. Measurements of abatement of particles and exhaust gases in a marine gas scrubber. *Proceedings of the Institution of Mechanical Engineers Part M: Journal of Engineering for the Maritime Environment*, 230(1):154–162, 2 2016.
- [67] Hulda Winnes, Erik Fridell, and Jana Moldanová. Effects of marine exhaust gas scrubbers on gas and particle emissions. *Journal of Marine Science and Engineering*, 8(4), 4 2020.
- [68] Azam Sharifi and Ali Mohebbi. A combined CFD modeling with population balance equation to predict pressure drop in venturi scrubbers. *Research on Chemical Intermediates*, 40(3):1021–1042, 2014.
- [69] Arkadiusz T. Sobczyk, Anatol Jaworek, Artur Marchewicz, Andrzej Krupa, Tadeusz Czech, Łukasz Śliwiński, and Adam Charchalis. Particulate Matter

- Emission Reduction from Marine Diesel Engines by Electrohydrodynamic Methods. *Journal of KONES*, 26(3):203–210, 9 2019.
- [70] Akinori Zukeran, Yuki Nanjo, Kohei Ito, and Takashi Inui. Removal of Polycyclic Aromatic Hydrocarbons Emitted from Diesel Engine Using an Electrostatic Precipitator and Heat Exchanger. *IEEE Transactions on Industry Applications*, 54(6):6430–6438, 11 2018.
- [71] A. Zukeran, Y. Sakuma, R. Yamagami, Y. Kawada, H. Kawakami, K. Yasumoto, T. Inui, and Y. Ehara. The effects of gas cooling on removal of SOF and sulphate by electrostatic precipitator for marine diesel. *WIT Transactions on Ecology and the Environment*, 183:165–176, 7 2014.
- [72] A. Bologna, H. R. Paur, H. Seifert, Th Wäscher, and K. Woletz. Novel wet electrostatic precipitator for collection of fine aerosol. *Journal of Electrostatics*, 67(2-3):150–153, 5 2009.
- [73] Anssi Järvinen, Kati Lehtoranta, Päivi Aakko-Saksa, Mikko Karppanen, Timo Murtonen, Jarno Martikainen, Jarmo Kuusisto, Sami Nyysönen, Päivi Koponen, Pekka Piimäkorpi, Eero Friman, Varpu Orasuo, Jaakko Rintanen, Juha Jokiluoma, Niina Kuittinen, and Topi Rönkkö. Performance of a Wet Electrostatic Precipitator in Marine Applications. *Journal of Marine Science and Engineering*, 11(2), 2 2023.
- [74] Seongho Jeong, Jan Bendl, Mohammad Saraji-Bozorgzad, Uwe Käfer, Uwe Etzien, Julian Schade, Martin Bauer, Gert Jakobi, Jürgen Orasche, Kathrin Fisch, Paul P. Cwierz, Christopher P. Rüger, Hendryk Czech, Erwin Karg, Gesa Heyen, Max Krausnick, Andreas Geissler, Christian Geipel, Thorsten Streibel, Jürgen Schnelle-Kreis, Martin Sklorz, Detlef E. Schulz-Bull, Bert

- Buchholz, Thomas Adam, and Ralf Zimmermann. Aerosol emissions from a marine diesel engine running on different fuels and effects of exhaust gas cleaning measures. *Environmental Pollution*, 316, 1 2023.
- [75] Yoshihiro Sakuma, Ryuta Yamagami, Akinori Zukeran, Yoshiyasu Ehara, and Takashi Inui. Reduction of SO₂ and DPM Using Heat Exchanger and Electrostatic Precipitation in Diesel Engine. *Marine Engineering*, 49(4):533–538, 2014.
- [76] Francesco Di Natale, Claudia Carotenuto, Arianna Parisi, Domenico Flagiello, and Amedeo Lancia. Wet electrostatic scrubbing for flue gas treatment. *Fuel*, 325, 10 2022.
- [77] Claudia Carotenuto, Francesco Di Natale, and Amedeo Lancia. Wet electrostatic scrubbers for the abatement of submicronic particulate. *Chemical Engineering Journal*, 165(1):35–45, 11 2010.
- [78] Tran Hong Ha, Osami Nishida, Hirotsugu Fujita, and Harano Wataru. Enhancement of diesel particulate matter collection in an electrostatic water-spraying scrubber. *Journal of Marine Science and Technology*, 15(3):271–279, 9 2010.
- [79] S Kojevnikova and Y Zimmels. Mechanism of aerosol collection by two- and three-dimensional in homogeneous arrays of charged drops. Technical report, 2000.
- [80] S Kojevnikova and Y Zimmels. MECHANISM OF COLLECTION OF AEROSOLS BY AN ARRAY OF OPPOSITELY CHARGED DROPS. Technical Report 4, 2000.

- [81] Haibo Zhao and Chuguang Zheng. Modeling of gravitational wet scrubbers with electrostatic enhancement. *Chemical Engineering and Technology*, 31(12):1824–1837, 2008.
- [82] Anatol Jaworek, Wamadeva Balachandran, Andrzej Krupa, Janusz Kulon, and Marcin Lackowski. Wet electroscrubbers for state of the art gas cleaning, 10 2006.
- [83] A. Jaworek, K. Adamiak, W. Balachandran, A. Krupa, P. Castle, and W. Machowski. Numerical simulation of scavenging of small particles by charged droplets. *Aerosol Science and Technology*, 36(9):913–924, 2002.
- [84] A Krupa, A Jaworek, M Szudyga, T Czech, A T Sobczyk, A Marchewicz, T Antes, W Balachandran, R Belega, F Di Natale, and L D’addio. Diesel Nanoparticles Removal by Charged Spray. Technical report, 2016.
- [85] Lipeng Su, Yu Zhang, Qian Du, Xianchao Dai, Jianmin Gao, Peng Dong, and Hui Wang. An experimental study on the removal of submicron fly ash and black carbon in a gravitational wet scrubber with electrostatic enhancement. *RSC Advances*, 10(10):5905–5912, 2020.
- [86] L. D’Addio, F. Di Natale, C. Carotenuto, W. Balachandran, and A. Lancia. A lab-scale system to study submicron particles removal in wet electrostatic scrubbers. *Chemical Engineering Science*, 97:176–185, 6 2013.
- [87] Song Zhou, Jinxi Zhou, and Yuanqing Zhu. Chemical composition and size distribution of particulate matters from marine diesel engines with different fuel oils. *Fuel*, 235:972–983, 1 2019.
- [88] Song Zhou, Jinxi Zhou, Yongming Feng, and Yuanqing Zhu. Marine Emission Pollution Abatement Using Ozone Oxidation by a Wet Scrubbing

- Method. *Industrial and Engineering Chemistry Research*, 55(20):5825–5831, 5 2016.
- [89] Arianna Parisi and Francesco Di Natale. Wet electrostatic scrubbing for fine and ultrafine particles removal in domestic biomass boilers. Technical report.
- [90] C. Y. Cha and B. J. McCoy. Thermal force on aerosol particles. *Physics of Fluids*, 17(7):1376–1380, 1974.
- [91] Anatol Jaworek, Andrzej Krupa, Arkadiusz T. Sobczyk, Artur Marchewicz, Michał Szudyga, Teresa Antes, Wamadeva Balachandran, Francesco Di Natale, and Claudia Carotenuto. Submicron particles removal by charged sprays. Fundamentals. *Journal of Electrostatics*, 71(3):345–350, 6 2013.
- [92] A. Jaworek, A. T. Sobczyk, A. Marchewicz, A. Krupa, and T. Czech. Particulate matter emission control from small residential boilers after biomass combustion. A review. *Renewable and Sustainable Energy Reviews*, 137, 3 2021.
- [93] Lord Rayleigh. XX. On the equilibrium of liquid conducting masses charged with electricity . *The London, Edinburgh, and Dublin Philosophical Magazine and Journal of Science*, 14(87):184–186, 9 1882.
- [94] Junke Guo. Motion of spheres falling through fluids. *Journal of Hydraulic Research*, 49(1):32–41, 2 2011.
- [95] Jason K. Kabarowski and Aditya S. Khair. Hydrodynamic slip significantly alters chaotic advection and scattering of small particles. *Physical Review Fluids*, 7(8), 8 2022.

- [96] Lin Yang, Ji Zhang, Han Yuan, and Ning Mei. Analysis of the motion of small-scale ellipsoidal particles in a horizontal laminar flow field. *Partic-uology*, 40:44–51, 10 2018.
- [97] Ao Wang, Qiang Song, and Qiang Yao. Behavior of hydrophobic micron particles impacting on dropletsurface. *Atmospheric Environment*, 115:1–8, 8 2015.
- [98] Jingye Ren, Lu Chen, Jieyao Liu, and Fang Zhang. The density of ambient black carbon retrieved by a new method: implications for cloud conden-sation nuclei prediction. *Atmospheric Chemistry and Physics*, 23(7):4327–4342, 4 2023.
- [99] Shurong Wang, Kaili Zhou, Xiaohui Lu, Hong Chen, Fan Yang, Qiang Li, Xin Yang, and Xiaofei Wang. Measurement of density and shape for single black carbon aerosols in a heavily polluted urban area. *Aerosol and Air Quality Research*, 21(12), 12 2021.
- [100] Jay L Devore. Probability and statistics. *Pacific Grove: Brooks/Cole*, 2000.
- [101] Douglas C Montgomery and George C Runger. *Applied statistics and prob-ability for engineers*. John wiley & sons, 2020.
- [102] David S Moore, George P McCabe, Layth C Alwan, and Bruce A Craig. *The practice of statistics for business and economics*. WH Freeman and Company, 2016.